



Chair of Reservoir Engineering

Master's Thesis



Fluid-Rock-Fluid Interactions Of Alkali-Polymer in 8 TH & 9 TH Matzen Reservoir

Ahmad Sidaoui

November 2022



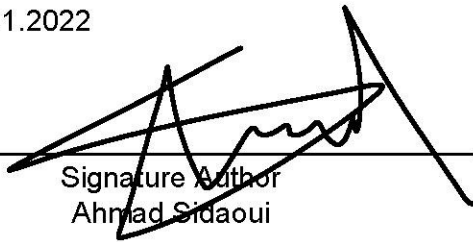
AFFIDAVIT

I declare on oath that I wrote this thesis independently, did not use other than the specified sources and aids, and did not otherwise use any unauthorized aids.

I declare that I have read, understood, and complied with the guidelines of the senate of the Montanuniversität Leoben for "Good Scientific Practice".

Furthermore, I declare that the electronic and printed version of the submitted thesis are identical, both, formally and with regard to content.

Date 07.11.2022



Signature Author
Ahmad Sidaoui



Ahmad Sidaoui
Hasnerstrasse 91, Apt. 17-18
1160 Wien

To the Dean of graduate Studies of the Montanuniversitaet Leoben

Declaration of Approval for the Digital Publication of Scientific Theses

I am aware that the thesis entitled "Fluid-Rock-Fluid Interactions Of Alkali-Polymer in 8 TH & 9 TH Matzen Reservoir" will be subject to a plagiarism assessment and may be stored by Montanuniversität Leoben for an unlimited period of time.

I agree that the University Library of Montanuniversität Leoben may publish the thesis open access in the World Wide Web. For embargoed theses this will be done after the embargo expires.

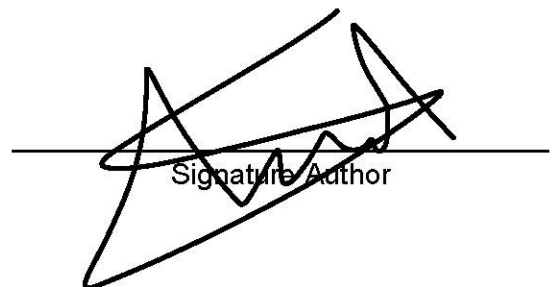
Note: in case you refuse the open access publication in the World Wide Web, the thesis will only be published in printed form (after a possible embargo has expired) in the University Library (dissertations also in the Austrian National Library).

I hereby agree with the open access publication of my thesis on the World Wide Web:

Yes

No

Date 07.11.2022


Signature Author

Ahmad Sidaoui

Master Thesis 2022

Petroleum Engineering

Fluid-Rock-Fluid Interactions of Alkali-Polymer in 8 TH & 9 TH Matzen Reservoir

Supervisor: Univ.-Prof. Dipl.-Phys. Dr.rer.nat.
Holger Ott

Co-supervisor/Advisor: Dr.-Ing. Rafael E. Hincapie

Chair of Reservoir Engineering

"I would like to dedicate my Master's Thesis to my parents, Oussama Sidaoui and Hiam Sabbagh, and my fiancée Claudia Ditel for being there for me and supporting me in hardship and ease. This thesis is dedicated to them and to whoever taught me a word."

Acknowledgements

I would like to express my gratitude to the oil company OMV, which gave me the opportunity to gain a lot of experience and to accomplish this work. Particularly, I would like to thank Dr. -Ing. Rafael Eduardo Hincapie Reina, for supervising me and guiding me throughout this project. Additionally, I would like to thank Magdalena Biernat and Ante Borovina for their technical and practical support in the laboratory.

Abstract

The chemical-enhanced oil recovery market has grown in the past few years. Studies have established that using chemical agents like alkali and polymers together has a synergetic effect in increasing oil production beyond additional recoveries reached by water flooding operations. The optimal chemical composition is essential because of the unique characteristics of reservoirs.

In this work, fluid-fluid and rock-fluid evaluations are carried out in the laboratory to select and optimise the chemical solution to be considered for further pilot testing applications in the 9 TH reservoir of the Matzen field northeast of Vienna, Austria. The evaluations consisted of measuring the IFT reduction effect of alkali and alkali-polymer solutions and analysing the emulsification process and the stability of the emulsions when the chemical agents meet the natural acids present in the oil samples. Spontaneous imbibition experiments were carried out to analyse and quantify the occurrence of a wettability alteration mechanisms. Finally, single-phase core flood experiments are carried out to analyse the effect of polymer retention on the core permeability and the additional resistance to flow when polymers are considered in the injected fluids.

In the evaluations, two oil types are analysed, an oil sample from the 8 TH reservoir and another from the 9 TH reservoir in the Matzen field. Both oil types have similar TAN and saponifiable acids. The chemicals consisted of different concentrations of two different types of alkalis, sodium and potassium carbonate, along with fixed concentrations of two types of HPAM polymers noted as KA 5265 and SNF 3630S. 1900 and 1850 ppm of SNF 3630S and KA 5265 consecutively were used in some prepared solutions.

A sound effect of IFT reduction was noted when an alkali agent was present in the analysed chemical solution. However, the presence of a polymer slightly reduced the IFT reduction effect due to the stability provided by the polymer. The added stability was also noticed in the phase behaviour experiments, the saponification and emulsification process were noticed with all the alkali-containing solutions, and the created emulsion middle phase was stabilised in cases where polymer was also present in the aqueous phase. An additional oil recovery of 7 % and 33 % was recorded for the 9 TH and 8 TH oil samples consecutively in the spontaneous imbibition tests. The low IFT mechanism contributed to the increase in oil production.

Moreover, the results were analyzed using the capillary diffusion coefficient. The results showed that the wettability alteration mechanism did not take a role in increasing oil production by spontaneous imbibition for the 8 TH cases. However for 9 TH cases wettability alteration was deduced by an combination of diffusion coefficient increase and IFT decrease. The Single-phase flooding evaluations showed that the concentration of 7500 ppm of sodium carbonate + 1850 ppm KA 5265 yields lower flow resistance factors and has a lower polymer retention capacity when it flows through the porous media.

Zusammenfassung

Der Markt für chemisch verstärkte Ölrückgewinnung ist in den letzten Jahren gewachsen. Studien haben ergeben, dass die gemeinsame Verwendung von chemischen Mitteln wie Alkali und Polymeren einen synergetischen Effekt bei der Steigerung der Ölproduktion hat, der über zusätzliche Gewinnungen hinausgeht, die durch Wasserflutungen erreicht werden. Die Mechanismen, die im Spiel sind, wenn es um chemisch verstärkte Ölrückgewinnung geht, sind eine Änderung der Benetzbarkeit und eine Verringerung der Grenzflächenspannung zwischen der Ölphase und der eingespritzten wässrigen Phase. Aufgrund der einzigartigen Eigenschaften von Lagerstätten ist die optimale chemische Zusammensetzung von entscheidender Bedeutung.

In dieser Arbeit werden Fluid-Fluid- und Gesteinsfluid-Bewertungen im Labor durchgeführt, um die chemische Lösung auszuwählen und zu optimieren, die für weitere Pilotversuchsanwendungen in der 9. TH-Lagerstätte des Feldes Matzen nordöstlich von Wien, Österreich, in Betracht gezogen werden soll. Die Bewertungen bestanden aus der Messung des IFT-Reduktionseffekts von Alkali- und Alkali-Polymer-Lösungen und der Analyse des Emulgierprozesses und der Stabilität der Emulsionen, wenn die chemischen Mittel auf die in den Ölproben vorhandenen natürlichen Säuren treffen. Spontane Imbibitionsexperimente wurden durchgeführt, um das Auftreten von Mechanismen zur Veränderung der Benetzbarkeit zu analysieren und zu quantifizieren. Schließlich werden einphasige Kernflutungsexperimente durchgeführt, um den Einfluss der Polymerretention auf die Kernpermeabilität und den zusätzlichen Strömungswiderstand zu analysieren, wenn Polymere in den injizierten Flüssigkeiten berücksichtigt werden.

In den Auswertungen werden zwei Ölsorten analysiert, eine Ölprobe aus der 8. Lagerstätte und eine weitere aus der 9. Lagerstätte im Feld Matzen. Beide Ölsorten haben ähnliche TAN und verseifbare Säuren. Die Chemikalien bestanden aus unterschiedlichen Konzentrationen von zwei verschiedenen Typen von Alkalien, Natrium- und Kaliumcarbonat, zusammen mit festen Konzentrationen von zwei Typen von HPAM-Polymeren, die als KA 5265 und SNF 3630S bezeichnet wurden. In einigen hergestellten Lösungen wurden nacheinander 1900 und 1850 ppm SNF 3630S und KA 5265 verwendet.

Ein deutlicher Effekt der IFT-Reduktion wurde festgestellt, wenn ein alkalisches Mittel in der analysierten chemischen Lösung vorhanden war. Die Anwesenheit eines Polymers verringerte jedoch leicht den IFT-Verringerungseffekt aufgrund der durch das Polymer bereitgestellten

Stabilität. Die zusätzliche Stabilität wurde auch in den Phasenverhaltensexperimenten festgestellt, der Verseifungs- und Emulgiervorgang wurde bei allen alkalihaltigen Lösungen festgestellt und die gebildete Emulsionsmittelfase wurde stabilisiert, wenn Polymer auch in der wässrigen Phase vorhanden war. Eine zusätzliche Ölwiederfindung von 7 % und 33 % wurde für die 9. und 8. Ölprobe nacheinander in den spontanen Tränkungstests aufgezeichnet. Der niedrige IFT-Mechanismus trug zum Anstieg der Ölförderung bei.

Darüber hinaus wurden die Ergebnisse anhand des Kapillardiffusionskoeffizienten analysiert. Die Ergebnisse zeigten, dass der Mechanismus der Veränderung der Benetzbarkeit bei der Erhöhung der Ölproduktion durch spontane Aufnahme für die 8 TH-Fälle keine Rolle spielte. Bei 9 TH-Fällen wurde die Benetzbarkeitsänderung jedoch aus einer Kombination aus einer Erhöhung des Diffusionskoeffizienten und einer Abnahme der IFT abgeleitet. Die Einphasenflutungsbewertungen zeigten, dass die Konzentration von 7500 ppm Natriumcarbonat + 1850 ppm KA 5265 niedrigere Strömungswiderstandsfaktoren ergibt und eine geringere Polymerrückhaltekapazität hat, wenn es durch die porösen Medien fließt.

Table of Contents

Acknowledgements.....	vii
Abstract.....	ix
Zusammenfassung.....	xi
Introduction.....	15
State of the Art or Literature Review.....	16
Introduction.....	16
Introduction to the Matzen Field.....	17
Enhanced Oil Recovery	19
Chemical Enhanced Oil Recovery	23
Fluid-Fluid interaction	28
Fluid Rock Interactions.....	35
Alkali - Polymer flooding	48
Experimental Setup and Methods	53
Fluid Characterization.....	53
Core Preparation and Analysis.....	56
IFT Evaluations.....	58
Routine core analysis	60
Spontaneous Imbibition Experiments	68
Phase Behavior Experiments	69
Single-Phase Core Floods	70
Results and Discussion	72
Conclusion	104
Interfacial tension.....	104
Phase behaviour:	104
Single-phase core floods:.....	105
Spontaneous imbibition experiment:	105
Analysis and capillary suction phenomena.....	106
Overall Conclusion	106
Future work:.....	107

References..... 109
References..... 109
List of Figures 113
List of Tables 115

Introduction

A Variety of chemical agents are use in Chemical Enhanced Oil Recovery, such as alkali agents to ultimately increase the oil production from a field. Previous studies have shown how alkali-polymer flooding contributes to the change of certain key physical parameters of the reservoir rock and fluids. Three main points take a great role in the Alkali-Polymer flooding, wettability alteration, the decrease of solution-oil interfacial tension, and the enhancement of the sweep efficiency. Some of these points contribute to the increase of the capillary number and others contribute to the reduction of the mobility ratio.

Prior field applications, EOR processes require a detailed feasibility evaluation that includes laboratory, modelling, and pilot testing. Previous laboratory and modelling evaluations performed for the 8 TH and the 16 TH Matzen have shown very promising results when applying alkali-polymer, leading to the field trials in 2022. This has attracted the interest in performing further rock-fluid interaction evaluations for the 8 TH Matzen field and enlarging the scope of alkali-polymer application to include the 9 TH Matzen field. Previous work presented by Leitenmüller (2019) addressed some of the issues generally, but without going into detail.

In the case of the 8 TH Matzen field, the rock-fluid interactions are an important uncertainty that needs to be investigated, while for the 9 TH Matzen field both rock-fluid and fluid-fluid interactions are required to be assessed to reduce uncertainties. This and other related aspects are expected to be covered in this work, through a detailed laboratory evaluation together with external partners. Detailed laboratory evaluations are presented in this work to cover the previously mentioned properties and aspects of Alkali-Polymer flooding in the Austrian Matzen Field.

To test the laboratory feasibility of applying alkali-polymer on the 8 TH and 9 TH, several parameters and evaluations are needed to be considered. First the fluids of interests some of which are the oil samples taken from the 8 TH and 9 TH reservoir, the synthetically prepared laboratory brines along side with other polymer and alkali chemicals are to be defined and characterized for further fluid-fluid and rock-fluid experimental evaluations. For the use of alkali-polymer in the targeted reservoirs, it is crucial to assess the impact of the polymer on viscosity and mobility. The rest of the evaluations can be subdivided into firstly, fluid-fluid evaluations including phase behavior experiments and IFT evaluations. Secondly, fluid-rock evaluations including core flooding experiment to determine the effect of polymer retention on

the effective permeability of the core plugs, and Spontaneous imbibition experiments to analyze the effect of Alkali-polymer chemicals on the rock wettability.

The Alkali-polymer application showed a significant alteration in the above discussed parameters. From a fluid/fluid interaction point, the interfacial tension between the 9 TH oil samples and the used chemical solutions was reduced significantly, and interaction between the two fluids lead to the creation of an emulsion phase. The emulsions formed with different chemical concentrations proved to have different stabilities. From a fluid/rock interaction point, the effect of interfacial tension was noted by a high early production of oil, and the effect of IFT reduction was noticed by higher ultimate oil recovery values while conducting the spontaneous imbibition test. Additionally, the single-phase core floods demonstrated the effect of polymer retention on the core plugs permeability.

The interaction between the steel metal lines and brine proved to be a challenge due to rust. Rust was noticed on the different faces of the cores after conducting the single-phase core flood experiments, it was also noticed on the edges of the metallic lines. This proved to be an issue as rust plugged the pore throats which led to a drastic increase in the differential pressure and a reduction in permeability. However, this issue was resolved by changing the metallic lines connecting the core holder to the pump and coating the inside faces of valves with a corrosion inhibitor. The results in which rust was noticed were disregarded.

The evaluations were divided into sections and chapters. A comprehensive literature review is presented in the first chapter in which the following topics were discussed: Introduction to the Matzen field, Enhanced oil recovery principles, chemical enhanced oil recovery, fluid-fluid interactions, rock-fluid interactions, and finally Alkali-Polymer flooding. Information about the used equipment and methodology are discussed in later chapters. Finally, the results of all the mentioned evaluations and experiments are shown and discussed, and conclusions are deduced in the last two chapters.

State of the Art or Literature Review

Introduction

This chapter provides an overview of Chemically enhanced oil recovery, in which chemicals such as Alkali-Polymer solutions, are used to increase oil production in different kinds of reservoirs. Chemical Enhanced oil recovery methods were used extensively in sandstone

reservoirs due to the additional complexities and heterogeneities that are accompanied by carbonate reservoirs.

First, the first subsection of this chapter provides a general definition of enhanced oil recovery. The many types and mechanisms that this recovery method offers are also described, along with a more thorough explanation of chemically enhanced oil recovery systems. A more thorough explanation will then be provided to highlight the various features that can be changed to boost oil production. These characteristics include the wettability of the rock surface and the interfacial tension at the surface where two non-miscible fluids meet.

The final section of this chapter will cover the subject of mobility control, emphasizing the value of using polymer solutions in a chemically enhanced oil recovery process. The different methods and tools that are used in measuring the different properties previously mentioned will also be reviewed.

Introduction to the Matzen Field

One of the biggest oil producing fields in Europe, the Matzen field is made up of several stacked reservoirs made of splay sands and interbedded shales. It had an estimated 190 million m³ of oil in it at first. The field has a long production history during which the production streamline and surface facilities were modified to account for the production from newly discovered reservoirs within the field. The field is located about 20 kilometers northeast of the city of Vienna in the Vienna basin.

As mentioned, the field is composed of multiple reservoirs, some of which will be highlighted in this section. The first reservoir to be discussed is the 16 Torton reservoir. It is a rectangular shaped reservoir with a length of 12 kilometers and a width of 3.5 kilometers. The sand layer has a maximum gross thickness of 70 meters and could be subdivided into 8 overlapping intervals. Each layer is made up of a prograding delta front deposit that is rich in sand, which is separated from it by a thin layer of limestone that was laid down during high sand events. The 16 Torton reservoir has an average initial water saturation of 15%, an average permeability of 1.2 Darcy, and an average porosity of 25%. The oil produced from this reservoir has a viscosity of 5 cP and an oil gravity of 25 API, and the reservoir's temperature is 60 °C. The first well drilled in this reservoir in 1949 yielded a constant production rate of 7000 m³ per day until a decline in production was observed in 1954. A 4 to 8 % reduction in oil production decline was achieved due to the application of water flooding operations in December 1967. In 1998, Gas was injected into the gas cap of the reservoir in the aim to stabilize the pressure of the reservoir. A volume of 42.8 million m³ of oil, along with 3.84 billion m³ of gas were produced up until the

year 2007, during which a water cut of 94% was reached (Poellitzer, Gruenwalder, Kienberger and Clemens, 2008).

The second reservoir of significance importance in the Matzen field is the 8 Torton reservoir. Formed of shallow marine sandstone deposits, the reservoir has a net thickness of 20 m and is characterized by an average permeability of 500 mD and a porosity range of 20 to 30 %. The reservoir situated 1150 m below the surface is neighboring a weak aquifer at the northern edge and possesses a gas cap. The oil produced from this reservoir was characterized with a viscosity of 50 cP at reservoir temperature of 50 °C and an oil density of 29 API. Production commenced in 1951 at a reservoir initial pressure of 113 bar. An oil production rate peak of 2000 m³ per day was achieved in 1957. Since then the reservoir production rate steadily declined to about 80 bars in 1960. Consequently, water flooding operations commenced in 1960 in an effort to stabilize the production rate. AS a result of the water flooding operations the water cut continuously increased until 96% at the year of 2016 (Sieberer, Jamek and Clemens, 2022).

Lastly the reservoir of interest for this research is the 9 Torten reservoir situated in the Matzen field. The 25 m thick reservoir located at a depth of 1150 m below the surface is composed of sandstone and mudstone deposits belonging to a deltaic depositional environment, these layers were deposited during sea level cycles. This complex depositional environment is the reason why the permeability of the reservoir is heterogeneous, some areas are highly permeable while other areas are less permeable. The reservoir has an average permeability of 400 mD and an average porosity of 20%. The reservoir is characterized by:

The presence of a gas cap.

The presence of an aquifer at the north easter edge.

A reservoir temperature of 52 °C.

An initial average reservoir pressure of 129.5 bar.

The 9 Torten reservoir has a production history of over 62 years, and a total of 250 wells with several re-completion. Production commenced in 1951 with an initial reservoir pressure of 129.5 bar. The peak production rate of 4400 bbl/d was achieved in 1957, after which oil production declined. It should be noted that drilling additional wells in the reservoir helped with maintaining the production rate over time. Finally, water flooding operations for this reservoir commenced in 1968 (Chiotoroiu, Clemens and Thiele, 2022).

Enhanced Oil Recovery

During the production life of an oil field, a reservoir can undergo multiple production stages, depending on the corresponding properties and conditions of the reservoir. An oil reservoir can undergo the following three stages, primary recovery, secondary recovery, and tertiary recovery.

The reservoir initially has enough natural energy during the primary recovery stage to displace the oil from the porous media all the way up to the surface.. This natural energy that the reservoir possess derives from different mechanisms, some of which are rock-fluid expansion, solution gas drive, the presence of a gas cap, gravity drainage, etc... During the primary recovery, there is no need for any additional energy. With time, the production rate of the reservoir decreases along with the reservoir pressure, indicating an overall decrease in the reservoir's natural energy. Thus, additional energy needs to be introduced to the reservoir for maintaining the pressure and increasing the production rate. This is done by implementing water flooding operations in which water is injected into the reservoir from one or multiple injection wells. The injected water does not only contribute to pressure maintenance but also contributes to the improvement of the sweep efficiency.

Tertiary recovery or Enhanced Oil Recovery is defined as the phase that comes after the secondary recovery, in which special fluids are injected into the reservoir to manipulate the rock and fluid properties to further increase oil recovery. Enhanced oil recovery has a wide range of applications, some of which are thermal recovery, miscible gas injection, and chemical recovery, in which certain predefined chemical composition is injected into the reservoir. Enhanced oil recovery is of great importance as it can contribute to a significant increase in oil production, in some cases EOR applications are even considered shortly after the beginning of the water flooding operations.

The term IOR or Improved Oil Recovery can be confused sometimes with EOR, however, IOR applications include processes that do not necessarily change the rock/oil/brine interactions such as horizontal well drilling, infill drilling, and improved reservoir management. EOR applications on the other hand are defined as processes that change oil/brine/rock interaction to ultimately increase oil production. EOR operations can be considered as a subsection of IOR applications (Sheng, 2016) (Stosur, Hite, Carnahan, and Miller, 2003).

Due to the fall of conventional oil production, EOR applications are on the increase, especially in the US (Taber, Martin and Seright, 1997). Some of the most important onshore basins located in Saudi Arabia, Russia, and China are witnessing a decline in production, however, the need

to extract the remaining recoverable oil from these reservoirs is increasing. Additionally, offshore technology has improved the applicability of certain operations in offshore reservoirs. All the above contribute to the growth of the enhanced oil recovery market which is to be expected by the year 2030 (Research, 2022).

Capillary Desaturation Curve

When it comes to Enhanced oil recovery, the targeted properties that dictates the amount of oil recovered can be divided into two, properties that affect oil recovery on a microscopic level, such as the interfacial tension, and properties that affect the recovery on a macroscopic scale.

To have a better understanding of the properties to be manipulated in EOR processes on both microscopic and macroscopic scale, a relation must be established between the different forces in a porous medium. The viscous force to capillary force ratio, as shown below, is what makes up the capillary number.

$$N_c = \frac{u\mu}{\sigma \cos \theta} \quad (1)$$

(Sheng, Modern chemical enhanced oil recovery 2016)

Where:

N_c is the capillary number [-]

u is the Darcy velocity of the displacing fluid [m/s]

μ is the viscosity of the displacing fluid [Pa*s]

θ is the contact angle

It should be mentioned that the capillary number is a dimensionless number.

However, the capillary number alone cannot describe the effect that these properties have on oil recovery. The Capillary Desaturation curve relates the trapped oil ganglion dimension and length with the capillary number, or in other words, the different forces applied to this oil ganglion. Literature has shown that above a critical oil ganglion size, a specific applied differential pressure can mobilize the ganglion (Yeganeh et al., 2016). It is indicated in the literature that when the capillary number increases, in other words, when the viscous forces are greater than the capillary forces, the residual oil saturation should decrease, indicating an increase in oil recovery.

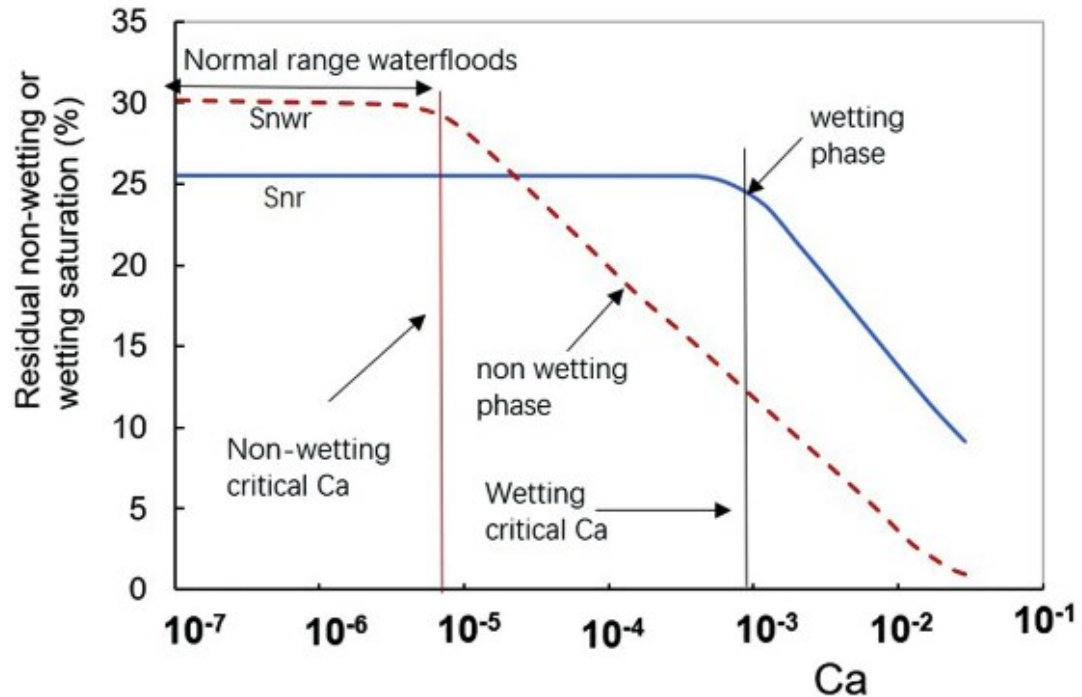


Figure 1: CDC curve for the wetting and non-wetting phase from Lake(1989, Fig.3–17, p.70).

Two capillary desaturation curves are shown in figure (1), the CDC curve for the non-wetting case is an imbibition curve, and the one for the wetting case is a drainage curve (Guo, Song and Hilfer, 2022). The critical capillary number above which the residual oil saturation is decreasing for the non-wetting phase is smaller than the one for the wetting phase. This is mainly due to the large capillary force that a non-wetting fluid needs to overcome to flow in the porous media.

Mobility Control

On a macroscopic level, EOR aims increase the stability of the flooding front. This is generally done by reducing the mobility of the injected fluid. A more stable front limits the bypassed oil regions brought by the viscous instabilities such as viscous fingering and increases oil production.

In order to analyze the stability of a front, it is necessary to define the mobility of both the displacing fluid—in the case of an EOR operation, the injected fluid—and the displaced fluid, or oil. In general, the relative permeability to viscosity ratio of a given phase determines a fluid's mobility (Sheng, 2016).

The mobility ratio M is a dimensionless unit that measures the stability of a displacement process in the absence of a gravity and capillary forces (Gbadamosi et al., 2019).

$$M = \frac{\lambda_{Displacing\ fluid}}{\lambda_{Displaced\ fluid}} = \frac{k_{r,displacing} / \mu_{displacing}}{k_{r,displaced} / \mu_{displaced}} \quad (2)$$

Where:

$k_{r,displacing}$ and $\mu_{displacing}$ are respectively the relative permeability and the viscosity of the displacing fluid.

$k_{r,displaced}$ and $\mu_{displaced}$ are respectively the relative permeability and the viscosity of the displaced fluid.

A mobility ratio greater than one indicates an unstable front, in which viscous instabilities can occur. However, a mobility ratio less than or equal to one indicates a stable front with a desirable sweep efficiency could minimize the bypassed oil regions in the porous media and increase the recovery of oil (Sheng, 2016).

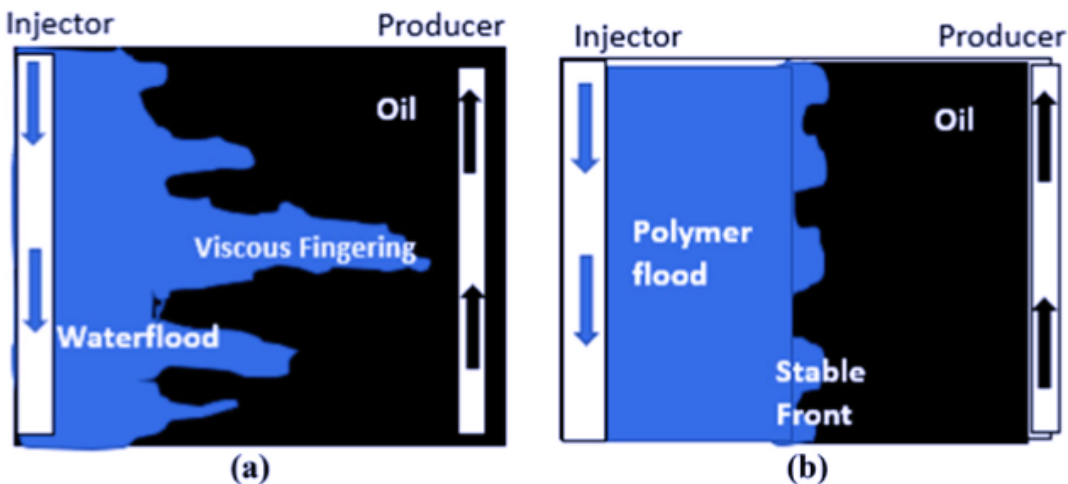


Figure 2: Displacement front in two different conditions, (a) unstable condition, (b) Stable condition without viscous fingering (Gbadamosi et al., 2019).

To achieve the desired mobility ratio, either the viscosity of the residing reservoir fluid needs to be changed by thermal applications or predefined polymeric solutions could be injected into the reservoir to increase the viscosity of the displacing fluid, decreasing the mobility ratio, and stabilizing the displacement process (Gbadamosi et al., 2019) (Sheng, 2016). By adjusting the polymer concentration in the solution, the viscosity of the polymer solution can be altered to a desired target viscosity (Sheng, 2016).

The different types of polymer solutions along with the parameters that affect the viscosity and the stability of the polymeric solutions will be further discussed in the Mobility control chapter.

To summarize the above, Enhanced Oil Recovery or tertiary recovery focuses on changing the reservoir rock/brine/oil interaction properties to increase oil production. The mechanisms applied in EOR processes serve two main objectives. The first goal is to increase the capillary number N_c by lowering the interfacial tension between the fluids being injected and those already present in the capillaries. To improve sweep efficiency and stabilize the displacement front, the second goal is to reduce the mobility ratio. Both goals will eventually boost oil recovery.

Chemical Enhanced Oil Recovery

Chemical Enhanced Oil Recovery utilizes chemical solutions to change properties affecting both microscopic and macroscopic displacement. This is usually done by determining the desired chemical composition in the lab through multiple screening criteria that would yield an optimized fluid composition. This fluid is then injected into the reservoir and displaces the residing fluids. The viscosity of the injected solution is also considered to ultimately increase the sweep efficiency and achieve a stable displacement front (Sheng, 2016).

The most important conventional EOR chemicals are Alkali, Polymers, and surfactants (Gbadamosi et al., 2019).

Screening Criteria for different chemicals

There is a wide range of chemicals in cEOR, thus a screening criterion has been adopted to optimize the chemical composition and to maximize the profits. Additionally screening for an optimized chemical composition comes in handy when it comes to simulating different scenarios in computer assisted tools for reservoir management (Taber, Martin and Seright, 1997). A generally adopted way to measure the success of an EOR process is the amount of chemicals injected in pounds per barrel of incremental oil produced (Sheng, 2016). When it comes to screening for chemical applications in cEOR processes, the following factors need to be considered:

1. Reservoir Temperature
2. Formation Type
3. Formation Water Salinity & Divalent Content
4. Oil Viscosity
5. Permeability

The formation composition is important in Alkali-Surfactant applications. Most of cEOR processes are done in sandstone reservoirs and not as much in carbonate reservoirs due to the high adsorption of anionic surfactants, which will be further discussed later on in this chapter, on the surface of carbonate rocks. Additionally, anhydrite can exist in carbonate rocks that would also cause high adsorption along with precipitation. Precipitation is undesired in cEOR processes because the precipitates can plug the small pore throats and reduce permeability. It should be noted that clay in sandstone reservoirs can also cause high polymer adsorption and alkaline consumption.

Water salinity and the presence of divalent ions such as calcium Ca^{2+} and magnesium Mg^{2+} has a significant impact on the type of polymers to be used, as an example biopolymer are less sensitive to high salinity and hardness than the hydrolyzed polyacrylamides or synthetic polymers. Thus, salinity and hardness are important factors to be considered when choosing the polymers to be used for a specific reservoir. Most of the cEOR operations have been applied generally in reservoirs with low salinities. In most Chinese polymer projects, the salinities are lower than 10000 ppm (Sheng, 2016). It should be noted that in this study salinity is used to indicate the total amount of anions and hardness refers to the multivalence.

Different reservoirs have different types of oil with different compositions and properties. Oil viscosity is a factor that should be considered when screening for chemical solutions as it has a direct effect on the mobility ratio and consequently on the sweep efficiency that would take place in the reservoir. Different surfactants/Alkali should be used with different oils as the composition of the oil plays an important factor in the chemical interactions between the injected solution and the oil.

Permeability is also an important factor when it comes to polymer injection, high permeable reservoirs are more favorable for polymer applications than low permeability reservoirs. Certain issues such as injectivity and polymer retention need to be accounted for in low permeable reservoir (Sheng, 2016)

Surfactants

According to published definitions, surfactants are amphiphilic surface-acting molecules made up of the hydrophilic group and the hydrophobic tail. The hydrophilic functional group is composed of ammonium salts, carboxylates COO^- , alcohols, sulfonates SO_3^- , and sulphate SO_4^{2-} while the hydrophobic group is formed of long chains for hydrocarbons that may not

be chained (Gong et al., 2016). Surfactants are classified according to the charge of the surfactant functional head, there are many types of surfactants some of which are:

Anionic surfactants

Cationic surfactants

Non-Ionic surfactants

Zwitterionic surfactants

The anionic surfactants characterized by a surface-active head bearing a negative charge are most used in EOR operations, mainly due to the applicability of EOR applications in sandstone reservoirs. The negative charge of the surfactant is most useful when it comes to its association of potassium K^+ and sodium Na^+ ions. Surfactants with sulphonates as a hydrophilic head are more stable in high temperatures compared to other anionic surfactants, however precipitation is an issue especially in the presence of divalent ions. On the other hand, Anionic surfactants with sulphates composed hydrophilic head are more tolerant to salinity and hardness, however they break down at high temperatures.

Cationic surfactants are characterized with a surface-active head bearing a positive charge. They are easily attracted to surfaces with negative charges such as surfaces with high clay content. The production of these types of surfactants requires a high-pressure hydrogenation reaction that makes them more expensive than anionic surfactants and less feasible.

Non-ionic surfactants are surfactants that do not ionize in the aqueous phase. Alkylbenzene or alkyl make up the hydrophobic tail, while the hydrophilic head is made up of substances like alcohol and phenol. These surfactants, according to published research, are more tolerant of salinity but have less of an impact on the interfacial tension at the interface of two immiscible fluids.

Last but not least, zwitterionic surfactants like sulfonier betaine are distinguished by having both an anionic and a cationic charge at the surface-active head. They are tolerant of both salinity and temperature well.

Alkali Salts

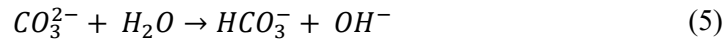
Alkalis are formed of ionic salts of an alkali metal or alkaline earth metals. They are of great importance when in EOR applications since they react with the natural acids present in heavy oil to form in situ surfactants. This process is further explained by the saponification reactions.

The most common Alkali agents are sodium carbonate and sodium hydroxide. It should be mentioned that the addition of such alkalis would change the pH environment in the reservoir, this is mainly the result of the dissociation of Alkali solutions shown below:

NaOH:



Na₂CO₃:



Alkaline flooding applications were recognized and applied as early as 1917. However, there application was not very common or successful (Kumar, Yen, Chilingarian and Donaldson, 1989). The modern successful application of alkali is usually done in the form of Alkaline-polymer flooding or Alkali-Surfactant-polymer flooding. ASP flooding operations were conducted in the Tanner field in Wyoming, USA, a sandstone reservoir with a reservoir temperature of 79 °C . The ASP flooding operation began in that field after a short waterflooding phase, the oil cut when ASP began was at 43, the application of this chemical flooding operation aims to produce an additional 17 % of the OOIP beyond what the water flooding phase could contribute (Mandal, 2015).

Polymers

Polymers have been used in EOR operations on a commercial scale. Secondary recovery can be effective up to a certain extent when the water cut increases and production is no longer feasible. At this point polymer flooding is considered as a tertiary process, or a EOR recovery process in which polymer are injected into the reservoir to reduce water breakthrough and to reduce the mobility ratio.

A wide range of polymer exists with different properties and characteristics commercially exists. However, the two most prominent types of polymers are Biopolymers and synthetic polymers. Biopolymers such as Xanthan gum, is a product of fermentation of glucose, it is composed of rigid poly saccharide chainz. The fermentation process itself is done by microorganisms such as Xanthomonas campestris, the most efficient bacteria in producing

Xanthan gum. Pilot tests involving this type of polymers were successfully implemented in Gudong oilfield in China, in which a decrease in water cut was observed along with an increase of oil production (Gbadamosi et al., 2019). This type of polymer acts as a semi rigid rod that can have a higher resistance to mechanical degradation than other types of polymers (Sheng, 2016).

Synthetic polymers such as polyacrylamide PAM and partially hydrolyzed poly acrylamide HPAM are widely used in polymer flooding operations, higher viscosities can be achieved with the same polymer concentration when synthetic polymers are used instead of bio-polymers. HPAM are composed of water soluble straight polymer chains, that are convenient in polymer flooding operations due to their insensitivity to bacterial activities, their low cost and their good solubility. These polymers are the result of copolymerization of sodium acrylate with acrylamide. However, they have some disadvantages that limits their utility, they are very sensitive to temperature, salinity, shear forces, hardness, and the pH environment in which they are used. All these parameters need to be considered before the utilization of this type of polymers. If not considered properly the injected polymer solution could lose its mobility enhancement properties due to its degradation and decrease in viscosity (Gbadamosi et al., 2019).

Polyacrylamide has a high tendency of adsorbing to the surface of the rock, this in turn would translate to the use of a higher quantity of polymer solutions that might affect the feasibility of the project. To reduce the adsorption of this polymer, sodium or potassium hydroxide is used to hydrolyze the polyacrylamide.

For the EOR operation, the right type of polymer needs to be selected based on the different properties of the reservoir. Some of these properties were mentioned before, Temperature, pH environment, Salinity, Hardness, shear force, etc.... Synthetic polymer or hydrolyzed polyacrylamides are sensitive to all the properties mentioned before thus an adequate screening process needs to be carried out in the laboratory before any pilot test is conducted. The advantage of using this type of polymer is that it is resistant to any bacterial degradation. It should be added that KIPAM, a Salinity resistant polyacrylamide, is being produced in Beijing Hengju (Sheng, 2016).

Biopolymers or Xanthan gum on the other hand demonstrates lower viscosity levels and higher sensitivity to bacterial degradation when compared with HPAM. However, Xanthan gum is more resistant to high salinity, temperature, and shear force levels (Gbadamosi et al., 2019) (Sheng, 2016).

Fluid-Fluid interaction

IFT reduction mechanism

IFT reduction increases the capillary number, it occurs when the hydrophilic head and the hydrophobic tail of the surfactant reacts with the oil and water phase consecutively. It is considered as an important recovery mechanism when surfactants are being either injected in the reservoir from surface facilities or being produced in-situ within the reservoir by alkali saponification reaction (Gbadamosi et al., 2019).

IFT Measurement Techniques

The spinning drop method was proposed to measure the interfacial tension between two immiscible fluids by Bernard Vonnegut in 1942. The concept consists of having a small bubble suspended in another liquid in a small capillary tube. These two fluids are immiscible thus a certain interfacial tension exists between them. The small bubble once the capillary tube starts rotating, the centrifugal forces are applied to the system and are balanced out by the surface tension force. As the centrifugal forces increases the droplet shape changes to a more cylindrical one. This elongation would stop when equilibrium between the centrifugal and the surface tension forces is achieved.

A relation between the interfacial tension σ , the density difference $\Delta\rho$ between the two fluids, the angular velocity ω and the cylindrical radius R can be established once the gravitational forces are insignificant compared to the large centrifugal forces at high rotational speeds (Viades-Trejo and Gracia-Fadrique, 2007) (Vonnegut, 1942).

$$\sigma = \frac{\Delta\rho\omega^2 R^3}{4} \quad (6)$$

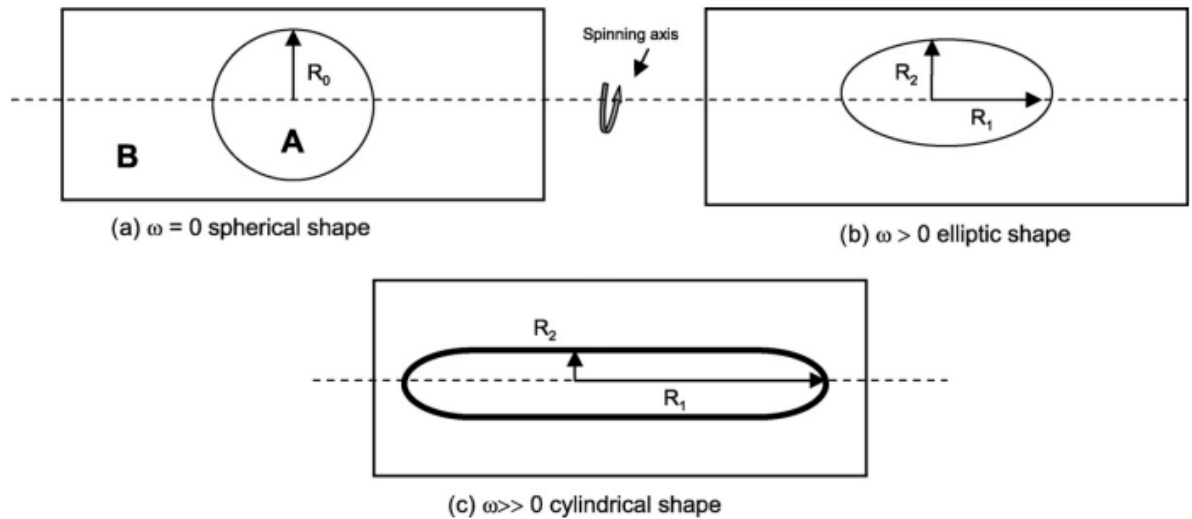


Figure 3: Spinning drop method (Viades-Trejo and Gracia-Fadrique, 2007)

Saponification Reaction

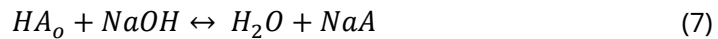
The literature has shown that minimal IFT values can be achieved with a narrow range of alkali concentrations. Additionally, it was shown that sodium-based alkali solutions are less reactive with the rock surface than sodium hydroxide. However, silicate precipitation can occur with these types of alkalis, which show a high degree of permeability reduction and plugging of the reservoir pore throats. On the other hand, when the precipitation issue is considered the use of sodium carbonates showed less permeability reduction. Furthermore, sodium carbonate precipitations can be removed from the production wells by acidizing operations, unlike silica containing precipitations. That is mainly the reason why sodium orthosilicate is not frequently used in EOR operations. Potassium based alkali solutions will not be discussed due to them being non feasible because of their high cost.

The saponification reactions are simply the generation of soap from the reaction of caustic alkali with the organic acid of the reservoir oil. The generated soap act as an in-situ surfactants that will in turn reduce the interfacial tension between the oleic and the aqueous phase (Gbadamosi et al., 2019).

The saponifiable components are petroleum acids, or naphthenic acids, the composition of these acids differs with the composition of the oil. The total acid number or TAN is a measure of how much the crude oil can generate surfactants, it is defined as the mass in milligram of

potassium hydroxide KOH required to neutralize one gram of crude oil. The literature has shown that potentiometric titration is a good method for determining the TAN. A high TAN number, larger than 0.5 mg of KOH/g, indicates an acidic oil (Behrang, Hosseini and Akhlaghi, 2021) (Fan and Buckley, 2006) (Sheng, 2016)..

When the caustic solution meets the organic acid the reaction shown in Eq(7) occurs. Where the generated soap acts as an in-situ anionic surfactant that in turn lowers the IFT. The extent of the overall reaction depends on the pH environment.



Where HA represents the acid species in the crude oil.

The overall all equation dependent on the distribution of acids between the oleic phase and the aqueous phase, demonstrated in Equ(8), where HA_o represents the acids present in the oil phase and HA_w represents the acids in the aqueous phase. The pH plays an important role in the partitioning of acid between both phases. In an acidic to neutral pH environment, the acid present in the oil phase is insoluble in the aqueous phase, it should be noted that keeping the acid from solubilizing into the aqueous phase is important during water flooding operations (Behrang, Hosseini and Akhlaghi, 2021). Eq(9) shows the hydrolysis of the acid in the aqueous phase releases the surfactants denoted by A^- (deZabala, Vislocky, Rubin and Radke, 1982).



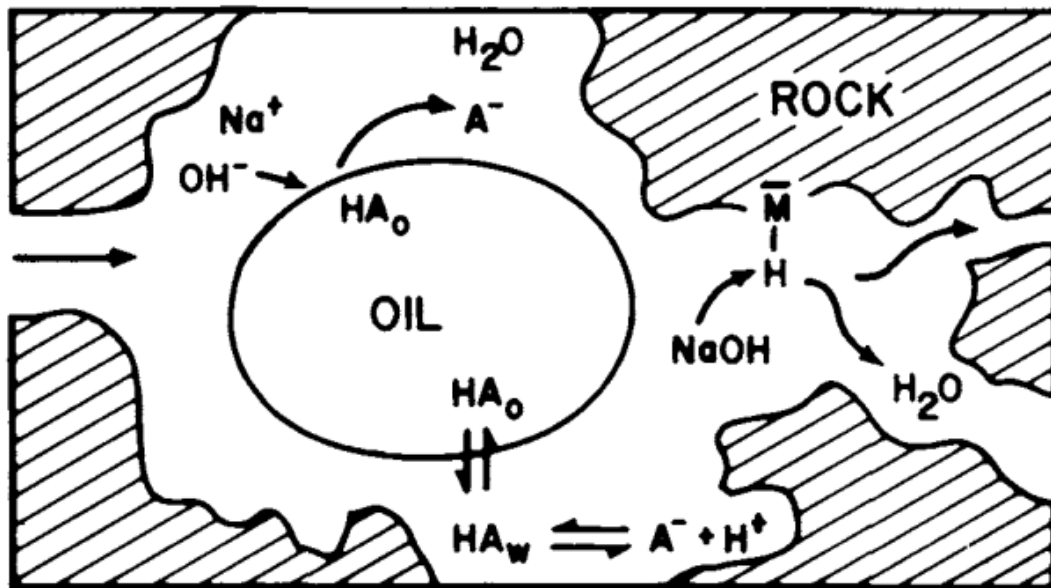


Figure 4: Alkali Recovery process (deZabala, Vislocky, Rubin and Radke, 1982).

Alkali scan & Salinity effect on pH and IFT reduction.

There is a small concentration window of alkali in which a reduction of IFT is noticed when the solution meets a specific crude oil. When the concentration of alkali is not in this window the interfacial tension values would not be as low, it should be noted that the pH environment (Alkali concentration) plays an important role in determining the extent of the saponification reaction. Hence an alkali scan is necessary.

An alkali scan is performed by preparing solutions with different alkali concentrations while keeping the salinity unchanged. The ionic strength (salinity) of a solution increase with the increase of alkali concentration, the higher the pH in a solution the stronger the ionic strength.

The effect of salinity and alkalinity in a solution is different, the literature shows that an increase in solution salinity would lead to a temporary decrease of the dynamic IFT compared to a permanent decrease of the IFT for solution with lower salinity levels (Sheng, 2016).

The literature shows that chloride salts such as $CaCl_2$, $MgCl_2$, KCl , and $NaCl$ can affect the IFT reduction. In previous studies when the pH environment was changed from an acidic state to a neutral or basic state a reduction in the interfacial tension was noticed due to the

saponification of organic acids. However, when the pH environment is high indicating a high concentration of caustic chemicals, increasing the ionic strength of the solution or in other words adding salts, had a negative effect by weakening the IFT reduction process. CaCl_2 presents an exceptional case, even in a low pH environment, the addition of calcium chloride decreased the IFT reduction mechanism. This could be explained by its molecular radius, which is big enough to form a stable complex that can keep the generated surfactants soluble in the bulk phase (Gong et al., 2016). It should be added that certain Alkali solutions are less sensitive to salinity than other solutions, Na_2CO_3 for example are less sensitive than NaOH (Sheng, 2016).

Divalent ions such as Ca^{2+} and Mg^{2+} are present in water. Precipitation occurs when the alkali solution meets water containing divalent ions, the interaction between the in situ generated surfactants and the multivalent ions renders them insoluble in water. This reaction is dependent on salinity, divalent ions concentration, and pH (Kumar, Yen, Chilingarian and Donaldson, 1989). The entrainment of the precipitates produced from this interaction could cause a significant reduction in the permeability of the reservoir leading to a decrease in oil production. It was shown that once NaOH and sodium orthosilicate is used in a divalent ion-rich environment, the produced precipitates are hydrated, flocculent and highly plugging. However, when sodium carbonate is used as an alkaline agent in a divalent ion-rich environment the precipitates are less plugging, smaller, less adherent to the surface, and do not aggregate to larger particles (Cheng, 1986). In specific cases, precipitation can play an important role by enhancing sweep efficiency. If properly located, the entrainment of the precipitates can block highly permeable flow paths, redirecting the flow towards non-swept areas of the reservoir (Kumar, Yen, Chilingarian and Donaldson, 1989).

Emulsions

Surfactants are absorbed on the interface of two immiscible fluids such as oil and water. They play an important role in reducing the interfacial tension and solubilizing the interfacial film. Once the film between two different fluids is solubilized, emulsification occurs (Gong et al., 2016). Fluid in fluid emulsion is defined as the dispersion of one immiscible fluid in another (Goodarzi and Zendehboudi, 2018).

A system in which two immiscible fluids exist is called a dispersion. There are many types of dispersion, but the three major types are foams, where a gas is dispersed in a liquid continuous phase, solids suspended in liquid, and finally dispersions in which one immiscible liquid is dispersed in another liquid. The third type of dispersion is the one that is considered in the case

where an emulsifying agent is added such as surfactants. The three types of fluid in fluid emulsions are oil in water emulsion, in which droplets of oil are suspended in water, Water in oil emulsions, where droplets of water are suspended in a continuous phase of oil, and finally, a more complex configurations of emulsions, such as oil in water in oil emulsion, where a droplet of oil is dispersed in a bigger droplet of water which in turn is dispersed in oil etc. It should be mentioned that oil in water emulsions is also called reverse emulsions.

Emulsions are further classified according to the size of the dispersed droplet in the continuous phase. Microemulsions are created due to the low interfacial tension between the two phases, and the size of the droplet is less than 10 nm. They are thermodynamically stable. While on the other hand, Macroemulsions have droplets size bigger than 1 μm ., and they are thermodynamically unstable due to the tendency of the two phases to coalesce in the aim of reducing the interfacial energies.

The physical properties of the emulsion phase differ from both the aqueous and the oleic phase. In terms of the emulsion phase equilibrium, Winsor classified microemulsion into 4 types. Winsor type I microemulsion is a oil in water emulsion, in which a small concentration of soluble surfactants exists in water in form of monomers. Winsor type II microemulsion is a water in oil emulsion in which the surfactants are preferentially soluble in the oil phase. Winsor type III is a three-phase system in which excess of water and oil coexist with a third phase in the middle, rich with surfactants. Winsor type IV is a micellar solution formed by the addition of surfactants with alcohol (Goodarzi and Zendehboudi, 2018). The breakdown of emulsions is

related to the involvement of various surface forces. Multiple breakdown processes can occur simultaneously or individually, they are illustrated in figure (7).

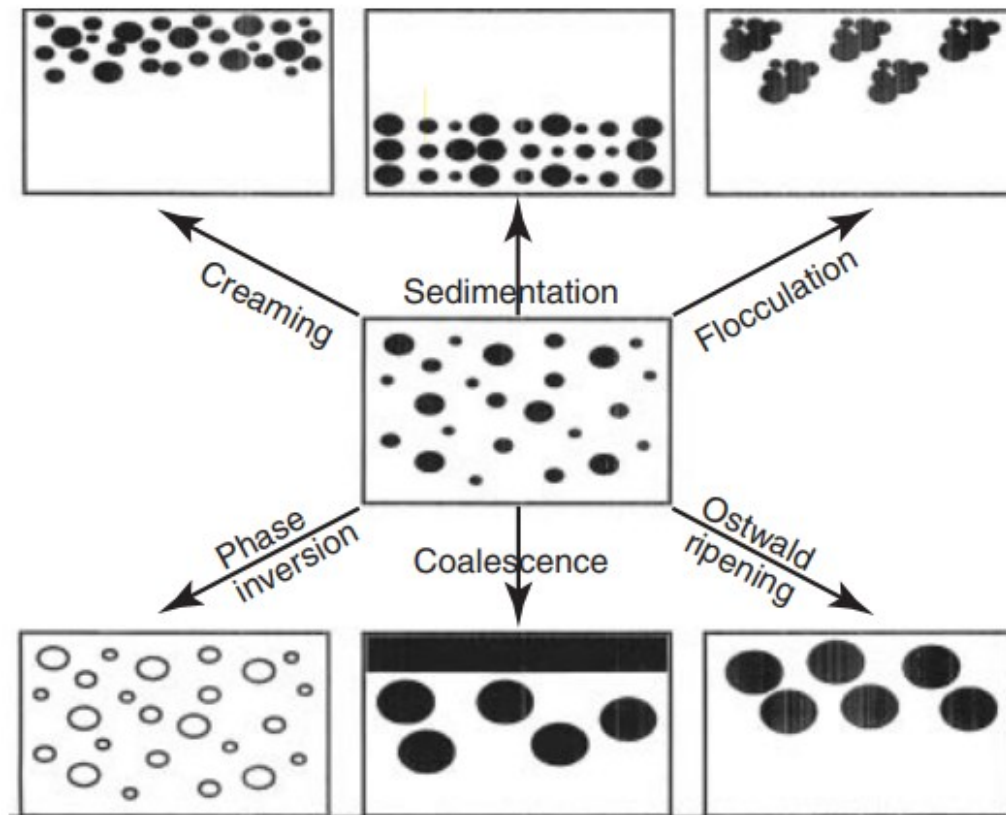


Figure 5: Different processes of de-emulsification (Tadros, 2013).

Gravitational and centrifugal forces play an important role in emulsion breakdown by exceeding the thermal motion of the individual dispersed droplets, when the density of the droplet is smaller than the density of the continuous phase the droplets migrate upward, this process is called creaming. However, when the density of the droplet is bigger than the density of the continuous phase, the droplets migrate downward, that process is called sedimentation. Ostwald Ripening or disproportionation on the other hand occurs due to the increased solubility values in smaller droplets, compared with larger droplets. With time the smaller droplets disappear and diffuse into the bigger droplets due to the curvature effect. Eventually the droplet size distribution shifts to larger values. The attraction of the droplets to each other can form aggregations without the diffusion of the smaller sized droplets into the bigger sized ones. This process is called flocculation and mainly occurs when the Van der Waals attractions are strong due to insufficient repulsion. Coalescence is the fusion of two or more bigger droplets

into one, resulting in the creation of a small film. The extreme case of coalescence is when there is a clear phase separation. And finally, phase inversion is a process in which there will be an exchange between the dispersed phase and the continuous (Tadros, 2013).

Emulsification entrainment & entrapment

Emulsification entrainment is when the stable oil in water emulsion phase formed is entrained and produced, the emulsion droplets have a small enough size to pass through the pore throats of the porous media.

Emulsification entrapment is when the formed emulsion phase is trapped in the porous media due to the large size of the emulsion droplets, typically larger than the average pore throat diameter in the porous media. It should be noted that this drive mechanism is based on the decrease of the aqueous phase relative permeability by plugging the high permeable channels in the porous media and redirecting the flow to other less permeable channels. This would increase sweep efficiency and reduce viscous instabilities such as viscous fingering (Kumar, Yen, Chilingarian and Donaldson, 1989).

Fluid Rock Interactions

Wettability Fundamentals

In a system composed of two or more immiscible fluids contacting a solid surface, the surface might show preference towards one of the immiscible fluids. This preference is demonstrated by the adherence of the chosen fluid onto the surface, it is defined as wettability of the surface. The water spreading across the surface of a tissue, in presence of air is a basic example of wettability in the day-to-day life. In that example it is safe to say that the surface is water wet, meaning that the surface prefers to stay in contact with the water phase.

In the case of reservoirs, the two immiscible fluids are generally water and oil. The wetting state of the reservoir affects the flow of a given fluid in the porous system. In a water wet reservoir as an example, the water would propagate easier within the porous media during water flooding operations. In that case, the water sticks to the surface of the reservoir rock, translating in lower mobility of water, thus oil is expelled easier from the reservoir pores.

To further understand wettability, the difference between cohesive and adhesive forces needs to be established. In short, cohesiveness is the attraction between two similar molecules, while

adhesiveness is the attraction between two different molecules. In the case of water spreading on the surface of the reservoir rock, cohesive forces are the forces trying to keep the water molecules together, while adhesive forces are the forces promoting the spread of water molecules across the surface of the rock. Thus, in a water wet situation, the adhesive forces are dominating the cohesive forces of the water molecules.

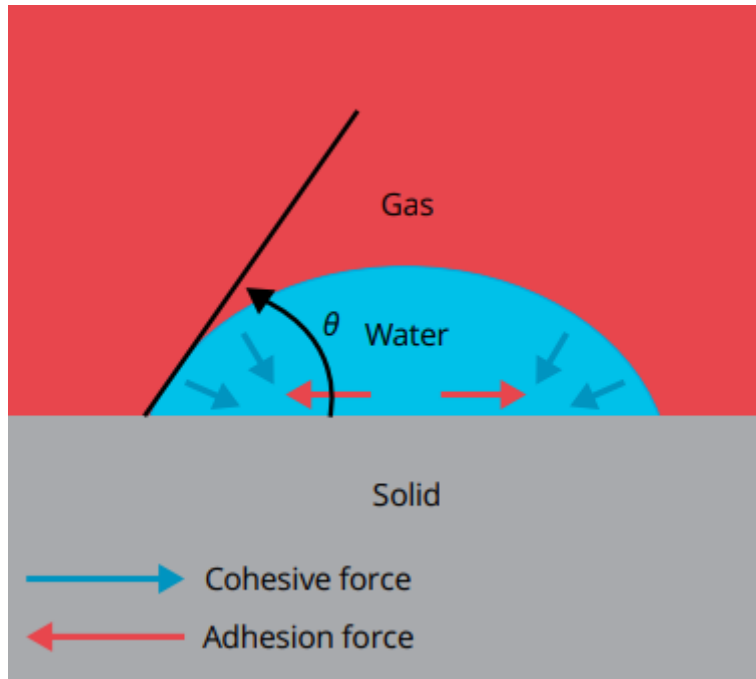


Figure 6: Schematic showing a droplet of water surrounded by gas on a solid surface (ALYAFEI, 2019).

The equilibrium of forces exercised at the point of contact between the two immiscible phases and the surface would provide a relation between the contact angle and adhesion tension, which is nothing other than the difference between the two solid-fluid surface tension. The relation is shown in Eq (10):

$$\cos \theta = \frac{\sigma_{sw} - \sigma_{so}}{\sigma_{wo}} = \frac{A_T}{\sigma_{wo}} \quad (10)$$

Where:

θ is the contact angle.

σ_{sw} the surface tension between the surface of the rock and water.

σ_{so} the surface tension between the surface of the rock and oil.

σ_{wo} the interfacial tension between oil and water.

A_T is the adhesion tension.

Multiple wetting cases exist, the water wet case as mentioned before is where water is adhering to the surface of the rock. In other words, it is when the contact angle is less than 90° and the water is spreading over inner and the outer surface of the porous media. The oil wet case is when oil is adhering over the surface of the rock, in this case the contact angle would be greater than 90° and the cohesive forces between the water molecules overcome the adhesive forces that are attracting the water molecules towards the surface of the rock. Thus, the water molecules will attract each other in the aim of minimizing the energy of the system by forming the shape of a sphere which has the smallest surface area.

The mixed wet case is the result of the rocks heterogeneity. The wettability depends on special location in the rock as in certain areas the rock prefers to stay in contact with water (water wet) and in other areas the rock prefers to stay in contact with oil (oil wet). Finally, in the neutral wet case or intermediate wet case the rock does not have a preference, meaning that it has equal tendency of being coated by either oil or water. In this case the contact angle is around 90° .

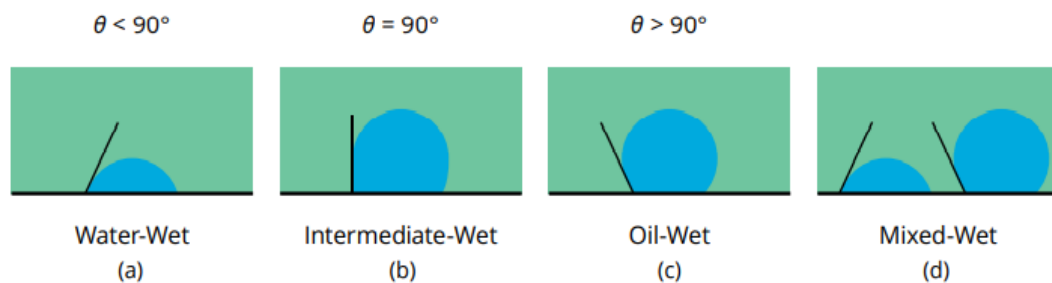


Figure 7: Schematic showing contact angle measurement on a solid surface for (a) water-wet, (b) intermediate-wet, (c) oil-wet, and (d) mixed-wet cases. (ALYAFEI, 2019).

Drainage, Imbibition & Wettability Measurement

The flow in porous media can be classified either as drainage or imbibition. Drainage of the reservoir rock is defined as the saturation decrease of the wetting phase, while imbibition is the saturation increase of the wetting phase in the rock. So for the example of a water wet rock, drainage is the decrease of water saturation in the porous media and imbibition is the increase

of the water saturation. In the situation where the oil is migrating towards the reservoir rock, the saturation of oil is gradually increasing, in other words, the saturation of water is decreasing, and this process is identified as primary drainage. Additionally for the same example, when the reservoir is flooding with water for a secondary recovery operation, the process would be imbibition due to the saturation increase of the wetting water phase.

The two different processes are represented with two different capillary pressure curves. During drainage, in the case of a water wet reservoir rock, the saturation of water decreases gradually with the increase of the capillary pressure, until the connate water saturation is reached, and remaining water remains immobile in the porous media. The drainage curve is shown in figure (10):

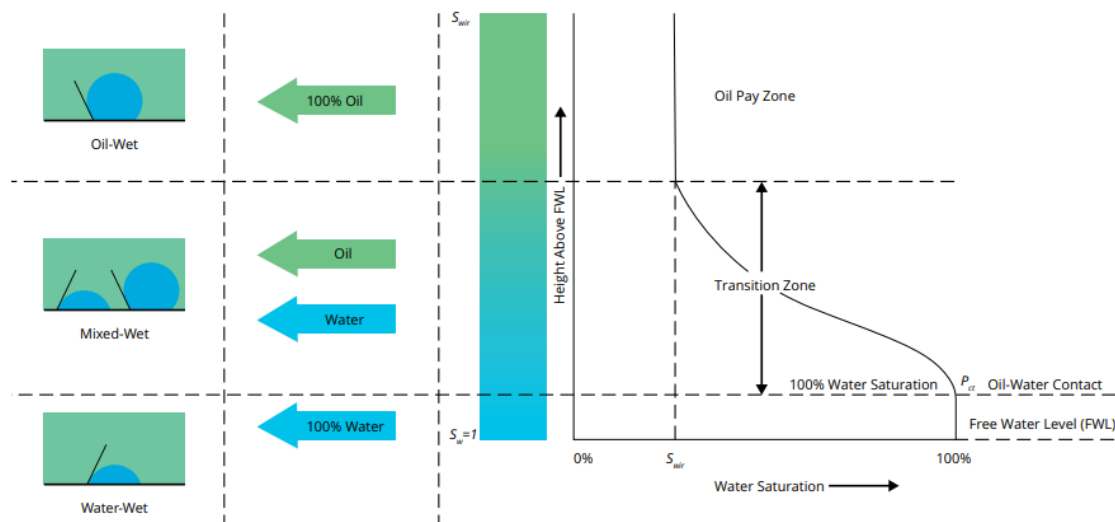


Figure 8: Schematic diagram of drainage capillary pressure with important labeling and wettability distribution in the reservoir. (ALYAFEI, 2019).

The transition zone is the zone in which the saturation of water is varying with the change of the capillary pressure. The height of this zone is influenced by the permeability of the reservoir rock. It usually starts at the oil-water contact (OWC) where the saturation of water still has a value of 1 before it starts to decrease, and the point at which irreducible water saturation has been reached. It should be added that the pressure at the OWC is also called the capillary threshold pressure. This threshold once exceeded in a water wet situation the saturation of the wetting phase would start decreasing.

During imbibition, the wetting phase is displacing the non wetting phase. There are two types of imbibition, forces imbibition, and spontaneous imbibition. Spontaneous imbibition of water occurs usually in a water wet or a mix wet case. The reason behind that is the positive value of

the capillary pressure, indicating a higher pressure in the oil phase. In a water wet reservoir rock, with an irreducible water saturation, water starts to imbibe in the narrowest pores possessing the highest capillary pressure values and then starts to invade the bigger pores with a lower capillary pressure value. All of this imbibition is spontaneous and occurs the moment the rock comes in contact with the water phase. During spontaneous imbibition, the increase of water saturation is to a certain point above which a negative capillary pressure is needed. A negative capillary pressure is achieved by undergoing water flooding operations in which the wetting phase pressure greater than the non wetting one. The increase of water saturation occurs to the point where oil becomes immobile due to capillary trapping mechanism, this is translated by the residual oil saturation. It should be noted that saturation hysteresis should be considered in the forced imbibition case.

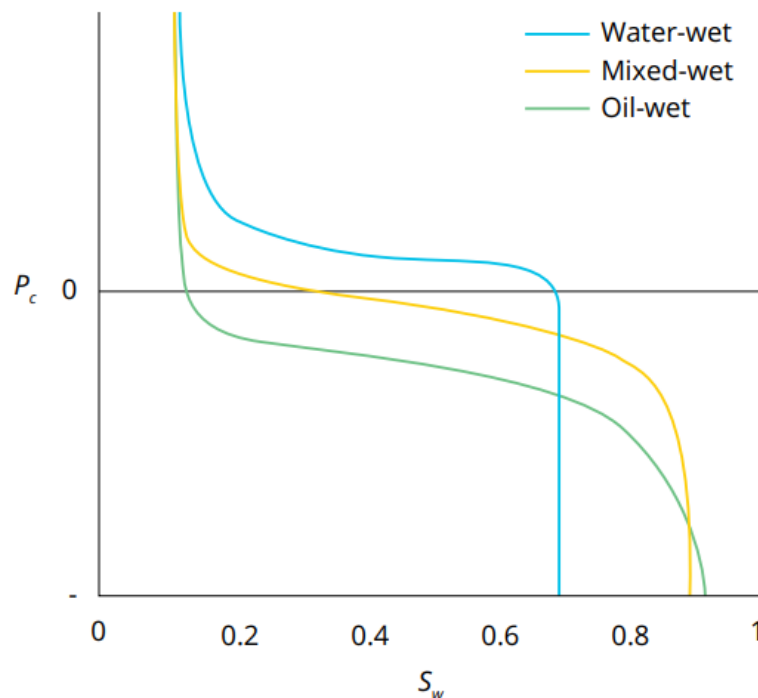


Figure 9: Schematic showing the effect of wettability on water re-saturation capillary pressure curves. (ALYAFEI, 2019).

The Amott imbibition test helps indicating the wettability of the reservoir since spontaneous imbibition is closely related to the wettability of the reservoir rock.

Since spontaneous imbibition and wettability are closely related, the Amott test would be a good method for quantifying the wettability of a reservoir rock. The test could be set up in two different ways, either to measure the Amott water index or to measure the Amott oil index. A reservoir core that is saturated with oil and submerged in water or other oil-displacing solution

would give a quantitative measurement of the amount of oil produced by spontaneous imbibition, so it could be further compared with the amount of oil produced from forced water injection, ultimately giving the Amott water index I_w . On the other hand, the experiment could be set in a way to measure the amount of water produced by spontaneous imbibition of oil and further compared by water produced by forced injection of oil to yield the Amott oil index I_o . This set-up consists of using a reservoir core fully saturated with water and submerged in an oil-filled Amott cell. The two setups are shown in figure (12):

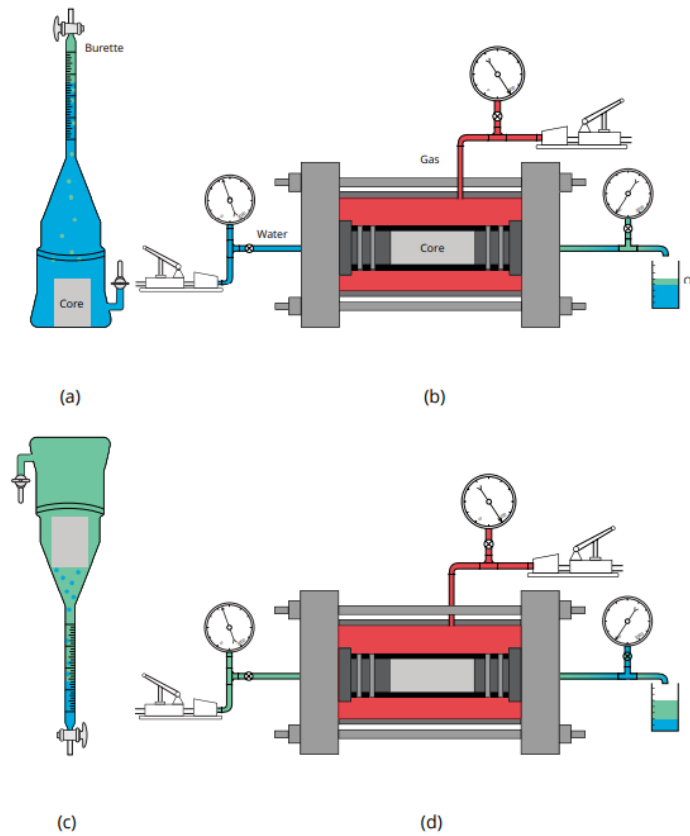


Figure 10: Schematic of the Amott experimental test (ALYAFEI, 2019).

The Amott water index and Amott oil index are shown in Eq (11) and Eq (12):

$$I_w = \frac{S_w(B) - S_w(A)}{S_w(C) - S_w(A)} \quad (11)$$

$$I_o = \frac{S_o(D) - S_o(C)}{S_o(E) - S_o(C)} \quad (12)$$

With:

I_o is the Amott oil index.

I_w is the Amott water index.

$S_w(B)$ is the water saturation after spontaneous imbibition.

$S_w(A)$ is the initial water saturation in the reservoir core before any spontaneous imbibition.

$S_w(C)$ is the water saturation after forced water injection.

$S_o(C)$ is the oil saturation after forced water injection.

$S_o(D)$ oil saturation after spontaneous oil imbibition.

$S_o(E)$ oil saturation after forced oil injection.

The Amott index (I_A) is then calculated by subtracting the Amott oil index from the Amott water index.

$$I_A = I_w - I_o \quad (13)$$

The value of the Amott index would then determine the wettability of the reservoir rock. the literature has shown that a water-wet reservoir rock has an Amott index of 0.3 to 1, a mixed-wet reservoir rock has an Amott index of -0.3 to 0.3 and finally, an oil-wet reservoir rock has an Amott index of -1 to -0.3 (ALYAFEI, 2019).

The USBM method is another way to determine the wettability of the reservoir core by calculating the work needed to displace one fluid with another for the first imbibition and secondary drainage case. It should be noted that the work done is the area under the curve.

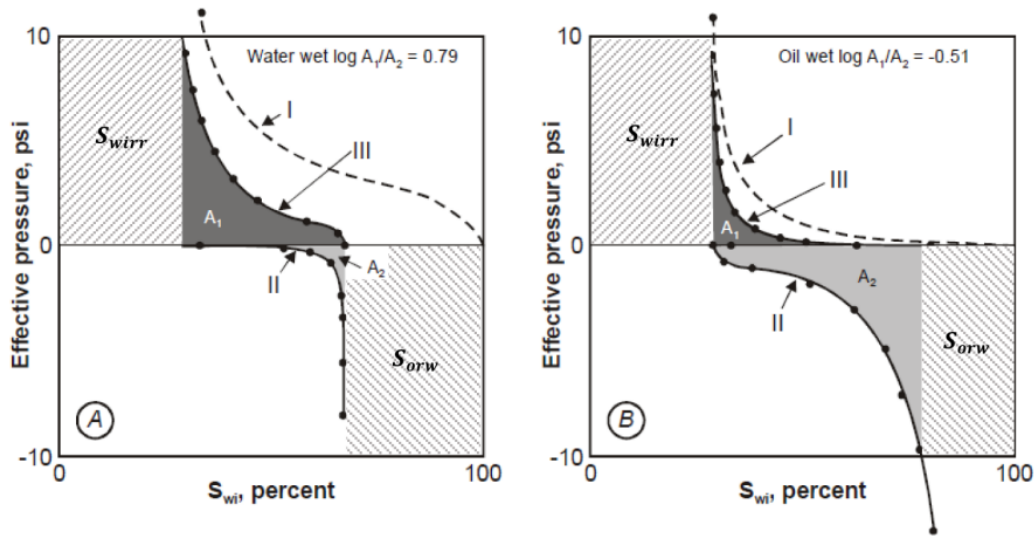


Figure 11: —USBM wettability measurement on (left) water-wet and (right) oil-wet samples (Costa Gomes, Geiger and P. Arnold, 2019)

$$WI = \log \frac{A_1}{A_2} \quad (14)$$

The logarithm of the area ratio is used as a wettability indicator. A negative wettability index indicates a oil wet reservoir rock, a positive wettability index indicated a water wet rock, and finally a wettability index of zero would indicates a neutral wet rock (Costa Gomes, Geiger and P. Arnold, 2019) (Donaldson, Thomas and Lorenz, 1969).

Low IFT Spontaneous imbibition

In a spontaneous imbibition process the dominating forces are the capillary forces. Besides the capillary forces other forces also contribute to the over system, such as viscous forces and gravity forces. The relationship between the capillary and gravity forces is described by the inverse Bond number.

$$N_B^{-1} = C \frac{\sigma \sqrt{\frac{\phi}{k}}}{\Delta \rho g H} \quad (15)$$

Where:

$C = 0.4$ for a capillary tube model.

H is the core height [meter].

σ is the interfacial tension [mN m^{-1}].

ϕ is the porosity [%].

k is the absolute permeability [mD].

$\Delta\rho$ is the density difference between the phases [kg/m^3].

The inverse bond number can be manipulated by increasing the core height or changing the IFT of the interface between the fluids in contact. The lower the IFT the smaller the inverse bond number and the weaker the capillary forces are, such is the case in the application of alkali-polymer or alkali solutions. In this case the resistance to flow is weaker and the production of oil happens mainly on the upper and lower faces of the core plugs in an Amott cell Spontaneous imbibition experiment, that is why this case is denoted as co-current spontaneous imbibition. The Stronger the interfacial tension, such as in the case of synthetic brine application, the higher the inverse bond number and the stronger the capillary forces are. In this case the production of oil occurs on all faces of the core plugs thus the name counter-current (Schechter et al., 1994).

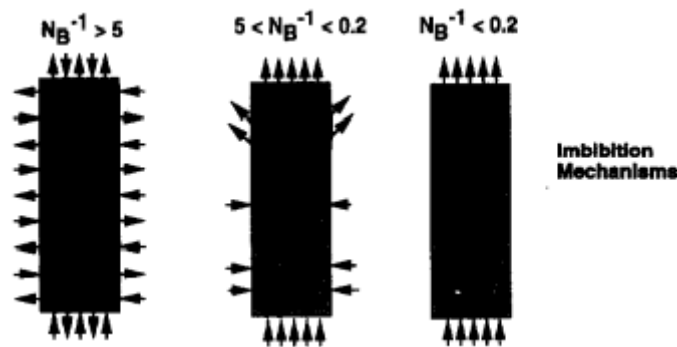


Figure 12: Effect of inverse bond number on capillary and gravity forces (Schechter et al., 1994).

Ion Exchange

To have a better understanding of fluid rock interaction, ion exchange process needs to be defined. Sorption of a certain chemical on a surface such as the surface of a porous media happens in 3 main forms. The first form of sorption is adsorption, which is defined as the

adherence of a chemical onto the surface of a solid. The second one is adsorption, which occurs when the chemical is taken up by the surface of the rock. Finally, the third most important form of sorption in chemical EOR is ion exchange. Ion exchange is defined as the replacement of one chemical already present at a surface with another chemical.

The ion exchange process in EOR operations is referred to as cation exchange. Initially all the fluids within the reservoir are at equilibrium with the reservoir rock. However, when a fluid with a different composition is injected into the porous media of the reservoir, a new equilibrium is established, and some ions would displace other ions. The injected ions would sorb on the surface and the displaced ions would be transported by the flow.

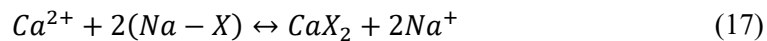
Based on the general law of mass action, the ion exchange equation is applicable to any type of reaction, such as the dissolution of minerals, the formation of complexes between dissolved chemicals and the dissolution of gases in water. The general ion exchange equation is shown in Eq (15):



The cation exchange is defined as the reaction between two ions at the solid surface, and the magnitude of the equilibrium constant of the reaction shown in Eq (16) describes the affinity of one ion to replace the other at the surface. The distribution of the components between the left and right side of the chemical reaction is given by the equilibrium constant.

$$K = \frac{[C]^c [D]^d}{[A]^a [B]^b} \quad (16)$$

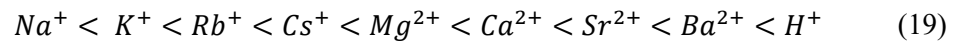
As an example, the reaction between sodium and calcium ions is shown below:



The equilibrium constant K in this case would be:

$$K_{Ca-Na} = \frac{[Ca - X_2][Na^+]^2}{[Na - X]^2 [Ca^{2+}]} \quad (18)$$

With X representing the clay surface. The higher the equilibrium constant for this case the higher the tendency of calcium ions to attach to the surface of clay compared to sodium ions. The following ions are ordered according to their order of affinity for the clay site:

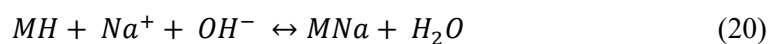


The cation exchange capacity is the capacity of ion exchange for a given rock. It is affected by temperature and the pH environment, the ion exchange process is enhanced in a high pH environment (Sheng, 2016).

Alkali-rock interaction

In Alkaline flooding or Alkaline-polymer flooding, there is an abundance of hydroxide ions in contact with the reservoir rock. The ion exchange mechanism dictates to a certain extent Alkaline-rock reaction. Typically, the higher the alkali concentration, the higher the pH value. As mentioned before the ion exchange process is enhanced in a basic environment with high pH values. In other words, the higher the pH the more the chosen alkali solution would react with the reservoir rock. It was shown that the extent of the ion exchange process can be increased by a factor of 2 to 3 when increasing the pH from a value of 11 to 13 (Cheng, 1986).

One important Alkali-rock reaction is the reversible sodium-hydrogen-base exchange in which the caustic chemical is consumed by the reservoir rock. In this reaction each hydrogen molecule is exchanged with both a sodium and hydroxide radical. It is reversible, meaning that the consumption of the alkali chemical by the rock is not permanent and could be reversed. The reaction is shown in Eq (20):



Where M denotes the mineral-hydroxide exchange site. The literature has shown that in previous experiments in which alkali solution is injected into sandstone cores, the higher the pH environment the longer it would take for the injected caustic solution to be detected in the effluent (deZabala, Vislocky, Rubin and Radke, 1982). The use of sodium carbonate as a caustic solution in EOR operations is more favorable to reduce alkali rock consumption and retention. It would take higher concentration of sodium carbonate to reach a specific pH value compared with sodium hydroxide with which it would take a lower concentration to reach the same pH value. Sodium hydroxide has a higher alkalinity and produce a higher pH value, Thus the use of Sodium carbonate would be more beneficial (Chenewog, 1986).

It should be noted that the electrostatic repulsion of the negatively charged minerals in a high pH environment causes a significant reduction in the adsorption of surfactants A- on the surface of the rock in this circumstance (deZabala, Vislocky, Rubin and Radke, 1982).

Wettability Reversal & Alteration

The use of Chemicals in EOR operations can lead to wettability alteration of the reservoir rock. Wettability alteration is an important mechanism in increasing oil production, the alteration can decrease the capillary forces and increase the relative permeability of oil. This mechanism was achieved by the use of surfactants and alkali solutions in both conventional and non-conventional reservoirs.

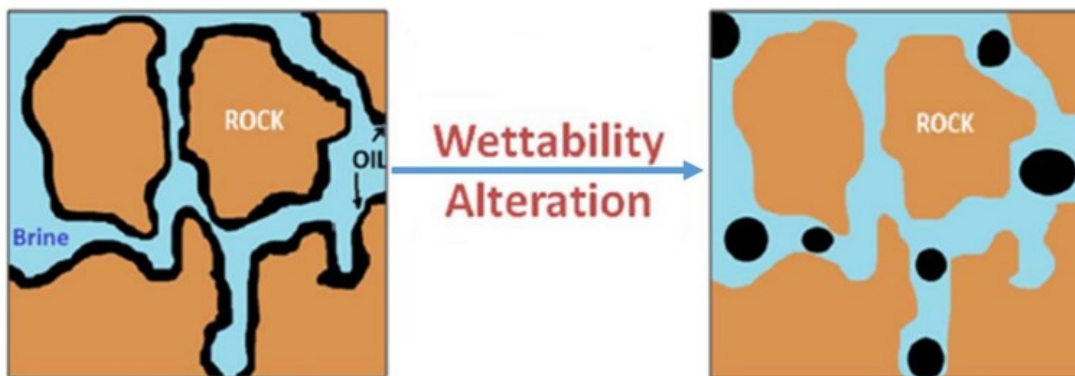


Figure 13:Wettability alteration process (Gbadamosi et al., 2019)

When it comes to surfactants and their use in chemical flooding, the type of reservoir they are being injected in is of great importance. For carbonate reservoirs, mainly cationic surfactants are used. Carbonate reservoirs possess generally a positively charged surface, on which negatively charged anionic components of oil such as carboxylate groups are attached. When the cationic surfactants are introduced to the reservoir, the formation of a strong ionic pair occurs between the positively charged head of the surfactant and the carboxylate components of the adsorbed oil. This interaction would promote water wetness and the desorption of oil off the mineral surface. In the case where anionic surfactants are added instead of cationic surfactants, a weaker interaction between the surfactant tail and the carboxylate group in oil occurs leading to minor wettability alterations with which neutral wetting conditions might be achieved.

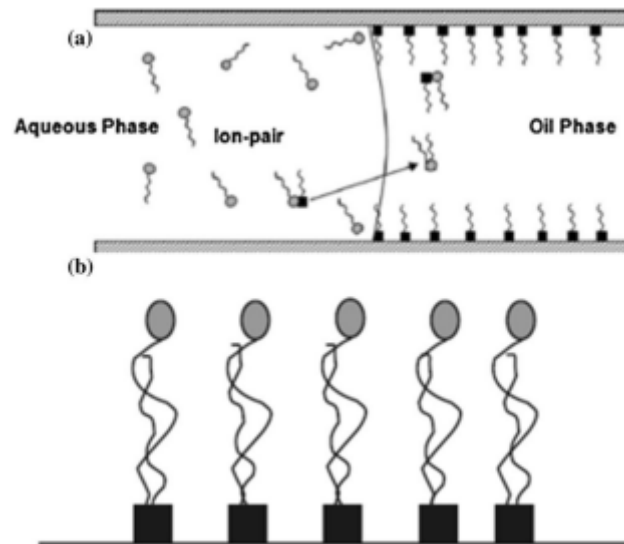


Figure 14: Wettability alteration by a cationic surfactant, b anionic surfactant (Gbadamosi et al., 2019)

Due to the presence of clay minerals, it is typically believed that the surface of sandstone reservoirs has a negative charge. The same mechanism, in which the positively charged surfactant head attracts the negatively charged carboxylic groups to increase water wetness, is also seen in sandstone reservoirs. The wettability alteration capacity is decreased when anionic surfactants are used. The weak hydrophobic interaction between the anionic surfactant's tail and oil is primarily to blame for this. According to Hou, Wang, and Huang (2015), the electrostatic attraction between the negatively charged surface and the negatively charged surfactant head groups is the cause of this weak interaction (Gbadamosi et al., 2019).

The use of alkaline agents, such as sodium or potassium carbonate also affects the wettability of the reservoir rock, promoting a wettability reversal mechanism with which more oil is released from the surface of the rock, increasing the overall oil production. The promotion of oil wetness in sandstone reservoirs as a result of alkali solutions was mentioned in the literature. Some studies showed that a change in contact angle from 24 degrees to 160 degrees indicated a change in wettability from a water-wet condition to an oil-wet condition. In turn, this would encourage the oil to adhere to the rock's surface and obstruct the water channels, lowering the water relative permeability and raising the relative permeability of the oil.

The mechanism, in which the wettability of the rock is brought back from water wet to oil wet is known as wettability reversal, and is sensitive to temperature, salinity conditions and the pH environment. The Anionic surfactants generated by the saponification reaction between the alkali solution and oil possess a negative charged hydrophilic group which is attached to the surface of the rock via electrostatic or hydrogen bonds. Furthermore, the heavy oil phase is

attracted and attached to the hydrophilic part of the anionic surfactant via Van Der Waals interactions, thus promoting a wettability alteration of the system towards a more oil wet state.

Alkali - Polymer flooding

Polymers are used in Chemical enhanced oil recovery operations. The main purpose of using polymers is the effect that they have on altering the injected fluid viscosity, in a way to minimize the bypassed oil-containing areas in the reservoir. As discussed before this is mainly done by stabilizing the displacing front and reducing viscous instabilities. The use of polymers can decrease the relative permeability of water (Sheng, 2016).

Due to high Alkali consumption in the reservoir rock either by retention on the rock surface by ion exchange or precipitation or mineral dissolution, made Alkali only flooding a non-desirable and non-feasible operation. Alkali polymer operations on the other hand provide an additional mobility control and a lower chemical consumption in the reservoir rock. The literature showed three methods of applying Alkali flooding, the first is the application of an alkaline flood followed by a polymer flood (A/P), the second one is the application of a polymer flood followed by an alkaline flood (P/A), and the third and the most efficient one is the injection of alkali and polymer simultaneously (Katsanis, Krumrine and Falcone, 1983).

Visco-elastic Effect

The viscoelastic behavior of the polymer is taken into consideration in polymer flooding or Alkali-Polymer flooding. The term "non-Newtonian fluid" refers to a fluid whose viscosity varies depending on the shear rate. On the other hand, the viscosity of a Newtonian fluid is constant. It should be noted that the polymer can exhibit Newtonian behavior at low shear rates. Two behaviors are to be highlighted, the first one is When the average time it takes for polymer molecules to move from one pore to the next is longer than the relaxation time, during which the polymer assumes a random coil configuration, shear thinning occurs in a porous medium.

The second crucial behavior is the thickening of shear bands. With an increase in shear rate, the fluid stretches and lengthens during shear thickening. fluid movement in a porous medium

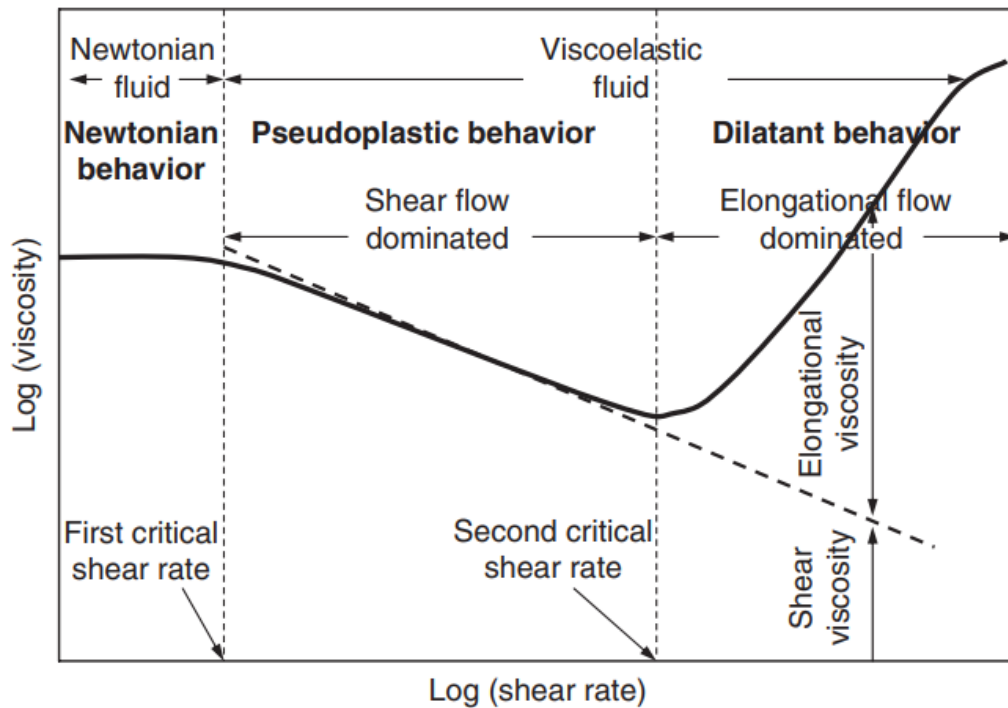


Figure 15: Visco-elastic fluid flow behavior (Sheng, 2016).

Three different regimes can be established with the increase of shear rate. A Newtonian regime in which the polymer solution does not change viscosity with the increase of the shear rate. A Shear thinning regime or a pseudoplastic regime in which the polymer molecules are untangled and the apparent viscosity of the solution decreases with the increase of shear rate. A shear thickening regime in which the polymer chains are elongated and stretched causing the increase of apparent viscosity with the increase of shear rate (Sheng, 2016).

Hydrolysis and Polymer Viscosity

When Alkali and Polymers are injected simultaneously in the reservoir, the two chemicals come in contact with and affect each other significantly. Synthetic polymers such as Polyacrylamide PAM when in contact with a base or an alkali agent are partially hydrolyzed. The hydrolysis is defined as the conversion of some of the amid groups CONH_2 present in the polymer chain to carboxyl groups denoted as COO^- . The fraction of the amid groups that have been converted to carboxyl groups is defined as the degree of hydrolysis, the higher the degree of hydrolysis the less stable the polymer solution is. However, the literature has shown that the higher the higher the degree of hydrolysis the less the polymers adsorb to the surface of the rock. In other words, the application of Alkali-Polymer flooding can be advantageous due to the presence of Alkali chemicals such as sodium or potassium carbonate that would lead to the hydrolysis of the

polymer solution. Stability of the solution needs to be considered. Even unhydrolyzed PAM could have a low percentage of 2 to 4 % of hydrolyzed groups.

The negative charge of the carboxyl groups introduced to the polymer chain affects the rheology of the Alkali polymer solution. At low salinity, the carboxyl groups, possessing the same charge, repel each other. This repulsion leads to the stretching of the polymer chain and consequently to the increase of the solution viscosity. However, the literature showed that above a certain threshold of hydrolysis (40 %), the flexible polymer chain would be subjected to a significant amount of compressive forces that would lead to flocculation and the distortion of the chain, consequently decreasing the solution viscosity.

Salinity is one of the factors playing an important role in controlling the solution viscosity. At high salinity levels, the abundance in electrolytes in the solution would shield the polymer chain, reducing its stretching capacity along with the solution viscosity. The hardness and the divalent effect on the solution is more complex. In a case in which the degree of hydrolysis is high, the presence of divalent ions such as calcium or magnesium would sharply reduce the viscosity, precipitation might occur.

The pH of the solution is another factor affecting the viscosity. The higher the Alkali concentration is the higher the pH. The addition of alkali salts to the solution has an effect like the salinity effect. The addition of alkali increases the electrolytes in the solution, shielding the polymer chain and decreasing the overall solution viscosity.

Additionally, it should be added that the increase in temperature at low shear rates decreases the viscosity of the solution (Sheng, 2016).

Polymer Stability

Polymer degradation is defined as any process that breaks down the polymer chain into smaller molecules. Degradation of the polymer chain can take many forms, chemical degradation, biological degradation and finally mechanical degradation.

Oxidation and reduction occur when oxygen molecules are present in the system. Once exposed to oxygen the polymer chain is subject to oxidative degradation. Literature has shown that oxidative degradation is proportional to the concentration of oxygen in the system. At low temperatures the effect can be insignificant, however, at high temperatures, the degradation is highly sensitive to the presence of oxygen. Thus, both the temperature and oxygen concentration control oxygen degradation.

The effect of ionic ions is another way of polymer chain degradation. When Fe^{3+} is present with a significant concentration in a system containing HPAM, degradation occurs and the viscosity of the solution decreases. The Fe^{3+} ions cross-link with HPAM to form an insoluble gel. It should be noted that in an open system Fe^{2+} is oxidized to Fe^{3+} . Literature showed that sodium carbonate and bicarbonate can play a role in stabilizing the polymer due to their effect on stability.

Hydrolysis as discussed in the previous section has a direct effect on polymer stability. From a thermal point of view, PAM is stable to temperature up to 120 °C. However, at high temperatures hydrolysis is promoted and the amid groups are replaced with carboxyl groups. In high-temperature reservoirs, the use of polymer with low initial hydrolysis is desired to improve the polymer injectivity.

Additionally, the hardness of the solution controls polymer stability. For HPAM, the negatively charged carboxyl groups strongly interact with the divalent ions in the solution promoting viscosity reduction, formation of gels and precipitation. The precipitation caused by this interaction can lead to the plugging of reservoir pore throats. The divalent ions such as Ca^{2+} crosslinks the acrylic group in HPAM resulting in the coagulation of the molecules, the higher the hydrolysis the lower the divalent concentration needed to have this coagulation (Sheng, 2016).

Polymer Retention and Acceleration

Polymer retention in the reservoir rock is an important factor as it can determine the feasibility of the Alkali-polymer operation. Three main retention mechanisms are highlighted in this section, polymer adsorption to the surface of the rock, mechanical entrapment of polymer molecules, and finally hydrodynamic retention (Gbadamosi et al., 2019) (Agi, Junin, Gbonhinbor and Onyekonwu, 2018).

Polymer adsorption is due to the interaction between the polymer molecules and the reservoir rock. In this type of retention, the polymer molecules are retained on the surface with the help of electrostatic forces, hydrogen bonds and Van der Waals interactions. The larger the contact area between the solution and the rock the higher the retention is (Agi, Junin, Gbonhinbor and Onyekonwu, 2018). In the case of Alkali polymer flooding both alkali and polymers are competing to be adsorbed on the surface of the rock, which consequently would reduce the overall consumption of polymer molecules compared to a polymer-only flood (Sheng, 2016).

Mechanical entrapment, in simple terms is the entrapment of molecule in narrow flow channels. This mainly happens when the polymer molecules are larger than the pore throats. Eventually

mechanical entrapment would lead to a higher concentration of molecules at the inlet of the flow and a polymer concentration lower than the desired one the further the flow propagates in the porous media. Mechanical entrapment of polymer could promote polymer acceleration, in which the flow is redirected away from the pores that are blocked by polymer molecules, usually referred to as inaccessible pore volume (IPV), towards areas with higher permeability. This is usually undesired since it decreases the sweep efficiency and leads to an early breakthrough of the injected solution.

Hydrodynamic retention is not well understood or defined; it is important on a laboratory experiment scale but not so important on a bigger scale. It was observed that a higher retention is recorded when the flow rate is adjusted. Reducing the polymer molecule size by pre-filtering or pre-shearing is a way to reduce the effect of the three retention mechanisms. Another way of avoided polymer retention is by simply applying polymer in reservoirs with higher permeability (Agi, Junin, Gbonhinbor and Onyekon).

Experimental Setup and Methods

In this section all the information relevant to the setup of the experiments and the utilized materials are listed and discussed.

Fluid Characterization

Characterization of the fluids to be used and studies in the various fluid-fluid and rock-fluid experiments are essential to have a comprehensive understanding of the different fluid-fluid and rock-fluid behaviours. The properties of interest are density, viscosity, pH, and interfacial tension.

Two different types of brine and oil were used for the experiments to be discussed in this, section. The first brine denoted as hardened brine was mixed and prepared with the presence of divalent ions. The second brine type denoted as softened brine did not contain any divalent ions, however, it is characterized by the addition of a buffer NaHCO_3 . The brine compositions are shown in table (1).

Table 1: Synthetic brine compositions.

	Formation Brine 8 TH	Formation Brine 9 TH	Softened Brine 8/9 TH
	[g/l]	[g/l]	[g/l]
NaCl	22.47	26.15	22.62
KCl	0.16	0.16	0.16
NaHCO_3	-		1.52
$\text{MgCl}_2 \cdot 6\text{H}_2\text{O}$	0.63	0.42	-
$\text{CaCl}_2 \cdot 6\text{H}_2\text{O}$	0.94	0.29	-

Two oils with two distinct compositions were investigated for the application of the AP project. The first oil sample denoted as 8 TH oil is produced from the 8 Torton reservoir. The second oil sample denoted as 9 TH oil is produced from the 9 Torton reservoir. Both reservoirs are in the Matzen field northeast of Vienna.

Two Alkali agents were considered for the experimental studies of the Alkali-Polymer project. sodium carbonate and potassium carbonate. However, it should be noted that sodium carbonate

was of greater interest in the investigations due to it being more feasible than potassium carbonate.

Alkali screening and pH measurements

The procedure follows the simple concept of measuring the electrical potential of a given solution. The solutions possessing higher positively charged hydrogen ions has a higher potential of producing an electrical current and thus this device operates like voltmeter. The measured potential is compared to a reference solution with a known pH value and the potential difference is calculated to deduce a difference in pH (Woodford, 2022).

The pH was measured using a pH meter. A range of alkali solutions with different concentrations were prepared and mixed with softened brine. A small sample of each alkali concentration was collected in small vials in which the pH meter was used. The pH was recorded at room temperature.

Additionally, an alkali screening test was performed, in which the prepared samples, with different alkali solutions and concentrations were preserved in sealed vials for 7 days at room temperature. This experiment would give a good indication on the alkali brine interaction by monitoring the samples for the occurrence of any precipitations.

Density Measurements

At a reservoir temperature of 51 °C, the density of fluids was measured using the Anton Parr Density meter apparatus shown in figure (17). The system utilizes the oscillating U-tube principle, with a digital record of the oscillation frequency. The sample-containing chamber has a certain capacity for oscillation; the mass of the sample determines the frequency of oscillation of this chamber.

The accuracy of the gadget is well known. To further reduce any errors caused by humans, each specific sample was measured three times. To regulate the reliability of the data, the average of

the repeated trials and the standard deviation were computed.



Figure 16: Anton Parr density meter (Meter, 2022)

Steady-State Shear Viscosity Measurement

Since Alkali-Polymer solutions were investigated, the rheological properties of the solutions were needed. An Anton Parr rheometer MCR-302 was used to measure the viscosity of different alkali-polymer concentrations at a temperature of 49 °C. The viscosity readings were collected at different shear rates, ranging from 1 s⁻¹ to 1000 s⁻¹.

To minimize error and increase the accuracy and reliability of the data, three measurements were conducted for each sample, from which the average and the standard deviation were calculated.



Figure 17: Anton Parr rheometer (MCR 102e/302e/502e, 2022)

Core Preparation and Analysis

For the rock-fluid interaction experiments, homogenous Berea sandstone outcrops were used. A total of 36 cores were subjected to a series of processes that aim to clean the cores from unwanted substances that might have been in contact with the cores during storage.

The Soxhlet extraction method was adopted in core preparation procedure for the Berea plugs. The core plugs were placed in a vacuum oven for 48 hours to reach a dry condition. A list of the number of laboratory equipment that was used to properly perform the extraction method is mentioned below:

- 1) Round bottom flask for solvent
- 2) Anti-bumping granules
- 3) Soxhlet apparatus containing the core samples
- 4) Distillation path
- 5) Siphon
- 6) O-ring

- 7) Lid
- 8) Condenser
- 9) Coolant inlet
- 10) Coolant outlet

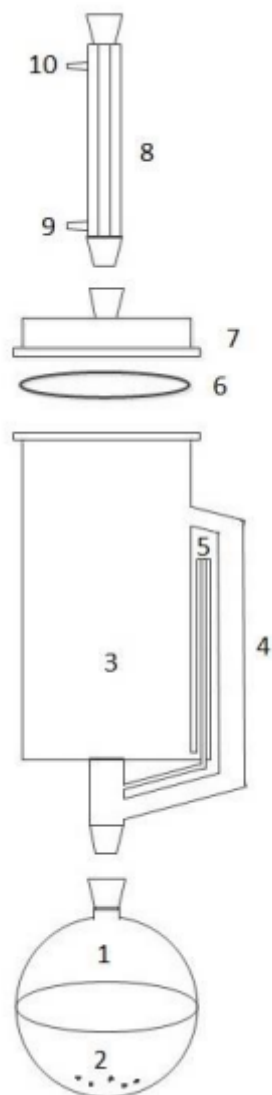


Figure 18: Soxhlet apparatus

A combination of polar/nonpolar solvents was used, toluene as a non-polar aromatic solvent that aims to dissolve the light hydrocarbons chains and evaporate water at high temperatures, and methanol as a polar solvent that helps with the dissolution of the heavier hydrocarbon chains remaining in the core plug.

The previously mentioned equipment was set up in a way that allowed the solvents to continuously flood the core plugs in a cyclic manner. With each cycle the solvents extracted a small concentration of unwanted components, and the core plugs were left in a cleaner state.

The scheme shown in figure (19) was implemented to carry out the experiment in the lab, Some bumping stones were placed in the bottom flask to help trigger the evaporation process of the solvents. The mounted equipment was properly supported by chain clamps and sealed with grease at glass joints to provide a closed environment and prevent the escape of vapor solvent.

At the end of the mounting process, the cores were situated in the Soxhlet apparatus, and the lower flask was filled with the chosen solvent.

Furthermore, the solvent concentration was chosen on the basis to form an azeotrope, a mixture that has the same proportion of solvents in the vapor phase and in the liquid phase. An azeotrope is convenient for the cleaning procedure for the main reason that it is formed of both polar and non-polar solvents, besides the point that it possesses a lower boiling temperature than the one possessed by each solvent.

At the end of the cleaning procedure, the AgNO_3 test was performed using the clear solvent mixture in the Soxhlet apparatus containing the cores. Two criteria were adopted as an indication of the end of the cleaning procedure, the first indicator was the exhibition of a clear solution in the Soxhlet apparatus and the absence of any leaching or discoloring material in the solution, the other indicator was a negative AgNO_3 test that was performed on the clear solvent sample taken from the apparatus before the solution was siphoned into the lower flask, the negative AgNO_3 test indicated the absence of chlorine, thus the absence of salts. AgNO_3 reacts with chlorine if present in the sample exhibiting a white precipitate.

IFT Evaluations

The interfacial tension measurements were conducted using a spinning drop tensiometer, with which oil samples from the 9 TH and 8 TH reservoirs were introduced to previously prepared alkali and alkali polymer solutions.

The solutions that were used for this experiment were prepared by diluting an alkali mother solution of 20,000 ppm to reach different concentrations ranging from 3,000 ppm to 15,000 ppm. The two different alkali agents that were utilized are sodium and potassium carbonate.

Additionally, polymer solutions were mixed and diluted with the alkali solutions to include interfacial tension values for alkali-polymer-oil solutions. The specific concentrations and solutions are mentioned in the results section.

To minimize human-made errors three trials were made for the same set of solutions. The values were averaged, and a standard deviation was calculated.

Different concentrations of the two alkali solutions were chosen to have a better understanding of the effect of pH on the interfacial tension between the solution and a given oil with a specific composition. The polymer was added to analyze the effect of polymers on the interfacial tension. The Krüss Spinning drop tensiometer was used due to its capability of measuring the tension of an interface between a heavy phase such as an alkali solution and a light such as oil. The device is shown in figure (20)



Figure 19: Spinning drop tensiometer (Spinning Drop Tensiometer-SDT, 2022)

The equipment that was used with this device are mentioned below, and shown in figure (22):



Figure 20: Equipment used in conducting IFT measurements.

Syringe

Plug

Capillary tube

Piston

Small rod

The procedure consisted of placing a small oil droplet on the plug with the help of an oil-filled syringe. Then, the capillary tube was filled with the heavy phase or with the alkali solution in other words with the help of another syringe. The piston was then placed inside the capillary tube with the help of a rod. And finally, the capillary tube containing the piston was carefully placed on top of the oil filled plug which helped introduce the oil droplet to the heavy phase contained within the capillary tube itself., the system was closed.

The capillary tube containing both phases was placed in the Krüss device. Interfacial tension measurements were taken at 51 °C and 5000 rpm. It should be added that the density of both phases at reservoir temperature were needed as input data to calculate the IFT based on the droplet shape.

Routine core analysis

Routine core analysis was conducted on each core to have relevant data such as porosity and permeability to gas for further fluid-fluid and rock-fluid evaluations.

Porosity Measurements

The porosity of the Berea sandstone plugs was determined using a porosimeter that follows Boyle's law. The porosity that was measured in this experiment is not the absolute porosity of the sample but really close to it. In other words, the porosity that was measured is reflecting the interconnected pores within the core samples. Since the presence of gas tight vugs in sandstone cores is not so common thus the measured porosity is really close to the absolute one. The gas used during this experiment was Helium, due to it being the smallest gas particle able to pass through the smallest pores and pore throats. The porosimeter is shown in figure (24):



Figure 21: Series of Porosimeters.

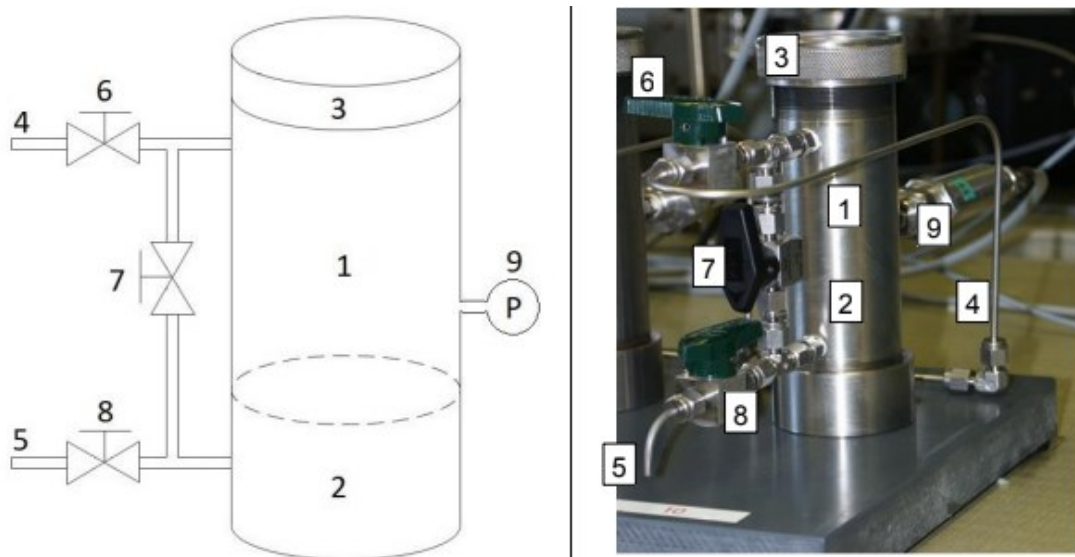


Figure 22: Porosimeter schematic.

The porosimeter is composed of the following element:

- 1) Sample chamber
- 2) Expansion chamber

- 3) Lid with O-ring
- 4) To gas supply (Helium)
- 5) Vent to atmosphere
- 6) Valve 1 (Inlet valve) – To pressurize the sample chamber with helium
- 7) Valve 2 (Balancing valve) – To equilibrate the pressures between sample- and expansion chamber
- 8) Valve 3 (Venting valve)- To vent to the atmosphere
- 9) Pressure transducer connected to recording device

The cores were taken out of the vacuum chamber and the dimensions were taken three consecutive times using a Vernier caliper, and then averaged to minimize human made errors. With the taken dimension the bulk volume of each cylindrical core was calculated V_{bulk} . The mass of each core was then measured and recorded.

Each sample was then placed in the first chamber of the porosimeter where the Helium was injected. The pressure P_1 was recorded in the first chamber after stabilization. The Valve connecting the first chamber to the second one was opened which resulted in a pressure drop. The pressure P_2 was then recorded after stabilization. It should be mentioned that the volume of the second chamber is known. Each measurement was repeated 3 times to ensure good quality data. By applying the equation of state, the matrix volume of the cores could be determined.

$$V_{grain} = V_S - V_E \frac{P_2}{P_1 - P_2} \quad (21)$$

With:

P_1 the pressure before opening the valve.

P_2 the pressure after opening the valve.

V_S the bulk volume of the solid.

V_E the volume of the second chamber.

V_{grain} the grain matrix volume.

The Bulk Volume of each rock was then cross checked with the volume calculated by mercury submergence technique. This technique consisted of determining the change of the core mass once submerged in a mercury bath. This change is assumed to be directly related to the bulk volume of the core. Finally, the pore volume is calculated by subtracting the grain volume from the bulk volume.

$$P_V = V_{grain} - V_{bulk} \tag{22}$$

$$\phi = \frac{P_V}{V_{grain}} \times 100 \tag{23}$$

With:

P_V the pore volume.

V_{bulk} the bulk volume of the core.

ϕ porosity.

Permeability to Gas – Nitrogen

A Hassler Cell type device was used to determine the permeability of the Berea sandstone cores to gas. Nitrogen was selected for this experiment as the gas to be injected through the core plug due to it being an inert, non-reactive gas.

The setup consists of a Hassler cell type composed of the following elements:

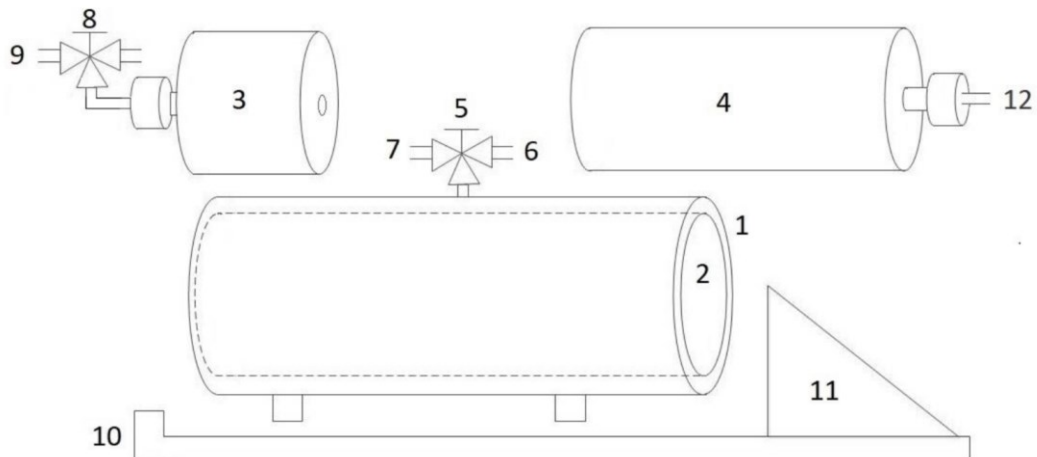


Figure 23: Hassler cell type schematic.

- 1) Body of the Hassler cell
- 2) Rubber sleeve
- 3) Gas inlet piece– fixed
- 4) Gas outlet - floating
- 5) Tree way valve for overburden pressure
- 6) Gas supply - overburden pressure (Nitrogen)
- 7) Gas outlet - To vent to the atmosphere
- 8) Three-way valve for test gas (Nitrogen to flow through sample)
- 9) Gas supply test gas (Nitrogen)
- 10) Base plate of safety rack
- 11) Movable part of safety rack
- 12) Optional: connector for backpressure for Klinkenberg corrected permeability

Nitrogen was injected into the core at a flow rate of 2,000 ml/min during which the pressure at the inlet was recorded. The permeability to gas was then calculated using Darcy's law. It should be noted that Klinkenberg effect was taken into consideration and corrected for in the calculations.

Permeability to Brine

After acquiring the porosity and gas permeability measurements, the cores were fully saturated with hardened brine. The used setup is shown in figure (26):



Figure 24: Fluid saturation unit.

Each core was placed in a vacuum chamber, composed of a lower part holding the cores and an upper part containing a three-way valve. The cores were placed inside, and the lower and upper parts of the chamber were sealed, Greece was applied at the connecting joint to ensure air tightness. The chamber was then connected to a pump with which the chamber was vacuumed, forcing out all gas and air particles contained within the porous media. The chamber remained under this condition for 2 hours, after which the valve was redirected from the pump towards a source of hardened water. The valve was then redirected towards the pump after the cores where completely submerged in hardened brine. It should be noted that air bubbles in the water phase were noticed.

Finally, after approximately 3 hours the pump was turned off and the cores were retrieved. The cores remained submerged in hardened brine to void any undesired displacement of brine from the pore holes.

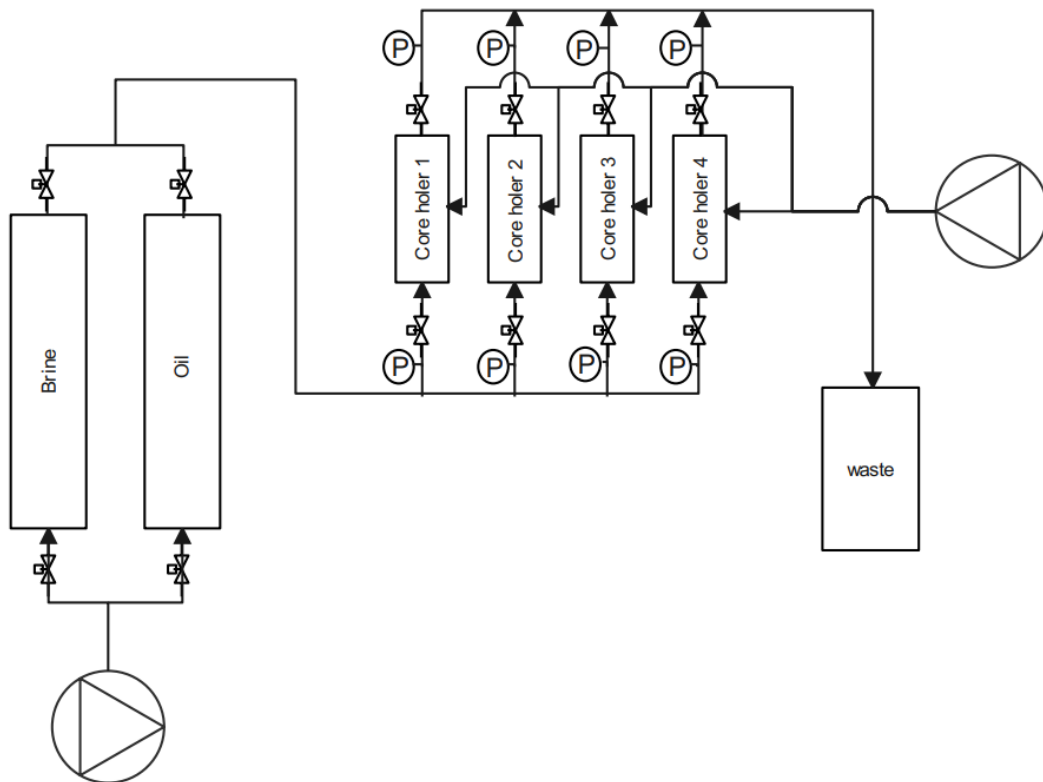


Figure 25: Core saturation setup schematic.

the permeability of the Berea core plugs to brine was measured by injecting hardened brine through the saturated cores with the use of a pump and multiple core holders. A custom setup was built using multiple absolute pressure transducers, metallic flow lines, valves, and finally

two pumps. The setup was designed to flood 4 cores simultaneously due to the high number of core plugs, a detailed schematic is shown in figure(27).

Using flow rate steps to inject brine, the absolute pressure at the inlet and outlet of the core holder was measured. A plateau in the pressure readings suggested that stability had to be attained at each flow rate.

Darcy's equation was then used to calculate the Permeability to Brine:

$$k_w = \frac{q_w \mu_w L}{\Delta P A} \quad (24)$$

With:

k_w – Water permeability [mD].

q_w – Water injection rate [m³ /s].

μ_w – Water viscosity [Pa*s].

L – Core plug length [m].

A – Core plug cross-section area [m²].

ΔP – Differential pressure along the core [Pa].

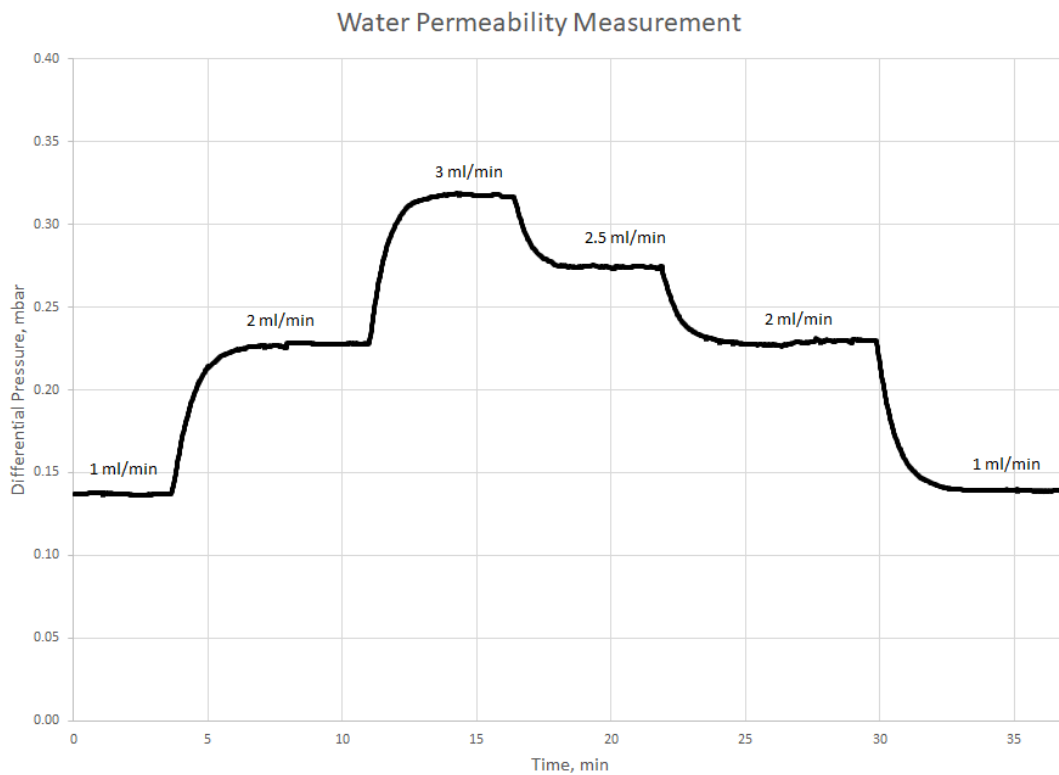


Figure 26: Differential pressure measurements at different brine flow rates for core (Be 05).

Oil Relative Permeability

Oil effective permeability was measured using the same setup shown in figure(27). A Pre injection phase of oil was applied at a rate of 0.05 ml/min for a minimum of 6 hours, which corresponds to a Darcy velocity of 1.4 ft/day. Once a specific oil saturation is achieved, oil was injected at different flow rates and the differential pressure was recorded as shown in figure(29).

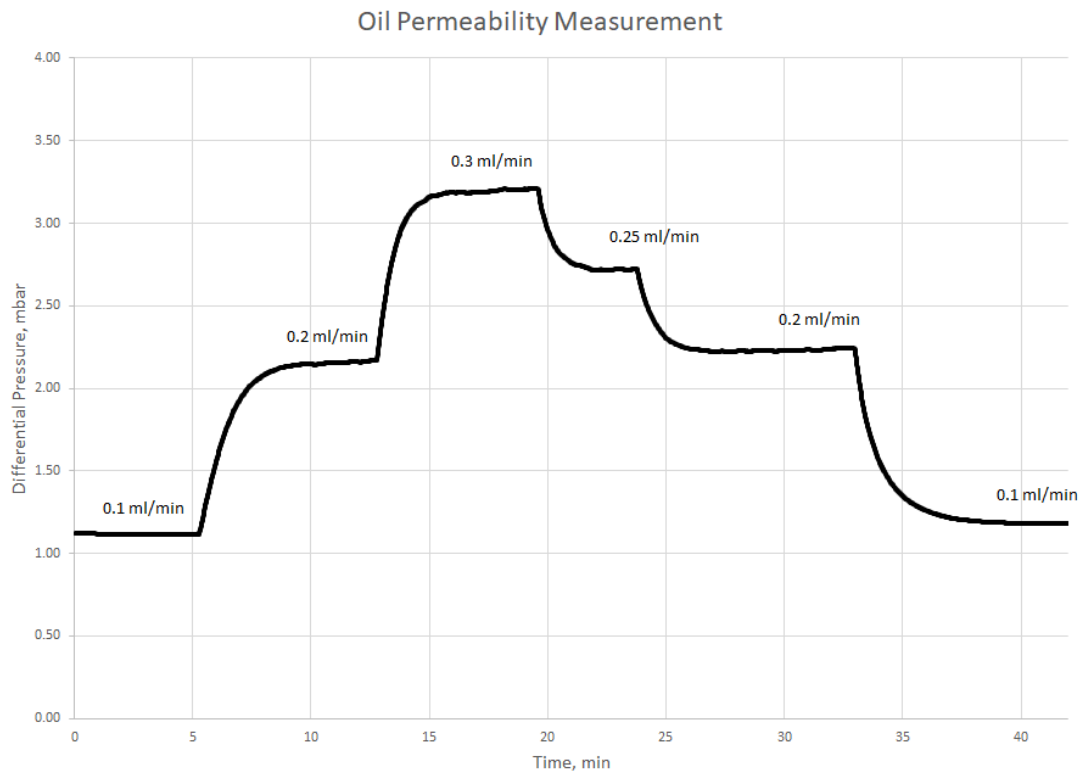


Figure 27: Differential pressure measurements at different oil flow rates for core (Be 05).

Since Swc could not be reached using this method, the oil effective permeability at lower water saturation values was calculated using Darcy's equation:

$$k_o = \frac{q_o \mu_o L}{\Delta P A} \tag{25}$$

With:

k_o – Oil effective permeability [mD]

k_w – Water effective permeability [mD]

q_o – Oil injection rate [m³ /s]

μ_o – Oil viscosity [Pa*s]

L – Core plug length [m]

A – Core plug cross-section area [m²]

ΔP – Differential pressure along the core [Pa]

The oil and water saturations of each core at the end of the oil flooding process were calculated using the water saturated weight of the core plugs and the weight after flooding them with oil. The saturations were calculated as shown in Eq (26) and (27).

$$S_o = \frac{\text{Pore volume} \times \rho_w - \text{Core mass after oil flooding} + \text{Grain mass}}{(\rho_w - \rho_o) \times \rho_o \times \text{Pore volume}} \quad (26)$$

$$S_w = 1 - S_o \quad (27)$$

Spontaneous Imbibition Experiments

The spontaneous imbibition experiment was done with the use of Amott cells. The cells is composed of an upper and lower part, with the upper part formed of a graduated tube which readings of produced oil were taken over time.

The oil saturated cores after measuring their absolute permeability to oil were extracted from the core holders and fully submerged in oil. The cores were then placed in the oven at a temperature of 51 °C for 30 days for the aging process to take place. The aged cores were then taken out of the oven and each core was placed in an Amott cell containing the displacing fluids.

It is worth noting that the moment the cores were submerged in the displacing fluid, spontaneous imbibition of the fluid was observed by the migration of oil droplets from the core towards the top of the cell. The Amott cells were finally placed in the oven at a temperature of 51°C and the oil production was measured daily.

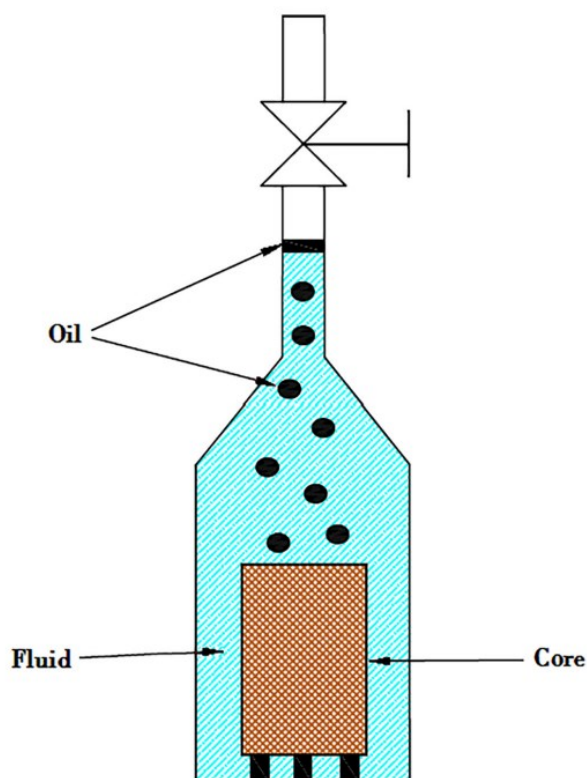


Figure 28: Schematic of Amott cell (Rezaeian, Mousavi, Saljoughi and Akhlaghi Amiri, 2020).

Phase Behavior Experiments

Phase behavior experiments were conducted with the different Alkali, and Alkali-polymer solutions. The samples were prepared in 10 ml pipettes. The pipettes were sealed from the bottom using a methane-oxygen open flame. The samples were then filled with 5 ml of aqueous solutions containing alkali or alkali-polymer along with another 5 ml of oil. The pipettes were closed from the top using the methane-oxygen flame ensuring a closed system.

A proper mixing was ensured by mixing the closed pipettes at a rate of 50 rpm for 48 hours with the help of a rotating shaker. Finally, the samples were stored in the oven at a reservoir temperature of 51 °C, in which the volume of the different phases in each sample were monitored. Multiple trials for each solution are prepared to increase reliability of the results.

Single-Phase Core Floods

Single phase flood experiments were carried out using a custom-made setup shown in figure (31). The setup was designed in a way to flood the Berea core samples with the different aqueous solutions containing different types of alkali and/or polymers to observe their effect on the effective permeability. The samples are listed in the results section.

The setup consisted of two pumps, the first provided a constant overburden pressure of 30 bars and the other was used to pump the aqueous solution through metallic pipes all the way through the core holder to the waste container. It should be highlighted that the setup was designed in a way that ensure a constant temperature of 51 °C was provided to the core holder by placing it in a convection oven.

The first stage of the flooding process consisted of injecting hardened brine in the core while measuring the pressure response, a step wise injection rate was adopted for this stage to evaluate the effective permeability of the core to hardened brine. The aqueous solution was injected overnight for approximately 8 hours at a rate of 0.05 ml/min all while the pressure response was recorded. For the third stage of the experiment, a step wise injection rate of the chosen aqueous solution was adopted to evaluate the effective permeability. Brine was re-injected into the core in the final stage of the single-phase core flood experiment in a step wise rate and the pressure was recorded again for effective permeability calculations. It should be noted that the effective permeabilities were calculated using Darcy's equation.

Finally, the cores were then taken out of the core holder and submerged in methane for further XRD, SEM and thin section analysis

At the end of the experiment, the effective permeability to the aqueous solution and to brine, before and after flooding the core with the aqueous phase, were calculated from the recorded differential pressure across the core holder. The recorded differential pressures were used to calculate the mobility of the different phases shown in Eq (29):

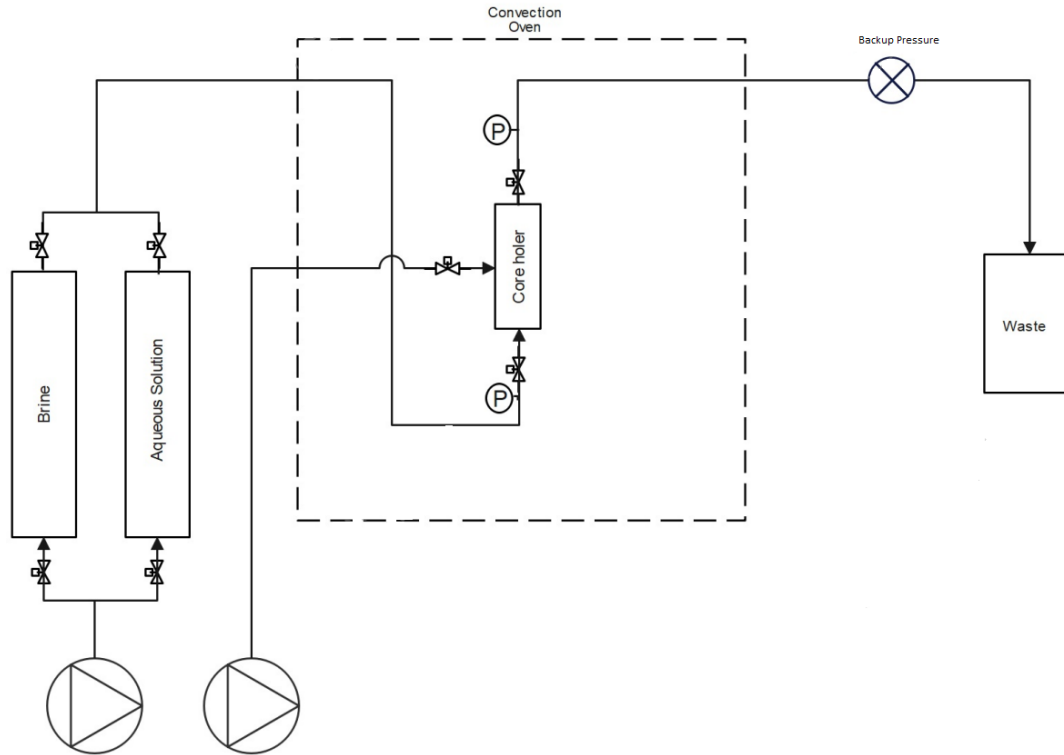


Figure 29: Core flooding experiment setup schematic.

In order to measure the flow restriction brought on by the aqueous phase adsorption to the rock, the resistance factor RF and the residual resistance factor RRF were calculated (Mishra, Berea and Mandal, 2022). The following equations were used to calculate the two parameters:

$$RF = \frac{\lambda_{brine}}{\lambda_{aqueous\ solution}} \quad (28)$$

$$\lambda = \frac{q \times L}{A \times \phi \times \Delta P} \quad (29)$$

$$RRF = \frac{\lambda_{brine\ before\ aqueous\ injection}}{\lambda_{brine\ after\ aqueous\ injection}} \quad (30)$$

Results and Discussion

This chapter presents the results of the different fluid-fluid and rock-fluid interaction experiments. First, the fluid characterisation results are presented and discussed, followed by the routine core analysis experiment results. Towards the end of this chapter, the results of the Amott imbibition, phase behaviour experiments, and IFT measurement results are presented and discussed.

Fluid Characterization

Oil characterization:

Two types of oil with different compositions were evaluated, the first oil sample was taken from the 8 TH reservoir in the Matzen field, and the second was taken from the 9 TH reservoir in the same field. The oil samples were chosen to evaluate the application of Alkali-polymer applications in the previously mentioned reservoirs.

All the relevant oil parameters, such as densities and viscosities, are noted in table (2):

Table 2: 9 TH and 8 TH oil properties.

	8 TH oil	9 TH oil
TAN [mg KOH / g]	2.15	2.17
VOS [mg TEGOtrant A100 / g]	17.18	18.52
Surfificant [mmol Surificant / g]	0.04	0.04
Density @ 22°C [g/cm ³]	0.93	0.91
Viscosity @ 22°C [cP]	210.27	154.77

Brine characterisation:

Three types of brines were used for the different fluid-fluid and rock-fluid evaluations. The first synthetic brine, softened brine, is a simplified brine that was prepared without adding any divalent cation. The softened brine's composition mimics the brine's composition to be injected into the reservoirs. The second synthetic brine is denoted as 8

TH Hardened brine. Its composition mimics the composition of the 8 TH reservoirs' formation water. The third and last synthetic brine is denoted as 9 TH Hardened brine, miming the composition of the 9 TH reservoirs formation water.

The compositions of the synthetic brine, along with their relevant properties, are shown in table (3):

Table 3: Synthetic Brine Viscosities and Densities.

	Formation Brine 8 TH	Formation Brine 9 TH	Softened Brine 8/9 TH
Denisty @ 22°C [g/cm3]	1.0154	1.0085	1.0137
Viscosity @ 22°C [cP]	0.974	0.974	-

Chemical solutions:

The chemical screening was conducted to determine the optimum concentration of both types of used alkalis and polymers. The chosen alkali agents to be investigated are sodium carbonate and potassium carbonate. In addition, two types of polymers were investigated SNF 3630S and KA 5265.

The Chemical solution evaluations are based on phase behaviour, Core flooding, and spontaneous imbibition experiments. The results of these experiments will be further discussed and explained in the following sections. The chemical solutions were prepared to have multiple samples allowing the comparison of different alkali concentrations for each alkali agent. The same also is done for Alkali-Polymer solutions in which specific concentrations of 1850 ppm of KA 5265 and 1900 ppm of SNF 3630S are considered.

Table (4) summarises the prepared solution's densities and pH values. An increase in solution pH is noticed with the increase in alkali concentration.

Table 4: Aqueous solutions densities and pH values.

	Concentration [ppm]	pH @ 22°C	Density @ 49 °C
Sodium Carbonate	3000	9.84	1.007427
	4000	9.98	1.008179
	5000	10.07	1.0097035
	6000	10.14	1.01046
	7000	10.21	1.0116193
	7500	-	1.0120883
	8000	10.25	1.012459
	15000	10.50	1.017988
Potassium Carbonate	3000	9.79	1.0068263
	4000	9.91	1.0081153
	5000	10.00	1.008953
	6000	10.07	1.0097123
	7000	10.14	1.0102847
	7500	-	1.0106867
	8000	10.20	1.0109547
	15000	10.48	1.0162723
Sodium Carbonate + 1900 ppm SNF 3630S	6000	-	1.0084
	7500	-	1.0093
	8000	-	1.0100
	15000	-	1.0142
Sodium Carbonate + 1850 ppm KA 5265	6000	-	1.0070
	7500	-	1.0103
	8000	-	1.0115
	15000	-	1.0177

Viscosity Measurements and Hydrolysis Effect

The viscosity of four alkali-polymer solutions was measured to analyse the change in viscosity at a specific shear rate of 7.944 s^{-1} over time at reservoir temperature. The results are shown in figure (32).

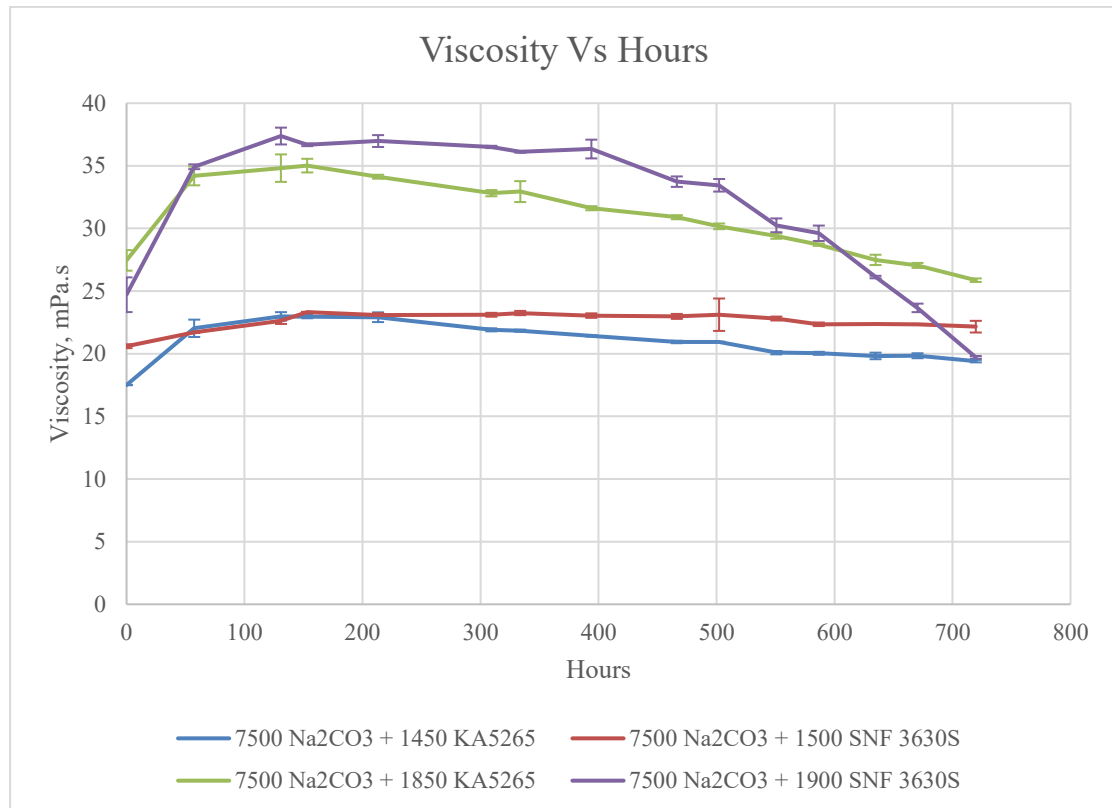


Figure 30: AP Viscosity Hours.

As soon as the alkali-polymer solutions were mixed, the hydrolysis process commenced. For the KA 5265, two concentrations were mixed with 7500 ppm of Na_2CO_3 , a concentration of 1450 and 1850 ppm, the solution with higher polymer viscosity marked a significant viscosity increase of 32.45 %, while the solution with the lower polymer viscosity had a viscosity increase of 32.54% after 11 days. For SNF solutions, two concentrations were mixed with the same concentration of sodium carbonate, a concentration of 1500 and 1900 ppm. Both SNF 3630S solutions resulted in higher viscosity values than KA 5265 at early monitoring stages. The hydrolysis effect is also noticed for the SNF cases by a significant viscosity increase of 59.7 % for the calcium carbonate mixed with 1900 ppm of SNF3630S case and a 16.03 % increase for the second case. The hydrolysis effect was more prominent for cases with higher polymer concentrations.

Table 5: AP viscosity measurements.

	Peak Viscosity [mPa.s]	Initial Viscosity [mPa.s]	Increase in Viscosity after 11 days [%]	Decrease in viscosity after reaching peak value [%]
7500 ppm Na ₂ CO ₃ + 1450 ppm KA 5265	23,22	17,52	32,54	16,71
7500 ppm Na ₂ CO ₃ + 1850 ppm KA 5265	35,59	26,87	32,45	27,59
7500 ppm Na ₂ CO ₃ + 1900 ppm SNF 3630S	23,70	37,85	59,70	17,13
7500 ppm Na ₂ CO ₃ + 1500 ppm SNF 3630S	24,03	20,71	16,03	6,41

An interesting behaviour was noticed for both the KA 5265 cases and the SNF 3630S higher polymer concentration case. The viscosity decreases with time after reaching the corresponding peak values in table (5). This can be explained by a decrease in polymer stability over time. As a result, the amid groups are constantly hydrolysed and replaced by carboxyl groups increasing the electrostatic repulsion and causing the coagulation of the polymer chain. This explains the observations made, in which fisheyes were noticed in the 7500 ppm Na₂CO₃ + 1900 ppm SNF 3630S.

Routine Core Analysis

A total of 36 cores were analysed, from which 16 were used for 8 TH spontaneous imbibition experiments and eight were used for 9 TH spontaneous imbibition experiments. The remaining 12 cores were used for the single-phase core flooding experiments.

The analysis consists of collecting data on water, Nitrogen, and oil effective permeability, along with helium porosity data. The results show a certain degree of uncertainty due to

the core heterogeneities. To have a better image of the consistency of the results and to determine the presence of any outliers several cross-plots are prepared.

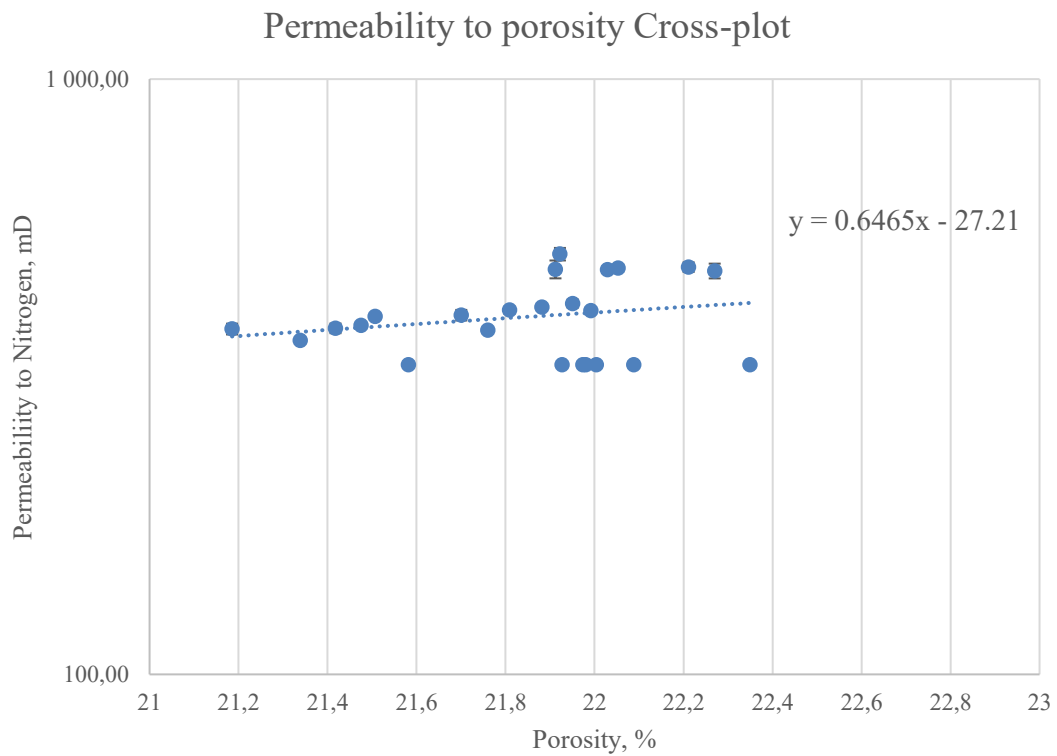


Figure 31: effective permeability - Porosity cross plot.

The First cross plots display the relation between helium porosity and effective permeability to Nitrogen. The displayed relationship shows that the data points are relatively clustered indicating a small uncertainty range. The relationship also indicates an increasing effective permeability with increasing porosity.

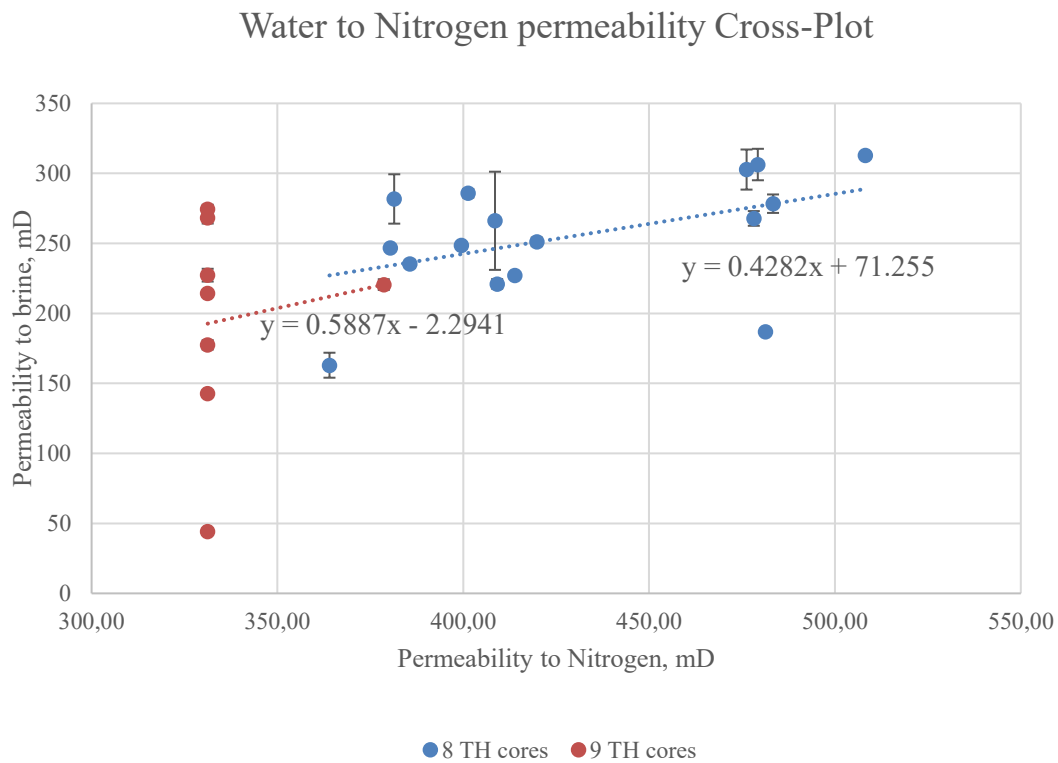


Figure 32: Water to Nitrogen effective permeability cross plot.

The second cross-plot considers the effective permeability to brine. It should be noted that the multi-rate measurements gave different effective permeability values for each core. A wide range of uncertainty can be due to the pressure reading limitations of the pressure transducers.

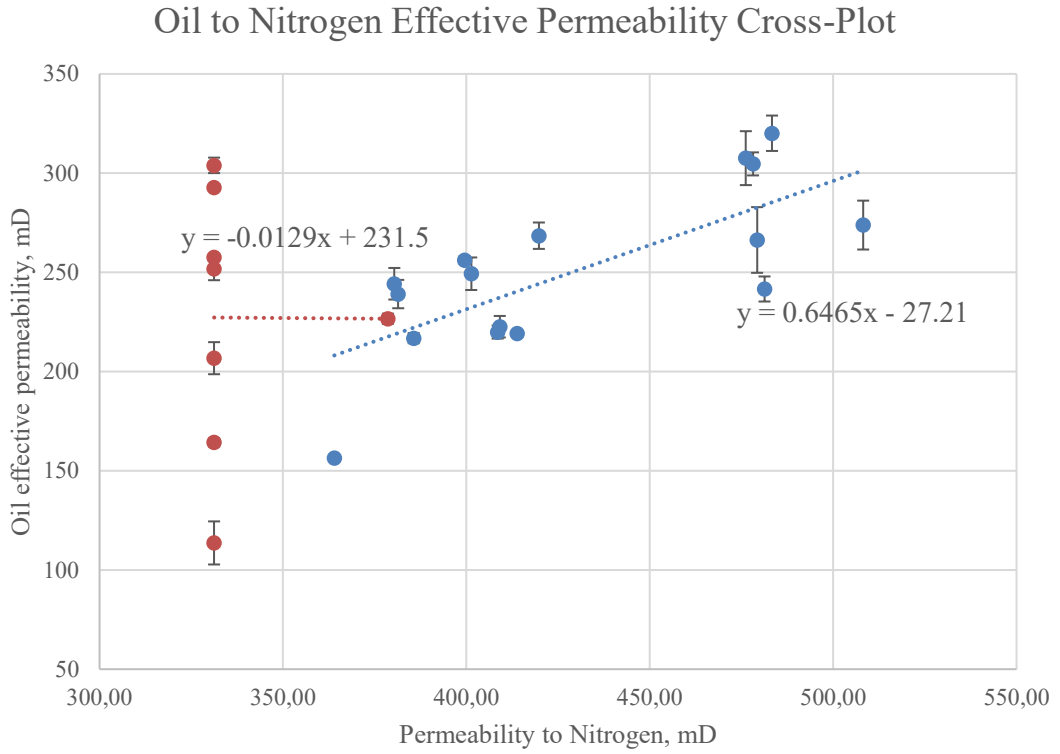


Figure 33: Oil to Nitrogen effective Permeability cross plot.

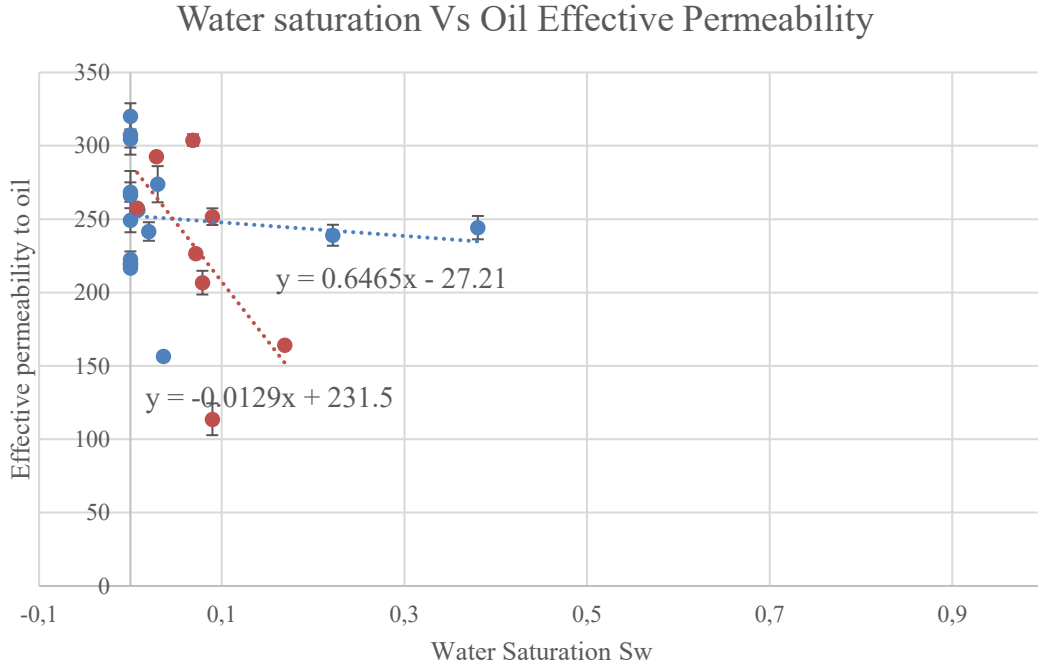


Figure 34: Sw Vs Oil effective permeability cross plot.

The effective permeability of oil is taken into account in the third cross-plot. The correlation between the irreducible water saturations and oil effective permeabilities is shown in a separate cross-plot. Table (6) presents the overall findings.

Table 6: Permeability and porosity of the used core plugs.

Sample ID	effective Permeability to Nitrogen [mD]	Average effective Permeability to Brine [mD]	Average effective Permeability to Oil [mD]	Swirr [-]	Porosity [%]
6/5	481,29	187,00	241,60	2,02	22,05
6/6	419,78	251,10	268,46	0,00	21,95
6/8	408,53	266,15	219,90	0,00	21,99
6/9	413,90	227,10	219,20	0,00	21,88
6/10	409,11	221,07	222,60	0,00	21,81
6/12	399,51	248,60	256,18	0,80	21,51
6/15	385,64	235,32	216,81	0,00	21,48
6/17	479,27	306,32	266,31	0,00	21,91
6/18	508,20	313,00	273,82	2,98	21,92
6/21	401,34	285,80	249,29	0,00	21,70
6/29	364,00	162,98	156,44	3,60	21,34
6/31	476,20	302,74	307,55	0,00	22,27
6/32	483,34	278,36	320,09	0,00	22,21
6/33	478,16	267,83	304,65	0,00	22,03
6/24	380,37	246,85	244,24	38,05	21,19
6/25	381,43	281,73	239,04	22,18	21,42
6/41	378,61	220,58	226,60	7,16	21,76
6/43	331,23	142,79	164,27	16,90	21,58
6/46	331,23	268,19	292,69	2,85	22,35
6/48	331,23	44,21	113,62	8,96	22,09
6/49	331,23	274,39	303,91	6,85	22,00
6/50	331,23	227,30	251,71	8,98	21,93
6/51	331,23	214,42	257,58	0,74	21,98
6/52	331,23	177,53	206,73	7,88	21,97

A large number of analysed core plugs reduces uncertainty and increases data reliability. When comparing the irreducible water saturation of the cores that were saturated with 8 TH oil and 9 TH oil, a larger saturation can be observed for the 9 TH cores, which is mainly due to the presence of water in the used oil sample (7 % water-oil ratio).

IFT Evaluations

Each solution's interfacial tension measurement was taken three times to increase data reliability and reduce uncertainty. The IFT results are taken as comparative indexers and not as exact values due to the high uncertainty level. It should be added that IFT evaluations were only conducted with 9 TH oil.

The shape of the oil droplets was observed for each experimental run. The droplets shape was significantly elongated at the beginning of the experiment. This is translated to a relatively lower initial IFT measurements when compared with the final equilibrium measurements. The shape of the droplet significantly changed at the later stages of the experimental run, the droplet was shrinking in size in a non homogenous manner, thus some parts of the droplet exhibited a more bulging shape while other parts of the droplet retained a non bulging, elongated shape. Upon closer observation the bulging shape had a distinguishable brown color which could indicate phase separation and the presence of a third micro-emulsion phase in the system. It should be mentioned that this observation was noted in most of the experimental runs, not all of them.

The data collected over 280 mins shows both the minimum values of IFT reached by each solution and the Equilibrium IFT at which stability is reached. The standard deviation shown in the results is related to a couple of parameters. The first parameter increasing the standard deviation is the splitting/collision of the oil droplets. A camera monitors the droplet while the capillary tube containing the solutions is rotating at 5000 RPM. During some of the experiments, the droplet splits into two smaller droplets or collides with another droplet leading to a significant volume change and thus affecting the IFT values. The second parameter increasing the standard deviation is the adoption of different algorithms for IFT calculations. Due to the elongated droplet shape, the Vonnegut method was adopted for low IFT values lower than 1 mN/m. On the other hand, the young-Laplace method is adopted for higher IFT values due to their spherical shape.

Alkali- Only cases:

For the alkali-only cases, table (7) summarises the obtained results. The effect of two alkali agents on the IFT was analysed, the first agent is sodium carbonate, and the second is potassium carbonate. The IFT values recorded for all the solutions containing alkali agents are lower than 2 mN/m. However, for the synthetic brine cases, higher IFT values

are recorded. The synthetic brine containing divalent ions recorded an equilibrium IFT 70 % higher than the Softened brine, in which no divalent cations are added.

Similarities in the dynamic IFT behaviour are drawn from the results. The interfacial tension starts initially at low levels indicating the undergoing of the saponification reactions at the aqueous-oil interface and the in-situ generation of surfactants leading to a reduction of the IFT. The initial IFT is at the lowest levels in most of the experiment runs. This could be related to how fast the saponification reaction occurs with this specific oil type. In other words, the saponification reaction and the IFT reduction occur almost instantaneously. An increase of IFT is observed for the alkali-containing solutions until a relative plateau is reached. The IFT value at the plateau is referred to as equilibrium IFT. The Equilibrium IFT is relatively higher than the initial lower IFT due to the consumption of the alkali agent and the diffusion of the surfactants of the aqueous solution-oil interface, and the lack of natural acids after the rearrangement of the molecules.

Another interesting behaviour can be drawn out from the results. The IFT increases at the early stages of the experiments to levels that exceed the Equilibrium IFT and then decreases again to reach its equilibrium value. This behaviour can be due to the diffusion of the generated surfactants off the interface between the two fluids, allowing more space for more saponifiable acids to react with the alkali solution and generate more surfactants, lowering the IFT to its equilibrium value. This behaviour is for the 7500 ppm Na_2CO_3 case in figure (37).

The IFT behaviour and values for the potassium carbonate and the sodium carbonate cases are very similar. For the Sodium carbonate cases, all the Equilibrium IFT values fall within a window between 0.1 and 1.05 mN/m. However, the higher the caustic concentration, the lower the Equilibrium IFT value. For example, a solution containing 7500 ppm of K_2CO_3 has an equilibrium IFT of 0.23 mN/m, which is 79% lower than the Equilibrium IFT of a solution containing 4000 ppm of K_2CO_3 and 96.16 % lower than the one reached in the Softened brine case.

The sodium carbonate gave similar results, with equilibrium IFT values overlapping within a specific window ranging from 0.11 to 0.6 mN/m. Again, a general trend can be seen with lower IFT values reached by solutions with a higher concentration of Na_2CO_3 . However, not all concentrations follow this trend.

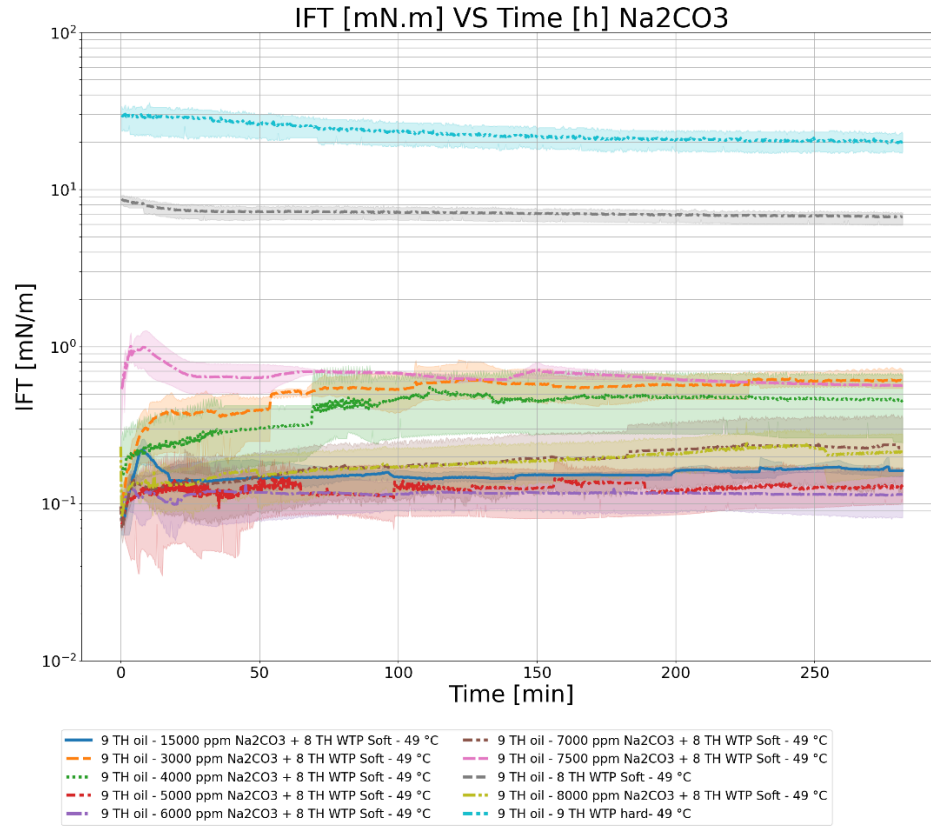


Figure 35: Sodium carbonate + 9 TH oil IFT results.

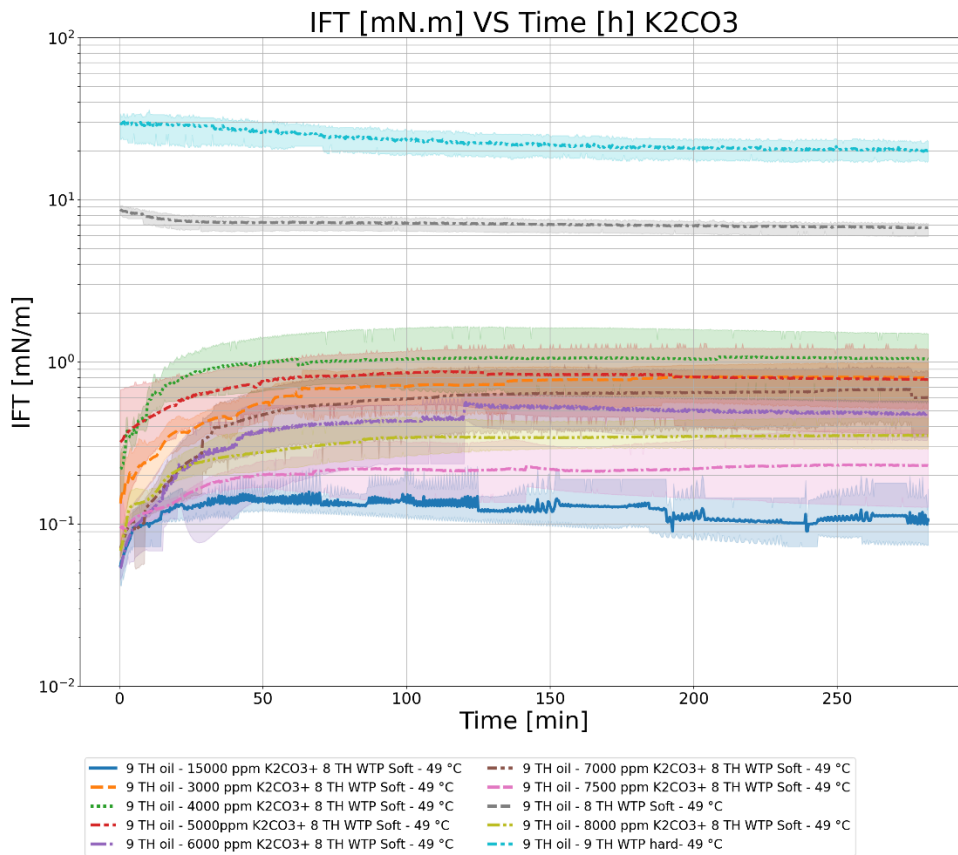


Figure 36: Potassium carbonate + 9 TH oil IFT results.

Alkali - Polymer cases:

Similar behaviour is observed for the alkali-polymer cases with the low recorded equilibrium values of 0,11 mN/m for the 7500 ppm of Na_2CO_3 with the Kamira 5265 polymer solution and 0.53 mN/m for the 7500 ppm of Na_2CO_3 with the SNF3630S polymer solution. The concentration of 7500 ppm of Na_2CO_3 is essential as it is the concentration to be considered for further applications. The IFT values when the cases containing polymer solutions are slightly higher than the ones without. This is mainly due to polymer molecules lowering the alkali concentration and the delay in the Na_2CO_3 diffusion towards the interface due to the higher solution viscosity. The IFT's gradual increase over time is due to the lack of surfactants on the solution-oil interface.

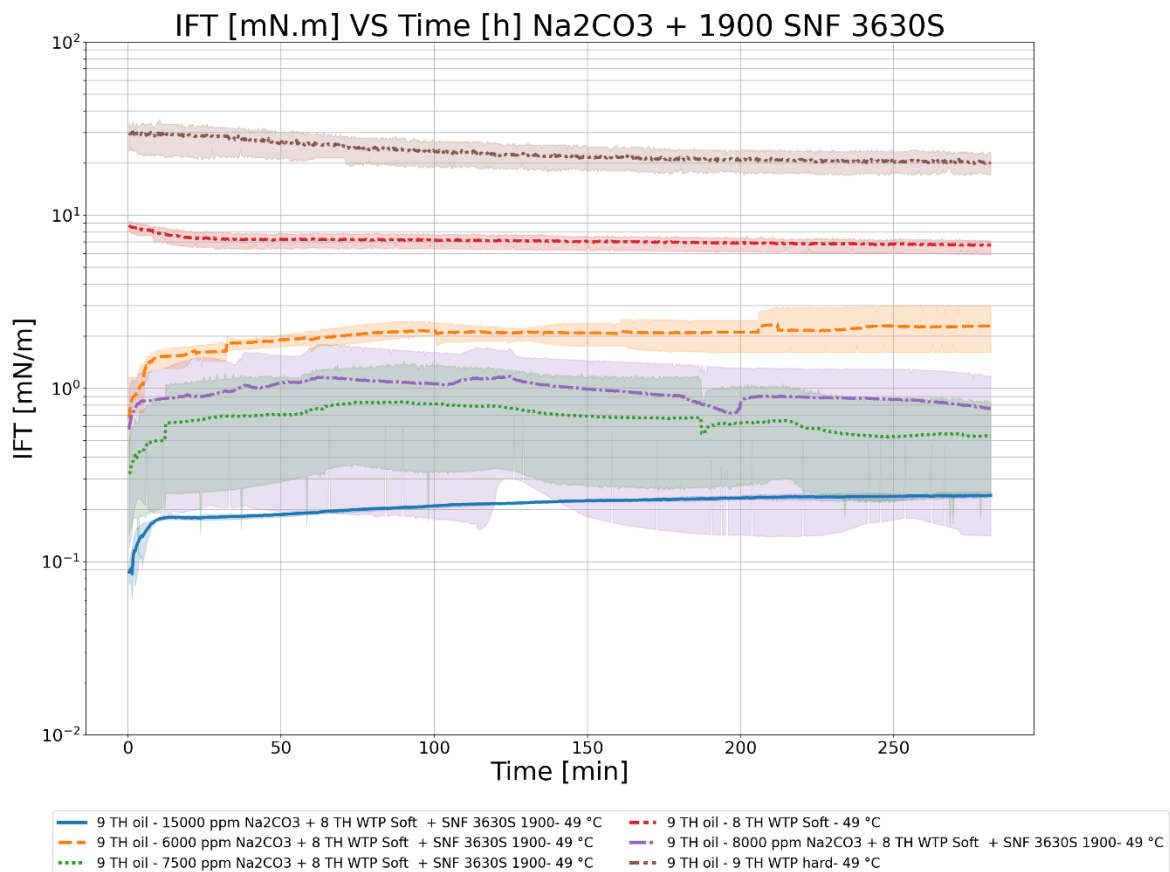


Figure 37: Sodium carbonate + 1900 ppm of SNF 3630S polymer + 9 TH oil IFT results.

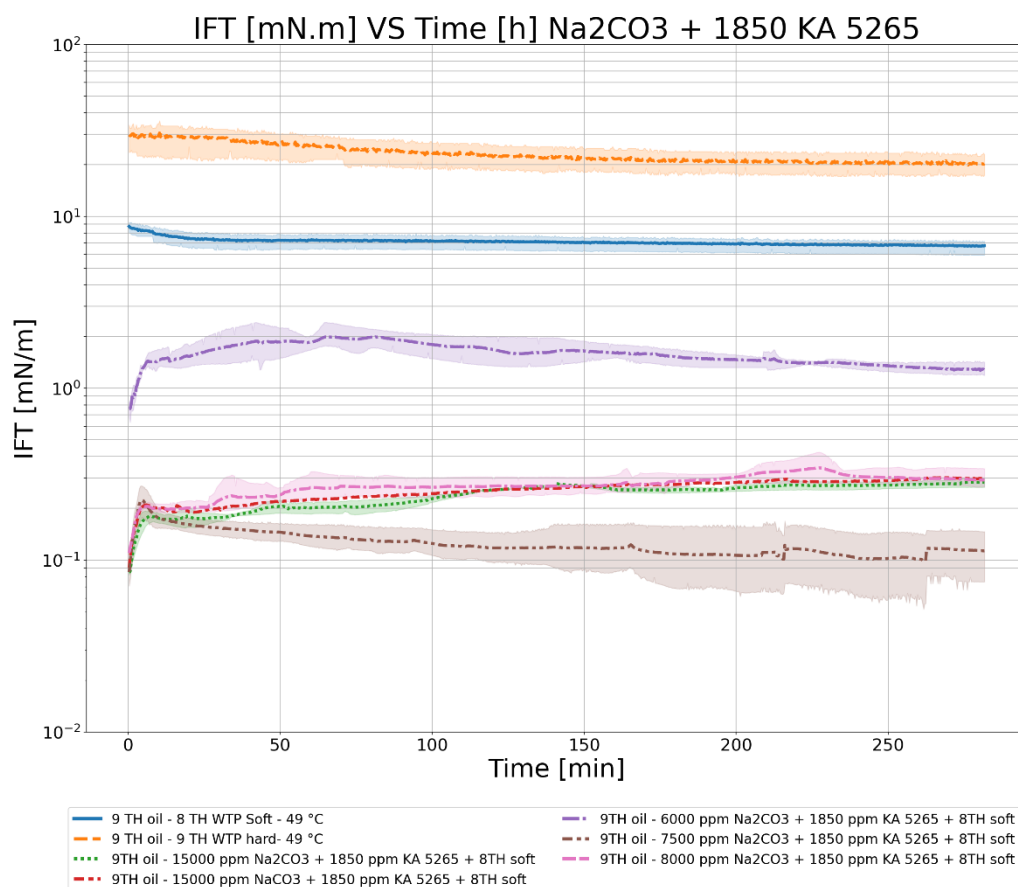


Figure 38: Sodium carbonate + 1850 ppm of KA 5265 polymer + 9 TH oil IFT results.

Every alkali-containing experiment run starts with a highly elongated droplet that corresponds to a low IFT value. The droplet significantly contracts as the IFT rises to stabilize. Table (7) shows the pertinent findings:

Table 7: Initial and Equilibrium IFT values.

	Alkali Concentration [ppm]	Initial IFT [mN/m]	Equilibrium IFT [mN/m]
Sodium carbonate	3000	0.109	0.609
	4000	0.160	0.459
	5000	0.078	0.128
	6000	0.103	0.114
	7000	0.072	0.234
	7500	0.590	0.567
	8000	0.088	0.213
	15000	0.079	0.164
Potassium carbonate	3000	0.146	0.801
	4000	0.224	1.048
	5000	0.325	0.782
	6000	0.056	0.480
	7000	0.073	0.611
	7500	0.096	0.230
	8000	0.072	0.352
	15000	0.058	0.106
Na ₂ CO ₃ + 1900 ppm SNF3630S	6000	0.752	2.290
	7500	0.334	0.531
	8000	0.628	0.778
	15000	0.089	0.240
Na ₂ CO ₃ +1850 ppm KA5265	6000	0.775	1.285
	7500	0.107	0.113
	8000	0.118	0.293
	15000	0.094	0.287
9 TH Hardened Brine	-	29.585	20.173
8 TH Softened Brine	-	8.633	6.733

Phase Behavior Experiments

The phase behaviour experiment was done to study the emulsification process and analyse the emulsion phase's stability. The emulsification process of the two oil samples was analysed for different alkali or alkali-polymer solutions, table (8) shows the different

solutions prepared for this experiment. Some prepared samples were repeated three times to narrow the uncertainty range.

It should be noted that some of the pipettes containing the mixed fluids broke while reading the emulsion volumes. These pipettes were discontinued and disposed of.

After the pipettes were mixed, almost all of them were formed of just a simple light brown emulsion phase. However, an aqueous phase was clear for the samples containing polymer solutions after mixing, indicating a Winsor type III micro-emulsion. This can be due to the polymer solution's high viscosity, rendering the diffusion of surfactants from one phase to the other more difficult.

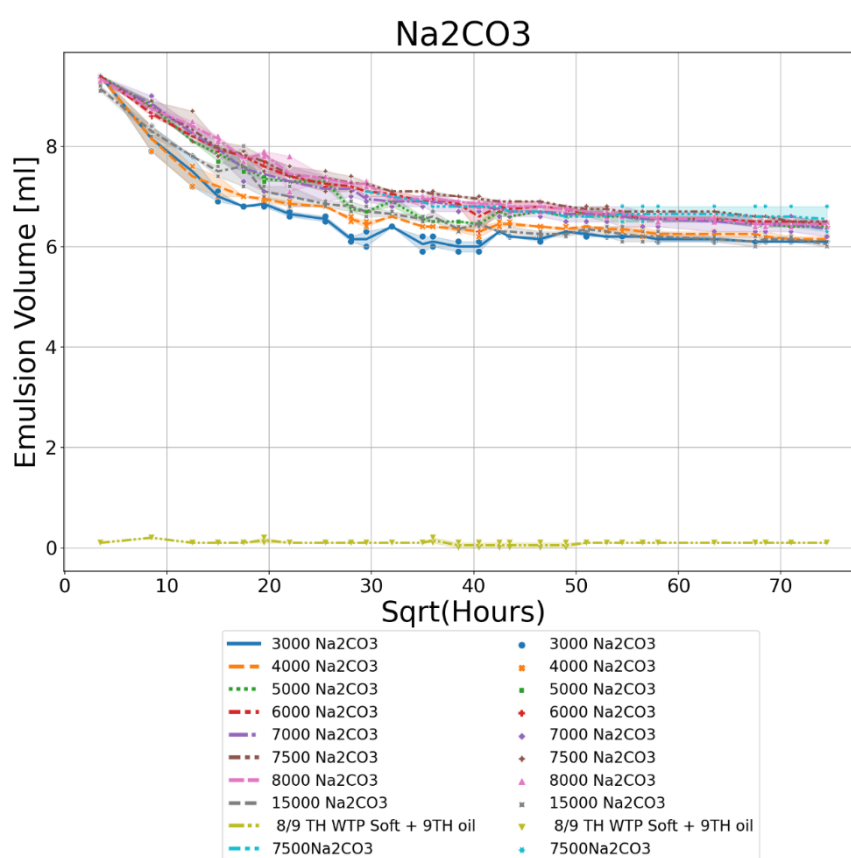


Figure 39:: Sodium carbonate emulsion volume Vs Sqrt(Hours).

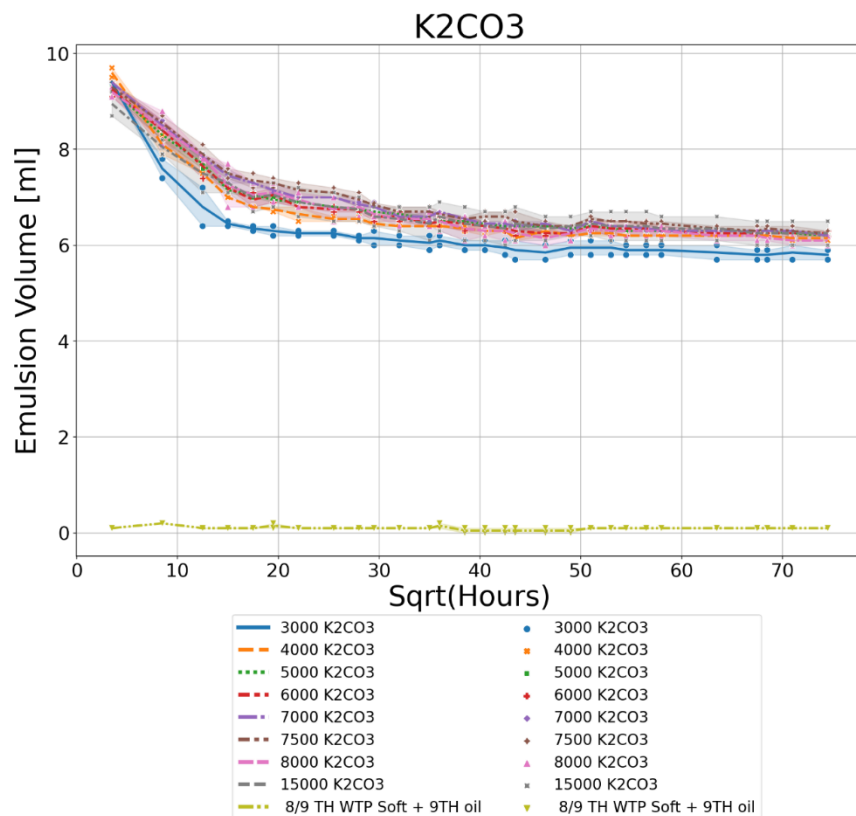


Figure 40: Potassium carbonate emulsion volume Vs Sqrt(Hours).

After storing the pipettes in the heat convection oven and monitoring them for a number of hours, phase separation started to occur and a three phase system was formed indicating the transition from Winsor type II to Winsor type III. This observation was clear for the alkali only cases, however for the alkali-polymer cases Winsor type III micro-emulsion was noticed immediately after mixing as mentioned before. The destabilization of the micro emulsion phase is the reason of the phase separation and the decrease of the micro-emulsion volume with time. Due to the ideal salinity conditions in which low interfacial tension values are achieved for both the Water-Emulsion interface and the Oil-Emulsion interface, both water and oil are solubilized in the micro-emulsion phase in Winsor type III micro-emulsions.

The breaking down of the micro-emulsion phase can be due to the increase of IFT at both of the above mentioned interfaces, until a certain equilibrium is reached. The results indicate that the higher the alkali concentration for the alkali only cases the higher the stability of the micro-emulsion phase and the lower the volume of the generated micro-emulsion. The generation of more surfactants help decreasing the IFT for both water-emulsion and oil-emulsion interfaces. With the increase of salinity, the solubility of the

generated surfactants in the water phase will decrease, which will result in a decrease of IFT at the oil emulsion interface.

The baseline case is formed of a mixture of softened brine and 9 TH oil; this mixture resulted in a narrow uncertainty range and a low to no emulsion phase due to the absence of the two caustic agents, the sodium carbonate and the potassium carbonate. For the sodium carbonate cases, all the used concentrations resulted in roughly the same behaviour and the same final emulsion volume over time. The higher the sodium carbonate concentration is, the higher the emulsion stability. This behaviour could be attributed to the higher alkali concentration resulting in a lower interfacial tension between the oleic phase and the aqueous phase, and the presence of alkali chemicals that keep reacting with the natural acids in the 9 TH oil samples. Consequently, the lower the IFT the more stable the micro emulsion phase. The potassium carbonate cases gave similar results.



Figure 41: Phase behavior results after 204 days, a) to the right a 7500-sodium carbonate + 9 TH oil, in the middle 7500-potassium carbonate + 9 TH oil, to the right 8/9 TH softened brine + 9 TH oil.



Figure 42: Phase behavior results after 204 days, a) to the right a 7500-sodium carbonate + 9 TH oil + 1900 SNF 3630S, in the middle 7500-potassium carbonate + 9 TH oil + 1850 KA 5265, to the right 8/9 TH softened brine + 9 TH oil.

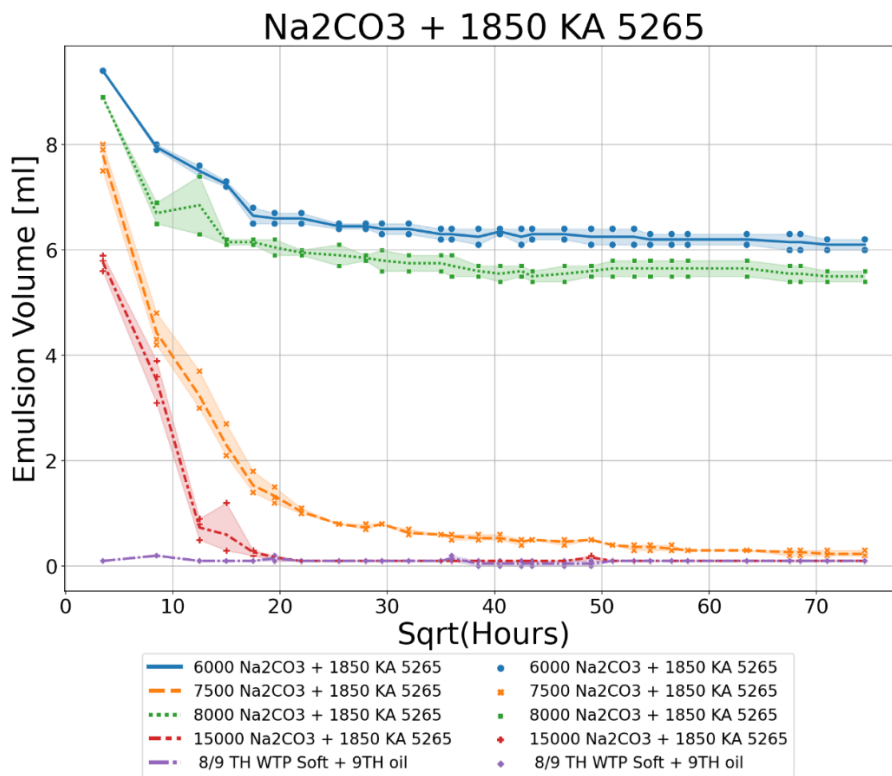


Figure 43: Sodium carbonate + 1850 KA 5165 + 9 TH oil, emulsion volume Vs Sqrt(Hours).

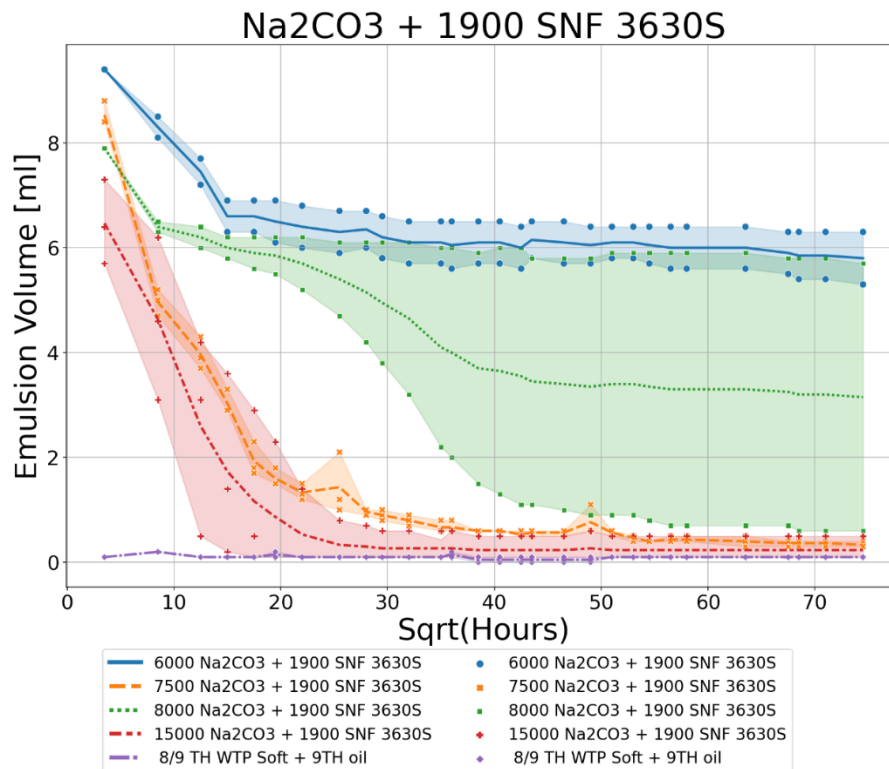


Figure 44 Sodium carbonate + 1900 SNF 3630S + 9 TH oil, emulsion volume Vs Sqrt(Hours).

For the alkali-polymer cases, similar behaviour is noticed in emulsion stability over time for the different concentrations. The concentration of interest composed of 7500 ppm of Na₂CO₃ and 1900 ppm of either SNF 3630S or KA 5265 gave lower emulsion volumes compared with a mixture of the same polymer but with an alkali concentration of 6000 and 8000 ppm. It should be added that a higher range of uncertainty is noticed for the cases containing SNF 3630S polymer, compared with the KA 5265. The emulsion stability of the alkali polymers with the lowest alkali concentration of 6000 ppm showed higher stability with a larger emulsion volume when compared with other alkali-polymer concentrations.

Furthermore, when the same solution is compared with the alkali-only cases, almost the same stability could be seen for the cases with the lowest alkali concentration of 3000 ppm.

Table 8: Phase behavior emulsion phase volume results.

	Concentration [ppm]	Initial Emulsion Volume [ml]	Final emulsion volume [ml]	Change in Volume [ml]
Sodium carbonate	3000	8.35	6.10	2.25
	4000	8.32	6.17	2.15
	5000	8.77	6.42	2.35
	6000	8.75	6.48	2.27
	7000	8.82	6.42	2.40
	7500	8.82	6.53	2.29
	8000	8.83	6.45	2.38
	15000	8.42	6.12	2.30
Potassium carbonate	3000	7.93	5.82	2.12
	4000	8.40	6.17	2.23
	5000	8.42	6.25	2.17
	6000	8.43	6.25	2.18
	7000	8.58	6.27	2.32
	7500	8.58	6.30	2.28
	8000	8.50	6.12	2.38
	15000	8.17	6.25	1.92
Sodium carbonate + 1900 ppm SNF 3630S	6000	8.38	5.83	2.55
	7500	5.82	0.36	5.47
	8000	6.83	3.18	3.65
	15000	4.57	0.23	4.33
Sodium carbonate + 1850 ppm KA 5265	6000	8.28	6.12	2.17
	7500	5.16	0.24	4.91
	8000	7.48	5.52	1.97
	15000	3.34	0.10	3.24
8 TH Softened Brine	-	0.13	0.10	0.03

Single-Phase Core Floods

A set of single-phase core flooding experiments were conducted to better understand the resistance factor and the residual resistance factor. First, a set of core plugs were flooded with a specific Alkali or alkali-polymer solution shown in table (9).

Two behaviours can be seen, a shear thinning behaviour exhibited by all polymer-containing solutions. The resistance to flow decreases with increasing interstitial velocity due to the de-clustering of the polymer chains. This is a shear-dominated flow. A shear thickening behaviour is also noticed at velocities greater than 0.06 ft/ day. With the increasing interstitial velocity, the turbulence of the flow increases resulting in the

elongation of the polymer chain, which in turn increases the solution's apparent viscosity. An increase in the solution viscosity translates into an increase to flow resistance. An additional behaviour was noted at higher velocities. The resistance factor showed a gradual decrease at higher shear rates. The shearing of the elongated polymer chains at high velocities could explain the decrease of the viscosity and the resistance to flow.

When comparing the two alkali polymer solutions composed of 7500 ppm of Na₂CO₃ and two different polymer solutions, the solution containing 1900 ppm SNF 3630S showed an overall higher resistance factor than the solution containing 1850 KA 5265. Using 7500 ppm of Sodium carbonate with 1850 KA 5265 resulted in the lowest RF values.

The residual resistance factor values are displayed in the table (9). For the cases representing the alkali injection without the use of polymer, the residual resistance factor was significantly lower than in the other cases. This is mainly due to the absence of polymer retention in the porous media. Additionally, the RRF for the Alkali-polymer cases was significantly lower than the values achieved by polymer-only injection. The lower retention on the surface of the porous media in the presence of sodium carbonate is due to alkali and polymers competing to be adsorbed on the rock surface, which reduces the overall polymer retention by adsorption.

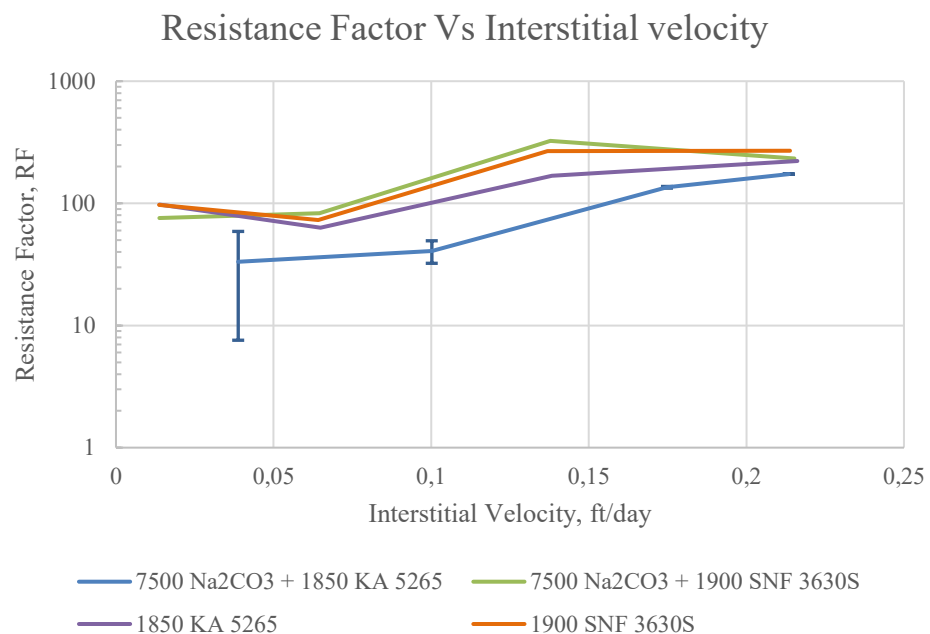


Figure 45: Resistance Factor Vs Interstitial Velocity.

Table 9: Residual Resistance factor, core flooding experiments.

Type	ID	RRF
Alkali Only	7500 Na ₂ CO ₃	1.24
Alkali/Polymer	7500 Na ₂ CO ₃ + 1850 KA 5265	12.95
Alkali/Polymer	7500 Na ₂ CO ₃ + 1900 SNF 3630S	15.52
Polymer Only	1850 KA 5265	21.47
Polymer Only	1900 SNF 3630S	32.14

It should be noted that some of the experiments were conducted multiple times due to the high differential pressure response that indicated core plugging. After thoroughly observing the core plugs, it was deduced that the cause of core plugging was rust seen in both the tubes connecting the piston accumulators to the core holder and on the cores themselves.



Figure 46: core plug showing corrosion on one of its faces.

Spontaneous Imbibition Experiments

In this section, the spontaneous imbibition experimental results are presented and discussed. The spontaneous imbibition experiment was conducted for 9 TH oil-saturated Berea sandstone core plugs and 8 TH oil-saturated Berea sandstone core plugs. The cores were submerged in different solutions, some of which contained a concentration of 7500 ppm of sodium carbonate and others contained different concentrations of alkali-polymer solutions. Oil production started as soon as the cores were placed in the solutions. The

production was noted by the migration of oil bubbles from the core, as shown in figure (49).

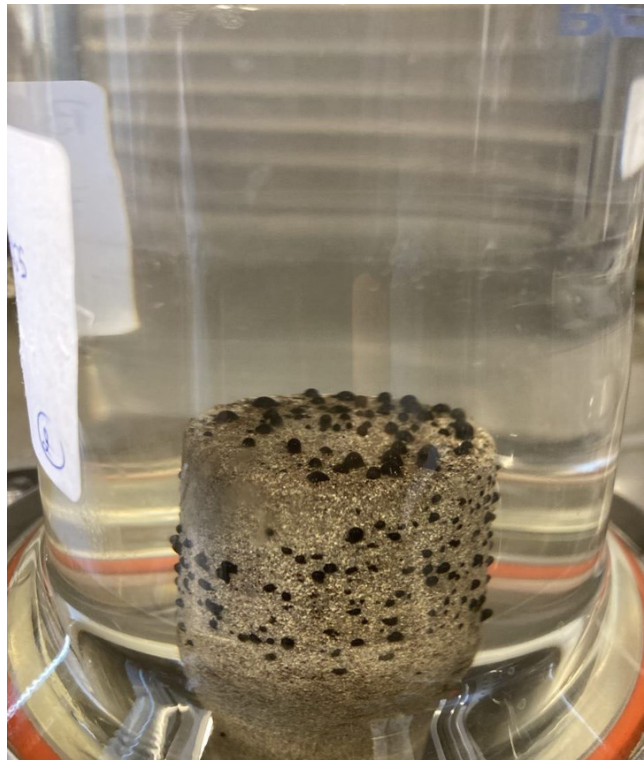


Figure 47: Submerged oil saturated core plug, oil droplets produced from all faces of the core plug.

Some of the experiments were repeated twice to reduce the uncertainty range. Finally, all the core plugs had a restored wettability state.

The analysis of the results showed an increase in oil production over time until a relative plateau is reached, indicating the final oil recovery value.

First, the 8 TH oil-saturated cases will be discussed and compared with the 9 TH oil-saturated cases. Figure (50) shows the oil recovery over the square root of time.

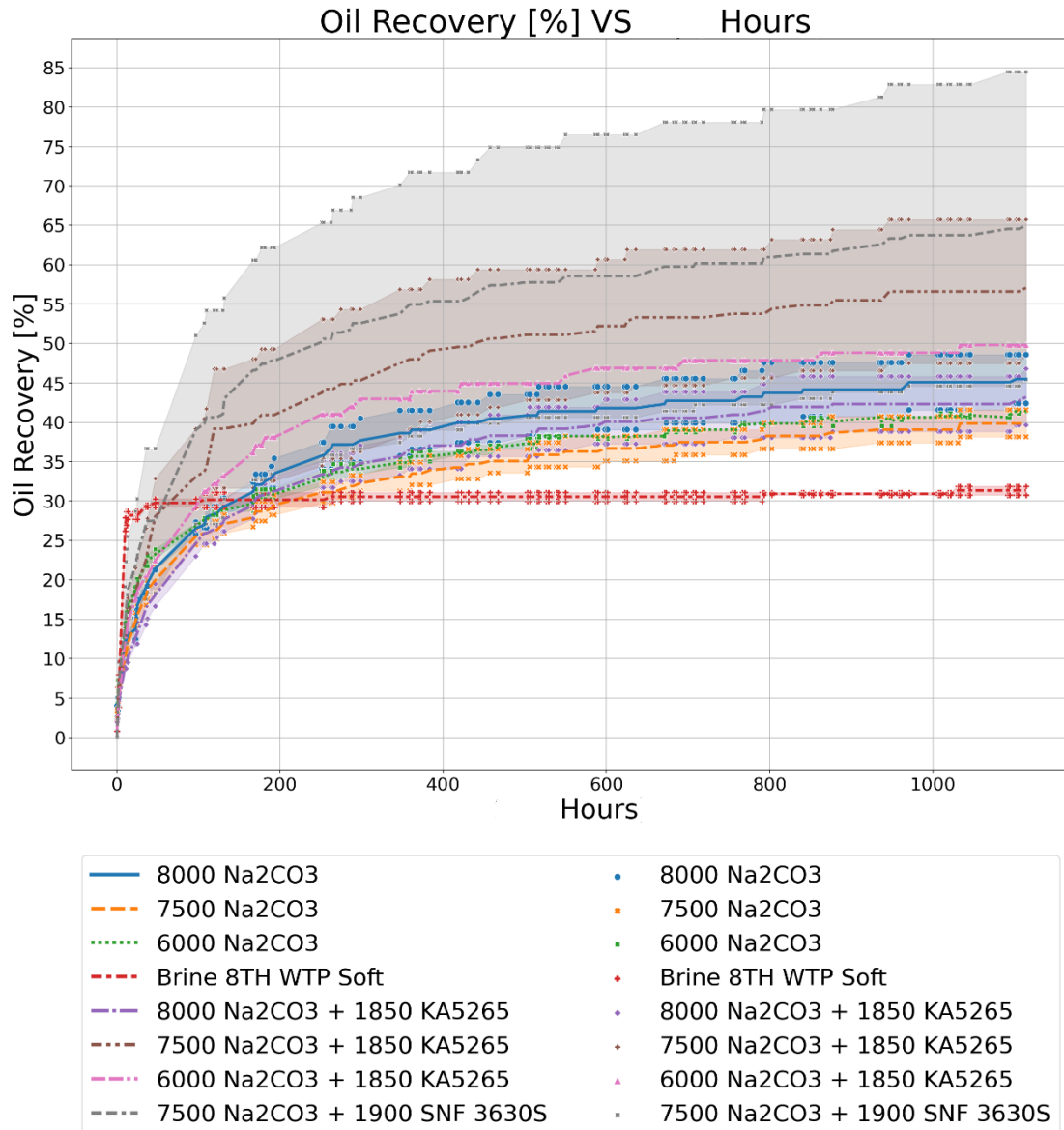


Figure 48: Oil recovery [%] Vs Sqrt (Hours), samples saturated with 8 TH oil.

The baseline case consists of an 8 TH oil-saturated core submerged in softened brine. The imbibition rate is larger in the baseline case due to the high interfacial tension at the oil-water interface. The higher the interfacial tension, the stronger the capillary forces and, in turn, the faster the imbibition rate. This explains the low imbibition rate observed in the alkali cases where a lower interfacial tension exists due to the in-situ generation of soap. In the Alkali-Polymer cases, the decrease of the imbibition rate or the capillary diffusion coefficient is also due to the large size of the polymer molecules in the solution.

The chemical solution provided a wide range of uncertainty with a maximum ultimate oil recovery of 85 %. The higher the Alkali concentration in the aqueous solution, the higher

the ultimate recovery. However, it should be added that the highest oil recovery levels of 64.61 and 56.69 % were achieved with the 7500 ppm of Na_2CO_3 mixed with 1900 SNF 3630S and 1859 KA 5265 consecutively. This significant difference in the ultimate oil recovery could not be simply explained by the lower IFT values since the equilibrium IFT values of the exact solutions were similar. The low IFT values lead to the destruction of the rigid oil films, drawing the oil from pores.

For the 9 TH oil-saturated cases, similar behaviour can be seen. The baseline case shows higher early production due to the higher capillary forces enhancing the spontaneous imbibition process. In the other cases in which Alkali or Alkali polymers are used, the production rate is slower, mainly due to the lower equilibrium interfacial tension values (weaker spontaneous imbibition mechanism). Higher ultimate recovery values are achieved when alkali or alkali-polymer invades the core pores.

It should be noted that the ultimate recovery values for the 9 TH oil-saturated core plugs are significantly lower than the ones for the 8 TH oil-saturated core plugs. This can be due to the higher water saturation in the core plugs because of the 9 TH oil samples' 7 % water-to-oil ratio.

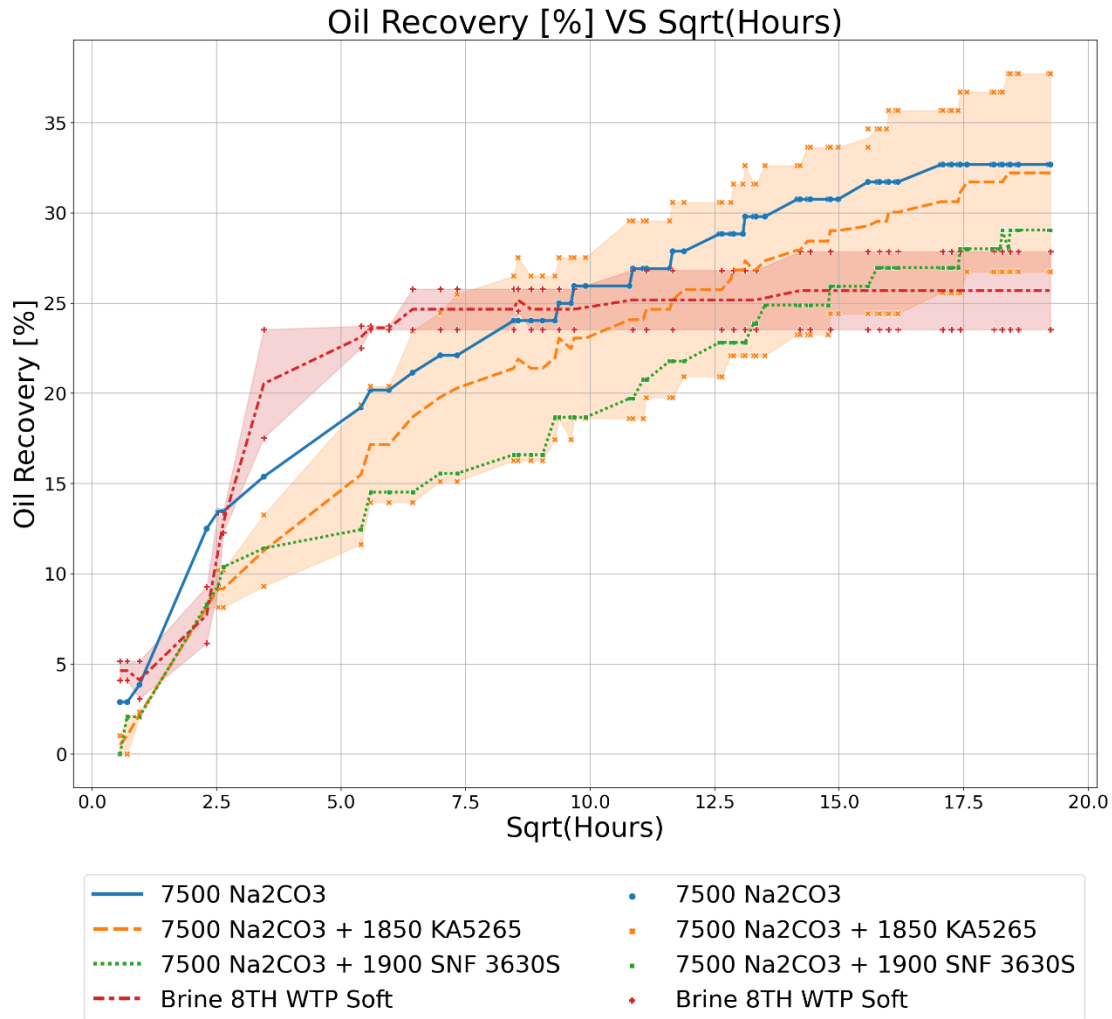


Figure 49: Oil recovery [%] Vs Sqrt (Hours), samples saturated with 9 TH oil.

Table 10: Ultimate oil recovery, Amott spontaneous imbibition experiment results.

	Concentration [ppm]	Ultimate recovery 8 TH [%]	Ultimate recovery 9 TH [%]
Sodium carbonate	3000	-	-
	6000	41.14	-
	7500	39.86	32.69
	8000	45.32	-
Na₂CO₃ + 1900 ppm SNF3630S	7500	64.61	29.05
Na₂CO₃ + 1850 ppm KA5265	6000	49.81	-
	7500	56.69	32.23
	8000	42.66	-
8 TH Softened Brine	-	31.33	25.70

Analysis & Capillary Suction Phenomena

The imbibition or flow of the wetting phase into the porous media is defined as spontaneous imbibition. Capillary forces drive the flow into the core without any viscous displacement resulting in the production of the non-wetting phase. Spontaneous imbibition consists of two flow regimes, the counter-current regime, and the co-current regime.

In the Counter-current case, the wetting phase flows through the same face the non-wetting phase is produced from. This flow behavior causes a decrease in mobility due to flow impedance. The capillary back pressure in this situation which is nothing other than the pressure required to be overcome to produce the non-wetting phase is increased.

In the Co-current case, the aqueous solution is forced into the porous media by spontaneous imbibition at one face of the core, while the production of the non-wetting phase is taking place at the other face. In this instance, mobility is considerably higher than in the counter-current flow regime.

The relationship between capillary and gravity forces is best described by the inverse bond number. The inverse bond number is defined as the ratio of the capillary forces to gravity forces. The wettability factor is not taken into account by the inverse bond number. So it is necessary to thoroughly analyze the capillary diffusion coefficient. You can estimate the capillary diffusion coefficient by ignoring the convective forces (Morrow & Mason, 2001).

As discussed previously, the spontaneous imbibition process is influenced by the capillary forces, and the diffusion of fluids is governed by an equation like Fick's law of diffusion. The diffusion coefficient is the coefficient that defines the rate with which the displacing fluid is imbibed into the porous media. It can be derived from Darcy's law for a two-phase flow system, neglecting convection and buoyancy, by rearranging the equation:

$$\phi \frac{\delta S_w}{\delta t} = -\nabla \left[\frac{1}{\lambda_w^{-1} + \lambda_o^{-1}} \nabla P_c(S_w) \right] \quad (31)$$

With:

ϕ – Porosity [-]

S_w – Water saturation [-]

K – Absolute Permeability [m²]

$\lambda_{w, o}$ – Mobility of water/oil [-]

P_c – Capillary pressure [Pa]

The above equation can be rewritten as diffusion equation:

$$\frac{\delta S_w}{\delta t} = D_c \nabla^2 S_w \quad \text{With} \quad D_c = \frac{\delta P_c}{\phi(\lambda_w^{-1} + \lambda_o^{-1})\delta S_w} \quad (32)$$

Where D_c is the capillary diffusion coefficient.

At a constant capillary diffusion coefficient, the solution can be solved analytically. The normalised oil saturation is defined as follows:

$$S_o^* = C_{ps} C_{cyl} = \frac{S_o - S_{of}}{S_{oi} - S_{of}} \quad (32)$$

$$C_{ps} = \sum_{n=0}^{\infty} \frac{8}{(2n+1)^2 \pi^2} \exp \left[-D_c (2n+1)^2 \pi^2 \frac{t}{4l^2} \right] \quad (33)$$

$$C_{cyl} = \sum_{n=1}^{\infty} \frac{r^2}{r^2 q_n^2} \exp \left[-D_c t q_n^2 \right] \quad (34)$$

With:

S_o^* – Normalized oil saturation [-]

C_{ps} – Concentration for the plane sheet solution [-]

C_{cyl} – Concentration for the cylinder solution [-]

S_{of} – Final oil saturation [-]

S_{oi} – Initial oil saturation [-]

D_c – Capillary diffusion coefficient [m^2 /s]

qn – the positive roots of the $J_0(rqn) = 0$ equation, being the first type Bessel function of order zero

r – Core plug radius [m]

l – Core plug half-length [m]

t – time [s]

The production data for early stages of SI was used to calculate the normalized oil saturation and plotted against time. To have a better fit, the Non linear least square method is used to note a constant diffusion coefficient at the early stages of the experiment. For the 8 TH samples the slowest imbibition rates are seen in the alkali and alkali-polymer cases. This can be due to the decrease of the capillary forces due to the reduction of the interfacial tension. The 9 TH cases demonstrated a different behavior, in most of the cores (with the exception of one Amott cell containing 7500 ppm sodium carbonate mixed with 1850 ppm KA 5265) an increase of diffusion coefficient is noticed along with the decrease of IFT. This behavior is a good indicator of wettability alteration towards a more water wet case . The variation of the capillary diffusion coefficient with respect to the base case of 8 TH softened brine is a good indicator of wettability alteration since the lower IFT values for the alkali and alkali-polymer cases slow the diffusion kinetics, an increase of the latter would indicate a wettability change to a more water wet state. In the displayed results the diffusion coefficients for 8 TH cases are highest in the base cases, no wettability alteration could be concluded. However, for the 9 TH cases an increase in the diffusion coefficient is noticed when alkali and alkali-polymer solutions are used, indicating wettability alteration.

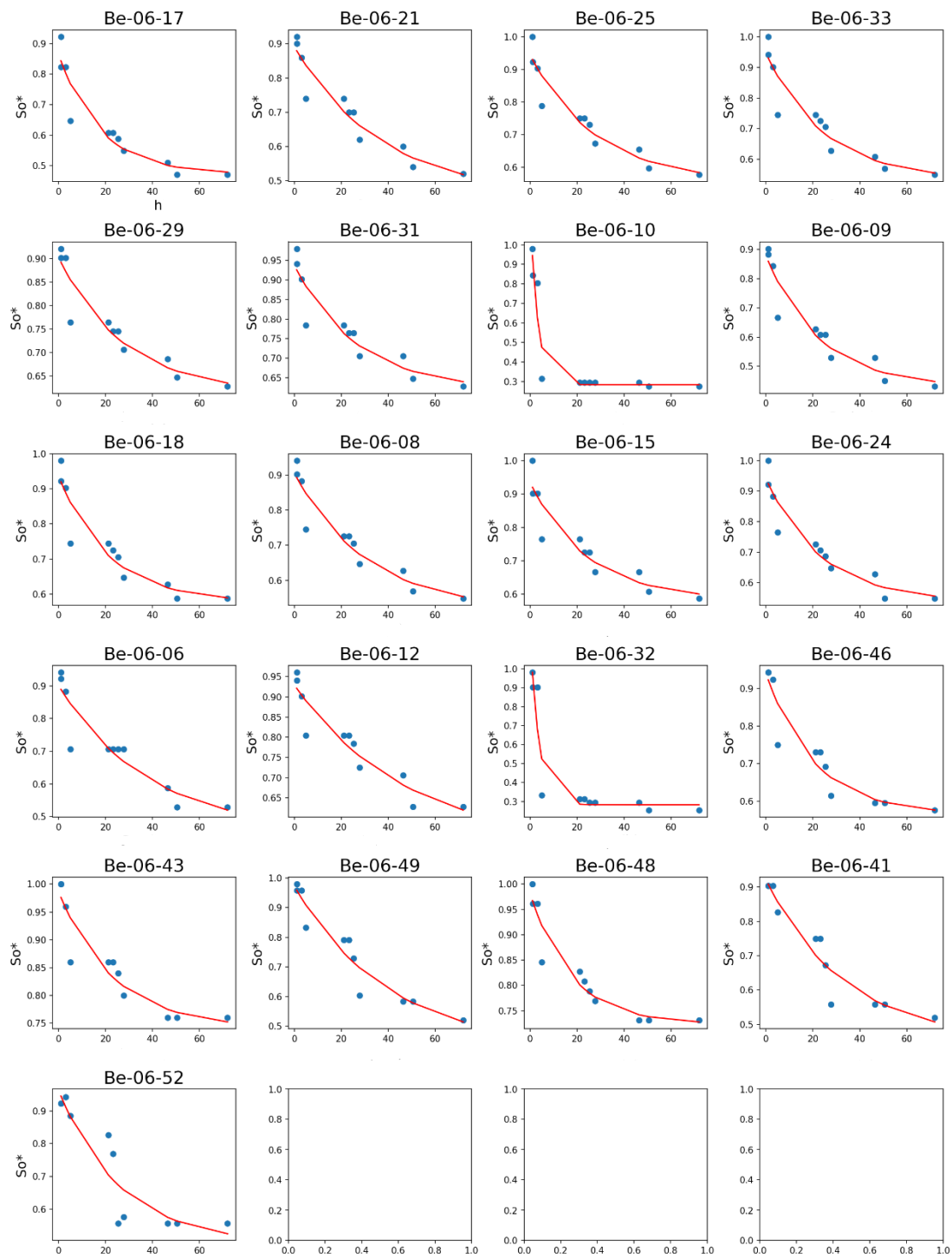


Figure 50: So^* Vs Hours using Non Linear Lease Square Fit

Table 11: Diffusion Coefficients

	core	Inverse Bond Number	Dc	ID	IFT	IFT change %	Dc change %
8 TH	Be-06-17	2.896394	1.56887E-05	6000 Na ₂ CO ₃	0.413	-85.952	- 81.930
	Be-06-21	3.424661	7.5384E-06	7500 Na ₂ CO ₃	0.515	-82.480	- 91.317
	Be-06-25	5.255386	9.8891E-06	7500 Na ₂ CO ₃ + 1850 KA5265	0.764	-74.027	- 88.610
	Be-06-33	3.395833	1.11833E-05	7500 Na ₂ CO ₃ + 1900 SNF 3630S	0.512	-82.582	- 87.119
	Be-06-29	3.840067	1.00072E-05	8000 Na ₂ CO ₃	0.760	-74.156	- 88.474
	Be-06-10	19.27361	8.68203E-05	Brine 8TH WTP Soft	2.940	0.000	0.000
	Be-06-09	2.49205	1.22749E-05	6000 Na ₂ CO ₃	0.413	-85.952	- 85.862
	Be-06-08	3.292267	8.99974E-06	7500 Na ₂ CO ₃	0.515	-82.480	- 89.634
	Be-06-15	4.74165	1.14538E-05	7500 Na ₂ CO ₃ + 1850 KA5265	0.764	-74.027	- 86.808
	Be-06-24	3.33396	1.1899E-05	7500 Na ₂ CO ₃ + 1900 SNF 3630S	0.512	-82.582	- 86.295
	Be-06-06	4.692772	7.31967E-06	8000 Na ₂ CO ₃	0.760	-74.156	- 91.569
	Be-06-32	21.43043	7.4203E-05	Brine 8TH WTP Soft	2.940	0.000	- 14.533
9 TH	Be-06-41	30.65407	8.34909E-06	Brine 8TH WTP Soft	6.733	0.000	- 20.358
	Be-06-43	0.429949	1.18199E-05	7500 Na ₂ CO ₃ + 1850 KA5265	0.113	-98.322	12.750
	Be-06-46	2.850613	1.34836E-05	7500 Na ₂ CO ₃	0.567	-91.579	28.620
	Be-06-48	1.123271	1.58148E-05	7500 Na ₂ CO ₃ + 1900 SNF 3630S	0.531	-92.113	50.857
	Be-06-49	0.590247	6.98628E-06	7500 Na ₂ CO ₃ + 1850 KA5265	0.113	-98.322	- 33.358
	Be-06-52	27.32713	1.04833E-05	Brine 8TH WTP Soft	6.733	0.000	0.000

Conclusion

This chapter draws out the conclusions deduced from the conducted experiments in sections.

Interfacial tension

The following is concluded from the measuring period of 4.72 hours:

- Adding alkali agents such as sodium carbonate or potassium carbonate reduced the interfacial tension measurements significantly to values below 1 mN/m. However, when the alkali-polymer solutions were measured, the results were slightly higher in some cases due to the higher solution viscosity stabilizing the oil bubble.
- Although the IFT measurements had a high level of uncertainty, a weak trend is seen. The equilibrium IFT values decrease as the alkali concentration increases. Not all measured concentrations fall under this.
- Due to the presence of divalent ions in the formation brine (higher ionic strength) and a buffer in the softened solution, NaHCO_3 , the softened brine case displayed lower IFT values when compared to the 9 TH formation brine.

Phase behaviour:

The phase behaviour experiments were used to study the emulsification process and the stability of the created emulsion phase. The following was concluded:

- The emulsification process is driven by the contact of an alkali agent with the natural acids of the 9 TH oil.
- The alkali-only cases exhibited similar behaviour with a relatively small uncertainty range. The higher the alkali concentration, the greater the emulsion volume created and the greater the emulsion stability.
- The concentrations of 6000 ppm of Na_2CO_3 + 1900 ppm SNF 3630S resulted in a considerably higher emulsion volume when compared with the concentration of interest of 7500 ppm of sodium carbonate mixed with either type of polymer.
- The Softened brine case showed low to no emulsion.

Single-phase core floods:

The single-phase core floods helped identify and quantify the different flow behaviours of alkali and alkali-polymer solutions. The resistance factor gave information about the visco-elastic flow behaviour, while the residual resistance factor gave a quantitative measure of alkali and polymer retention in the porous media. The following was concluded:

- For all of the alkali-polymer solutions that were analyzed, the shear thinning and shear thickening flow behaviors were both present. Finally, the shearing of the polymer chains at faster speeds may be the cause of a decrease in flow resistance. Little to no resistance to flow was observed for the alkali injection due to the absence of a polymer solution.
- The alkali-polymer solutions containing KA 5265 have a lower resistance factor and a lower residual resistance factor than the polymer-only cases. In other words, the polymer adsorption to the rock's surface is lower due to the presence of alkali, which is also adsorbing on the same surface.
- When compared to the case in which 1900 ppm of SNF 3630S was used in place of 1850 ppm of KA 5265, the concentration of interest (7500 ppm of sodium carbonate mixed with 1850 ppm of KA 5265) showed the lowest values of adsorption and flowed resistance. (7500 ppm of sodium carbonate mixed with 1850 ppm of KA 5265) showed the lowest values of adsorption and flowed resistance.

Spontaneous imbibition experiment:

The Spontaneous imbibition experiment gave a concrete and quantified image of the alkali wettability alteration mechanism. The results are summed up with the following:

- A high range of uncertainty was observed for the alkali and the alkali-polymer cases.
- The softened brine cases resulted in a high oil recovery value at the early stages of the experiment due to the higher interfacial tension values shown in the IFT section. The higher the IFT values, the stronger the capillary forces and the stronger the spontaneous imbibition. However, the ultimate oil recovery for this

case was not as high as in other cases containing alkali or alkali-polymer chemicals.

- 8 TH oil cases yielded higher ultimate oil recovery than the 9 TH oil cases due to the 9 TH oil samples' 7 % WOR.

Analysis and capillary suction phenomena

- The diffusion coefficient of the displacing fluids, in this case, the aqueous solutions, is a good indicator of the flow kinetics. Therefore, the analytical solution was obtained by assuming a constant diffusion coefficient.
- No gain in diffusion was observed for the 8 TH cases when comparing the alkali and alkali-polymer Dc cases with the base-softened brine Dc case.
- For the 9 TH cases an increase in the diffusion coefficient is noticed when alkali and alkali-polymer solutions are used, indicating wettability alteration.

Overall Conclusion

Generally, using Alkali-Polymer chemicals enhanced the parameters affecting the ultimate oil recovery from the 8 TH and 9 TH oil reservoirs in the Matzen field. Sodium carbonate is considered a favourable Alkali chemical due to its feasible price and ability to reduce the interfacial tension between the oleic and the injected aqueous phase. The Polymer chemicals, on the other hand, proved to improve the stability of the emulsion phase, which is the product of the saponification reaction between the natural acids in the oil and the alkali chemicals. When it comes to polymer retention, it was evident that the synergetic effect of 7500 ppm of sodium carbonate and 1850 ppm of KA 5465 chemicals contributes to relatively lower retention and lower effective permeability reduction when flooding the core samples. Interestingly, the mentioned solution also showed the highest ultimate oil recovery values when conducting spontaneous imbibition experiments. Thus, this concentration should be considered in future AP pilot tests in the 9 TH Matzen reservoir. Further spontaneous imbibition tests with a broader range of alkali concentrations would give a better picture of the significant increase in the ultimate oil recovery.

Future work:

- Performing XRD, SEM, and Thin section analysis on flooded core samples to closely examine changes in mineralogy after alkali and alkali-polymer flooding.
- Conducting more core flooding experiments with different polymer types and concentrations.

References

- Agi, A., Junin, R., Gbonhinbor, J., & Onyekonwu, M. (2018). Natural polymer flow behaviour in porous media for enhanced oil recovery applications: a review. *Journal of Petroleum Exploration and Production Technology*, 8(4), 1349–1362. <https://doi.org/10.1007/s13202-018-0434-7>
- ALYAFEI, N. A. Y. E. F. (2019). *Fundamentals Of Reservoir Rock Properties*. BLOOMSBURY QATAR FOUNDATI.
- Behrang, M., Hosseini, S., & Akhlaghi, N. (2021). Effect of pH on interfacial tension reduction of oil (Heavy acidic crude oil, resinous and asphaltenic synthetic oil)/low salinity solution prepared by chloride-based salts. *Journal of Petroleum Science and Engineering*, 205, 108840. <https://doi.org/10.1016/j.petrol.2021.108840>
- Cheng, K. H. (1986). Chemical Consumption During Alkaline Flooding: A Comparative Evaluation. *SPE Enhanced Oil Recovery Symposium*. <https://doi.org/10.2118/14944-ms>
- Chiotoroiu, M.-M., Clemens, T., & Thiele, M. (2022). *Experiences with History Matching of a Complex Austrian Reservoir with 250 Wells and 62 Years of Production Using Global and Local Techniques*. Retrieved 2022, from https://www.researchgate.net/publication/272706918_Experiences_with_History_Matching_of_a_Complex_Austrian_Reservoir_with_250_Wells_and_62_Years_of_Production_Using_Global_and_Local_Techniques
- Costa Gomes, J., Geiger, S., & P. Arnold, D. (2019). An Open Access Carbonate Reservoir Benchmarking Study for Reservoir Characterisation, Uncertainty Quantification & History Matching. *Day 1 Tue, September 17, 2019*. <https://doi.org/10.2118/196674-ms>

- deZabala, E. F., Vislocky, J. M., Rubin, E., & Radke, C. J. (1982). A Chemical Theory for Linear Alkaline Flooding. *Society of Petroleum Engineers Journal*, 22(02), 245–258. <https://doi.org/10.2118/8997-pa>
- Donaldson, E. C., Thomas, R. D., & Lorenz, P. B. (1969). Wettability Determination and Its Effect on Recovery Efficiency. *Society of Petroleum Engineers Journal*, 9(01), 13–20. <https://doi.org/10.2118/2338-pa>
- Fan, T., & Buckley, J. S. (2006). Acid Number Measurements Revisited. *All Days*. <https://doi.org/10.2118/99884-ms>
- Gbadamosi, A. O., Junin, R., Manan, M. A., Agi, A., & Yusuff, A. S. (2019). An overview of chemical enhanced oil recovery: recent advances and prospects. *International Nano Letters*, 9(3), 171–202. <https://doi.org/10.1007/s40089-019-0272-8>
- Gong, H., Li, Y., Dong, M., Ma, S., & Liu, W. (2016). Effect of wettability alteration on enhanced heavy oil recovery by alkaline flooding. *Colloids and Surfaces A: Physicochemical and Engineering Aspects*, 488, 28–35. <https://doi.org/10.1016/j.colsurfa.2015.09.042>
- Goodarzi, F., & Zendejboudi, S. (2018). A Comprehensive Review on Emulsions and Emulsion Stability in Chemical and Energy Industries. *The Canadian Journal of Chemical Engineering*, 97(1), 281–309. <https://doi.org/10.1002/cjce.23336>
- Guo, H., Song, K., & Hilfer, R. (2022). A Brief Review of Capillary Number and its Use in Capillary Desaturation Curves. *Transport in Porous Media*. <https://doi.org/10.1007/s11242-021-01743-7>
- Hou, B.-feng, Wang, Y.-fei, & Huang, Y. (2015). Mechanistic study of wettability alteration of oil-wet sandstone surface using different surfactants. *Applied Surface Science*, 330, 56–64. <https://doi.org/10.1016/j.apsusc.2014.12.185>
- Katsanis, E. P., Krumrine, P. H., & Falcone, J. S. (1983). Chemistry of Precipitation and Scale Formation in Geological Systems. *SPE Oilfield and Geothermal Chemistry Symposium*. <https://doi.org/10.2118/11802-ms>
- Kumar, S., Yen, T. F., Chilingarian, G. V., & Donaldson, E. C. (1989). Chapter 9 Alkaline Flooding. *Developments in Petroleum Science*, 219–254. [https://doi.org/10.1016/s0376-7361\(08\)70461-8](https://doi.org/10.1016/s0376-7361(08)70461-8)
- Lake, L.: Enhanced Oil Recovery. Prentice Hall, Englewood Cliffs (1989)
- Mandal, A. (2015). Chemical flood enhanced oil recovery: a review. *International Journal of Oil, Gas and Coal Technology*, 9(3), 241. <https://doi.org/10.1504/ijogct.2015.069001>
- MCR 102e/302e/502e, M. (2022). *Modular Compact Rheometer: MCR 102e/302e/502e* :: Anton-Paar.com. Anton Paar. Retrieved 2022, from

<https://www.anton-paar.com/us-en/products/details/rheometer-mcr-102-302-502/>

- Meter, D. (2022). *Density Meter :: Anton-Paar.com*. Anton Paar. Retrieved 2022, from <https://www.anton-paar.com/corp-en/products/group/density-meter/>
- Mishra, S., Bera, A., & Mandal, A. (2022). *Effect of Polymer Adsorption on Permeability Reduction in Enhanced Oil Recovery*. Retrieved 2022.
- Morrow, N.R. and Mason, G. (2001) "Recovery of oil by spontaneous imbibition," *Current Opinion in Colloid & Interface Science*, 6(4), pp. 321–337. Available at: [https://doi.org/10.1016/s1359-0294\(01\)00100-5](https://doi.org/10.1016/s1359-0294(01)00100-5).
- Poellitzer, S., Gruenwalder, M., Kienberger, G., & Clemens, T. (2008). How to Optimise Oil Recovery after almost 60 Years of Production from the Matzen Field, Austria. *All Days*. <https://doi.org/10.2118/113303-ms>
- Research, P. (2022). *Enhanced Oil Recovery Market Size to Hit US\$ 78.24 Bn by 2030*. GlobeNewswire News Room. Retrieved 2022, from <https://www.globenewswire.com/news-release/2022/03/30/2413054/0/en/Enhanced-Oil-Recovery-Market-Size-to-Hit-US-78-24-Bn-by-2030.html>
- Rezaeian, M. S., Mousavi, S. M., Saljoughi, E., & Akhlaghi Amiri, H. A. (2020). Evaluation of thin film composite membrane in production of ionically modified water applied for enhanced oil recovery. *Desalination*, 474, 114194. <https://doi.org/10.1016/j.desal.2019.114194>
- Schechter, D. S., Zhou, D., & Orr, F. M. (1994). Low IFT drainage and imbibition. *Journal of Petroleum Science and Engineering*, 11(4), 283–300. [https://doi.org/10.1016/0920-4105\(94\)90047-7](https://doi.org/10.1016/0920-4105(94)90047-7)
- ShamsiJazeyi, H., Verduzco, R., & Hirasaki, G. J. (2014). Reducing adsorption of anionic surfactant for enhanced oil recovery: Part I. Competitive adsorption mechanism. *Colloids and Surfaces A: Physicochemical and Engineering Aspects*, 453, 162–167. <https://doi.org/10.1016/j.colsurfa.2013.10.042>
- Sheng, J. (2016). *Modern chemical enhanced oil recovery*. Gulf Professional.
- Sheng, J. J. (2015). Investigation of alkaline–crude oil reaction. *Petroleum*, 1(1), 31–39. <https://doi.org/10.1016/j.petlm.2015.04.004>
- Sieberer, M., Jamek, K., & Clemens, T. (2022). *Polymer Flooding Economics, from Pilot to Field Implementation at the Example of the 8 TH Reservoir, Austria*. Retrieved 2022.
- Spinning Drop Tensiometer-SDT*. Kruss-scientific.com. (2022). Retrieved 2022, from <https://www.kruss-scientific.com/en/products-services/products/sdt>

- Stosur, G. J., Hite, J. R., Carnahan, N. F., & Miller, K. (2003). The Alphabet Soup of IOR, EOR and AOR: Effective Communication Requires a Definition of Terms. *All Days*. <https://doi.org/10.2118/84908-ms>
- Taber, J. J., Martin, F. D., & Seright, R. S. (1997). EOR Screening Criteria Revisited— Part 1: Introduction to Screening Criteria and Enhanced Recovery Field Projects. *SPE Reservoir Engineering*, *12*(03), 189–198. <https://doi.org/10.2118/35385-pa>
- Tadros, T. F. (2013). Emulsion Formation, Stability, and Rheology. *Emulsion Formation and Stability*, 1–75. <https://doi.org/10.1002/9783527647941.ch1>
- Viades-Trejo, J., & Gracia-Fadrique, J. (2007). Spinning drop method. *Colloids and Surfaces A: Physicochemical and Engineering Aspects*, *302*(1-3), 549–552. <https://doi.org/10.1016/j.colsurfa.2007.03.033>
- Vonnegut, B. (1942). Rotating Bubble Method for the Determination of Surface and Interfacial Tensions. *Review of Scientific Instruments*, *13*(1), 6–9. <https://doi.org/10.1063/1.1769937>
- Woodford, C. (2022). *How do pH meters work? | Measuring acidity*. Explain that Stuff. Retrieved 2022, from <https://www.explainthatstuff.com/how-ph-meters-work.html>
- Yeganeh, M., Hegner, J., Lewandowski, E., Mohan, A., Lake, L. W., Cherney, D., Jusufi, A., & Jaishankar, A. (2016). Capillary Desaturation Curve Fundamentals. *All Days*. <https://doi.org/10.2118/179574-m>

List of Figures

Figure 1: CDC curve for the wetting and non-wetting phase from Lake(1989, Fig.3–17, p.70).	21
Figure 2: Displacement front in two different conditions, (a) unstable condition, (b) Stable condition without viscous fingering (Gbadamosi et al., 2019).	22
Figure 3: Spinning drop method (Viades-Trejo and Gracia-Fadrique, 2007).	29
Figure 4: Alkali Recovery process (deZabala, Vislocky, Rubin and Radke, 1982).	31
Figure 5: Different processes of de-emulsification (Tadros, 2013).	34
Figure 6: Schematic showing a droplet of water surrounded by gas on a solid surface (ALYAFEI, 2019).	36
Figure 7: Schematic showing contact angle measurement on a solid surface for (a) water-wet, (b) intermediate-wet, (c) oil-wet, and (d) mixed-wet cases. (ALYAFEI, 2019).	37
Figure 8: Schematic diagram of drainage capillary pressure with important labeling and wettability distribution in the reservoir. (ALYAFEI, 2019).	38
Figure 9: Schematic showing the effect of wettability on water re-saturation capillary pressure curves. (ALYAFEI, 2019).	39
Figure 10: Schematic of the Amott experimental test (ALYAFEI, 2019).	40
Figure 11: —USBM wettability measurement on (left) water-wet and (right) oil-wet samples (Costa Gomes, Geiger and P. Arnold, 2019)	42
Figure 12: Effect of inverse bond number on capillary and gravity forces (Schechter et al., 1994).	43
Figure 13: Wettability alteration process (Gbadamosi et al., 2019).	46
Figure 14: Wettability alteration by a cationic surfactant, b anionic surfactant (Gbadamosi et al., 2019)	47
Figure 15: Visco-elastic fluid flow behavior (Sheng, 2016).	49
Figure 16: Anton Parr density meter (Meter, 2022).	55
Figure 17: Anton Parr rheometer (MCR 102e/302e/502e, 2022)	56
Figure 18: Soxhlet apparatus	57
Figure 19: Spinning drop tensiometer (Spinning Drop Tensiometer-SDT, 2022).	59
Figure 20: Equipment used in conducting IFT measurements.	60
Figure 21: Series of Porosimeters.	61
Figure 22: Porosimeter schematic.	61
Figure 23: Hassler cell type schematic.	63
Figure 24: Fluid saturation unit.	64
Figure 25: Core saturation setup schematic.	65
Figure 26: Differential pressure measurements at different brine flow rates for core (Be 05).	66
Figure 27: Differential pressure measurements at different oil flow rates for core (Be 05).	67
Figure 28: Schematic of Amott cell (Rezaeian, Mousavi, Saljoughi and Akhlaghi Amiri, 2020).	69
Figure 29: Core flooding experiment setup schematic.	71
Figure 30: AP Viscosity Hours.	75
Figure 31: effective permeability - Porosity cross plot.	77
Figure 32: Water to Nitrogen effective permeability cross plot.	78
Figure 33: Oil to Nitrogen effective Permeability cross plot.	79
Figure 34: Sw Vs Oil effective permeability cross plot.	79
Figure 35: Sodium carbonate + 9 TH oil IFT results.	83
Figure 36: Potassium carbonate + 9 TH oil IFT results.	83
Figure 37: Sodium carbonate + 1900 ppm of SNF 3630S polymer + 9 TH oil IFT results.	84
Figure 38: Sodium carbonate + 1850 ppm of KA 5265 polymer + 9 TH oil IFT results.	85
Figure 39: Sodium carbonate emulsion volume Vs Sqrt(Hours).	87
Figure 40: Potassium carbonate emulsion volume Vs Sqrt(Hours).	88

Figure 41: Phase behavior results after 204 days, a) to the right a 7500-sodium carbonate + 9 TH oil, in the middle 7500-potassium carbonate + 9 TH oil, to the right 8/9 TH softened brine + 9 TH oil..... 89

Figure 42: Phase behavior results after 204 days, a) to the right a 7500-sodium carbonate + 9 TH oil + 1900 SNF 3630S, in the middle 7500-potassium carbonate + 9 TH oil + 1850 KA 5265, to the right 8/9 TH softened brine + 9 TH oil. 90

Figure 43: Sodium carbonate + 1850 KA 5165 + 9 TH oil, emulsion volume Vs Sqrt(Hours). 90

Figure 44Sodium carbonate + 1900 SNF 3630S + 9 TH oil, emulsion volume Vs Sqrt(Hours). 91

Figure 45: Resistance Factor Vs Interstitial Velocity. 93

Figure 46: core plug showing corrosion on one of its faces. 94

Figure 47: Submerged oil saturated core plug, oil droplets produced from all faces of the core plug. 95

Figure 48: Oil recovery [%] Vs Sqrt (Hours), samples saturated with 8 TH oil..... 96

Figure 49: Oil recovery [%] Vs Sqrt (Hours), samples saturated with 9 TH oil..... 98

Figure 50: S_o^* Vs sqrt(time) using Non Linear Least Square Fit 102

List of Tables

Table 1: Synthetic brine compositions.	53
Table 2: 9 TH and 8 TH oil properties.	72
Table 3: Synthetic Brine Viscosities and Densities.	72
Table 4: Aqueous solutions densities and pH values.	74
Table 5: AP viscosity measurements.	76
Table 6: Permeability and porosity of the used core plugs.	80
Table 7: Initial and Equilibrium IFT values.	85
Table 8: Phase behavior emulsion phase volume results.	91
Table 9: Residual Resistance factor, core flooding experiments.	94
Table 10: Ultimate oil recovery, Amott spontaneous imbibition experiment results.	98